Fusion Engineering and Design 6 (1988) 3–64
North-Holland, Amsterdam

MODELING, ANALYSIS AND EXPERIMENTS FOR FUSION NUCLEAR TECHNOLOGY

M.A. ABDOU, A.H. HADID, A.R. RAFFRAY, M.S. TILLACK, and T. IIZUKA *

Mechanical, Aerospace and Nuclear Engineering Department, University of California, Los Angeles, Los Angeles, CA 90024, USA

P.J. GIERSZEWSKI

Canadian Fusion Fuels Technology Project, Mississauga, Ontario, Canada L5J 1K3

R.J. PUIGH

Hanford Engineering Development Laboratory, Westinghouse Hanford Company, Richland, WA 99352, USA

D.K. SZE and B. PICOLOGLOU

Argonne National Laboratory, Argonne, IL 60439, USA

Submitted May 1987; accepted November 1987
Handling Editor: R.W. Conn

Selected issues in the development of fusion nuclear technology (FNT) have been studied. These relate to (1) near-term experiments, modeling, and analysis for several key FNT issues, and (2) FNT testing in future fusion facilities.

A key concern for solid breeder blankets is to reduce the number of candidate materials and configurations for advanced experiments to emphasize those with the highest potential. Based on technical analysis, recommendations have been developed for reducing the size of the test matrix and for focusing the testing program on important areas of emphasis. The characteristics of an advanced liquid metal MHD experiment have also been studied. This facility is required in addition to existing facilities in order to address critical uncertainties in MHD fluid flow and heat transfer.

In addition to experiments, successful development of FNT will require models for interpreting experimental data, for planning experiments, and for use as a design tool for fusion components. Modeling of liquid metal fluid flow is a particular area of need in which substantial progress is expected, and initial efforts are reported here. Preliminary results on the modeling of tritium transport and inventory in solid breeders are also summarized. Finally, the thermo-mechanical behavior of liquid-metal-cooled limiters is analyzed and the parameter space for feasible designs is explored.

Because of the renewed strong interest in a fusion engineering facility, a critical review and analysis of the important FNT testing requirements have been performed. Several areas have been emphasized due to their strong impact on the design and cost of the test facility. These include (1) the length of the plasma burn and the mode of operation (pulsed vs. steady-state), and (2) the need for a tritium-producing blanket and its impact on the availability of the device.

1. Introduction

The importance of moving forward with the development of fusion nuclear technology (FNT) has been clearly recognized by all of the world's major fusion programs. Furthermore, there has been an increased awareness of the complexity of the research and development (R&D) problems of FNT and of the need for careful technical planning of experiments and facilities. FNT is concerned with fuel production and processing, energy extraction and use, and radiation protection of personnel and components. The primary fusion reactor components include the blanket, plasma-interactive components (such as first wall, limiter, and divertor), and radiation shield, and tritium system. In 1984–1985, the FINESSE study identified the key technical issues

* Visiting scientist. Permanent address: Japan Atomic Energy Research Institute, Tokai-mura, Naka-gun, Ibaraki-ken, 319-11, Japan.

0920-3796/88/$03.50

and developed, based on technical evaluations, recommendations on the types, sequences and characteristics of major experiments and facilities in a logically consistent path for FNT development. The results were presented in the two major FINESSE reports [1,2], with comprehensive summaries in refs. [3] and [4]. Although technical planning was the driving goal for FINESSE, substantial contributions have also been made to the advancement of the understanding of fusion nuclear components and to the capability of predicting their performance.

Implementation is the logical next step to technical planning. The results from FINESSE showed that the present activities on FNT need substantial enhancement through:

(a) construction of a number of well defined, small-scale facilities;
(b) performance of a number of new specific experiments in existing facilities; and
(c) development of analytical and computational models for predicting the performance of nuclear components.

This article describes two technical studies which relate to the implementation phase of FNT.

The first, which is a follow-up to FINESSE, focuses on specific key questions for: (a) very near-term (0–3 years) nonfusion experiments and facilities, and (b) FNT testing in a fusion facility.

The second is the initial stage of a detailed effort to develop theory, models and computer codes for predicting the performance of nuclear components.

Section 2 addresses a number of selected technical problems for the very near-term experiments of solid and liquid breeders. In previous FINESSE work, a number of advanced solid breeder experiments in fission reactors have been identified. These next-generation experiments are relatively costly and, hence, need to be limited to materials and configurations with the highest potential. An important part of Section 2 is an assessment of the relative advantages of the many solid breeders, neutron multipliers and configurations. Recommendations have been developed for reducing the size of the test matrix and for focusing the testing program on important areas of emphasis for the near-term experiments.

The need for a near-term advanced MHD facility, called LMF1, has been identified in FINESSE. This facility is required in addition to existing facilities (e.g., ALEX at Argonne National Laboratory) in order to address critical MHD fluid flow issues. The characteristics and cost of this facility and the experiments which might be performed in it are also discussed in Section 2.

Major initiatives are underway to plan and design a fusion engineering test facility (e.g., NET [5] in Europe, FER [6] in Japan, and TIBER [7] in the U.S.). The requirements of FNT testing on the major parameters and features of such a facility have been addressed previously in FINESSE. Examination of the impact of these requirements on the design and cost of a fusion engineering facility revealed the need for further examination of a number of issues. A particularly important issue relates to the length of the plasma burn time and to the mode of operation (steady state or pulsed). Another important issue pertains to the need for a tritium-producing blanket and to its impact on the operational availability of the device. These issues are examined in Section 3. Because of the renewed strong interest in a fusion engineering facility, a reasonably complete summary of the important FNT testing requirements is also provided.

Successful development of the predictive capabilities necessary to design, construct and operate fusion nuclear components requires a highly interactive program of theory, modeling and experiments. While Sections 2 and 3 are concerned with FNT experiments, Section 4 reports on the progress of the initial stage of an effort to develop theory and analytical and numerical models for nuclear components. A major part of the effort to date has focused on modeling of MHD effects for liquid metal blankets. Progress has also been made on modeling tritium transport and inventory in solid breeder blankets and the thermomechanical behavior of liquid-metal-cooled limiters.

2. Non-fusion experiments and facilities

Experiments in non-fusion facilities can play a key role in the development of fusion nuclear technologies prior to testing in the fusion environment. This was recognized in earlier studies and incorporated as a central element in the FINESSE test plans for blankets and other nuclear components [2]. Recent effort in the Technical Planning Activity (TPA) [8] has confirmed the importance of these experiments.

Non-fusion facilities include non-neutron test stands, fission reactors, and 14 MeV point neutron sources. Each of these provide unique testing capabilities for blanket experiments. The key issues for solid breeder blankets are shown in table 1. Because of the dominant role that radiation plays in tritium production, tritium transport, and breeder thermomechanical behavior, fission reactors play a major role in the solid breeder test program. Table 1 also summarizes the key issues for

Table 1
Key blanket issues

Solid breeder
Tritium self-sufficiency
Breeder/multiplier tritium recovery and inventory
Breeder/multiplier thermomechanical behavior
Corrosion and mass transfer
Structural response and failure modes
Tritium permeation and processing from the blanket
Liquid breeder
Tritium self-sufficiency
Magnetohydrodynamic effects
Corrosion and mass transfer
Structural response and failure modes
Tritium permeation and processing from the blanket

liquid breeder blankets. Here, the key issues generally involve thermomechanical behavior (including MHD effects), material compatibility, and tritium recovery. Experiments addressing these issues are generally best treated in non-neutron test stands. For all blankets, fuel self-sufficiency is a key issue. 14-MeV neutron sources are needed for experiments on tritium breeding as well as other neutronic and radiation damage issues.

A framework for technical planning of fusion nuclear experiments has been developed earlier in FINESSE [2]. This framework defines four phases that are summarized in table 2. During these phases, the emphasis shifts in the level of integration from separate effect, to multiple effect, to partially integrated and, finally, to fully integrated fusion testing. The key elements of the test plans for both solid and liquid breeder blankets are summarized in figs. 1 and 2. Both plans culminate in the design of experimental modules for testing in the fusion environment and in an assessment of the feasibility and attractiveness of blanket components and systems. The objectives and milestones for each phase are also shown in table 2.

As part of the previous FINESSE effort, many of the technical features of experiments and facilities of the four phases have been defined. The work reported here examines a number of selected technical problems for the near-term experiments of Phase I.

For solid breeder blankets, material selection and characterization are currently at the center of a worldwide effort. On-going and near-term experiments are focused on fabrication, unirradiated properties and in-reactor open and closed capsule tests. At the same time, the world programs include a large number of candidate materials and configurations. This work assesses the relative advantages of the various solid breeders and provides recommendations for reducing the size of the test matrix in upcoming experiments. This is particularly important because of the increased cost of the more complex next-generation experiments.

Section 2.1.1 describes the detailed analyses that have been performed to compare different solid breeder materials and configurations. The comparison was based on various performance parameters directly dependent on the solid breeder properties. Prior to the analysis, these properties (and corresponding uncertainty ranges)

Table 2
Phases of blanket testing

	Approximate time frame	Level of integration	Primary objectives	Milestones
Phase I	0–10 yrs	Properties, separate effects	Develop understanding of material behavior and blanket phenomena	Select material combination [a]
Phase II	5–15 yrs	Multiple effects	Understand phenomena, develop predictive capabilities for complex configurations	Select blanket configurations
Phase III	10–20 yrs	Partially integrated (non-fusion)	Design concept verification in non-fusion environment	Select primary blanket design options for fusion testing
Phase IV	15–25 yrs	Integrated	Design concept verification in fusion facility	Successfully operate test modules

[a] To the extent possible with limited high fluence irradiation data

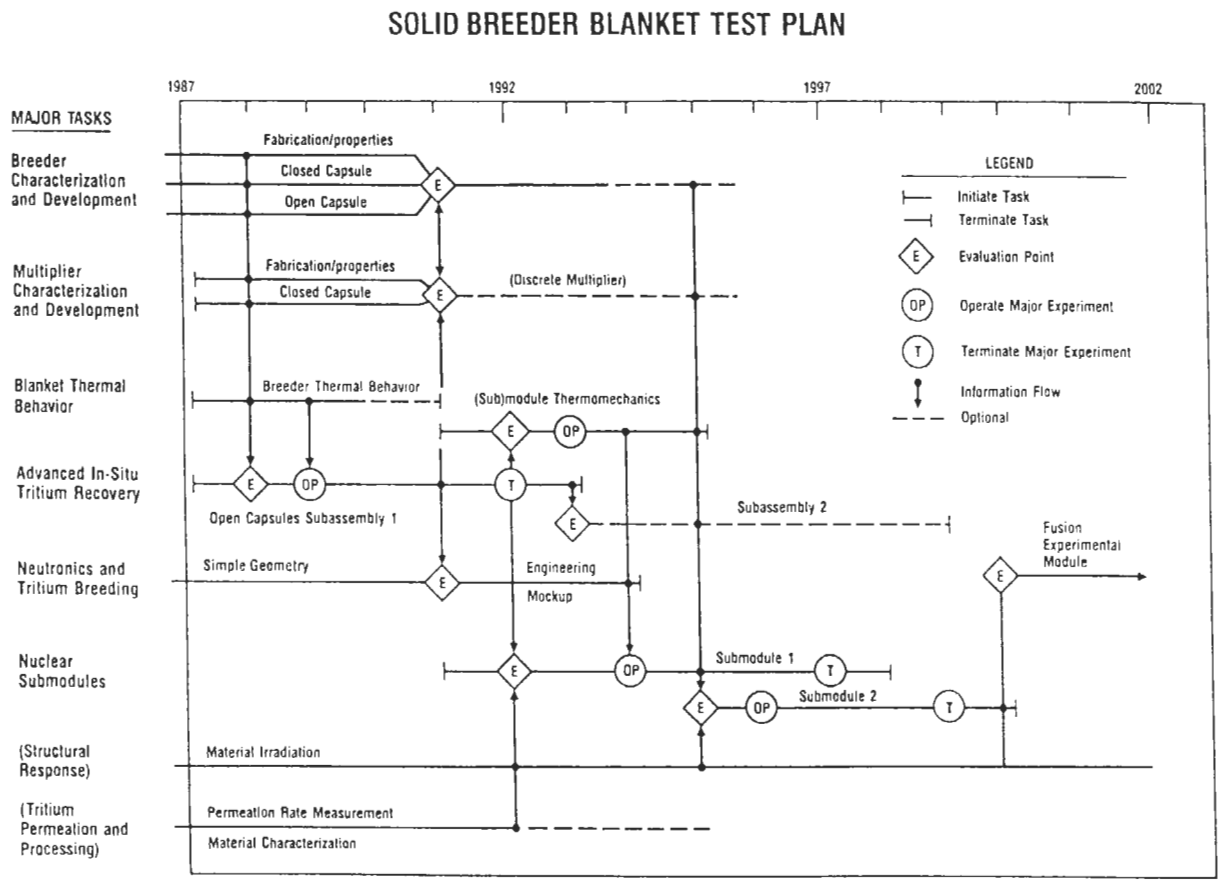

Fig. 1. Solid breeder blanket test plan.

were assembled from data taken from the literature and past experiments (see ref. [9]). The calculated performance parameters were then used to identify the more attractive solid breeder candidates and configurations, and recommendations on important areas of emphasis in near-term experiments were derived.

The capabilities of three existing fission reactors with significantly different neutron spectra also have been assessed in order to provide recommendations on the optimum facilities in which to perform future solid breeder experiments. The objective was to explore how well the three fission reactors would match tritium production and temperature profiles in macroscopic test specimens. The results are discussed in Section 2.1.2.

For liquid breeder blankets, there is not one central element in the test program. There are many issues, some of which depend strongly on the choice of materials and configuration. For the large and important class of designs, known as self-cooled liquid metal blankets (for which the breeding material also functions as the coolant), MHD effects are the dominant concern. Separate effect tests are currently planned or underway in several countries to address MHD fluid flow and pressure drop issues. An example of a current experiment is ALEX in the U.S. [10]. After ALEX and similar experiments, the need for an advanced MHD facility, called LMF1, has been identified (see fig. 2). The characteristics of this facility and the experiments which might be performed are explored in Section 2.2.

2.1. Solid breeder experiments and facilities

2.1.1. Solid breeder comparison and testing priorities

2.1.1.1. Objectives and calculation framework

Solid breeder blanket research is in a material development and selection phase which requires the consideration of a large number of potential solid breeder materials, properties, behaviors, and test conditions. A consistent comparison of the effect of solid breeder material choice on blanket attractiveness has been performed to focus the test matrix by reducing the number

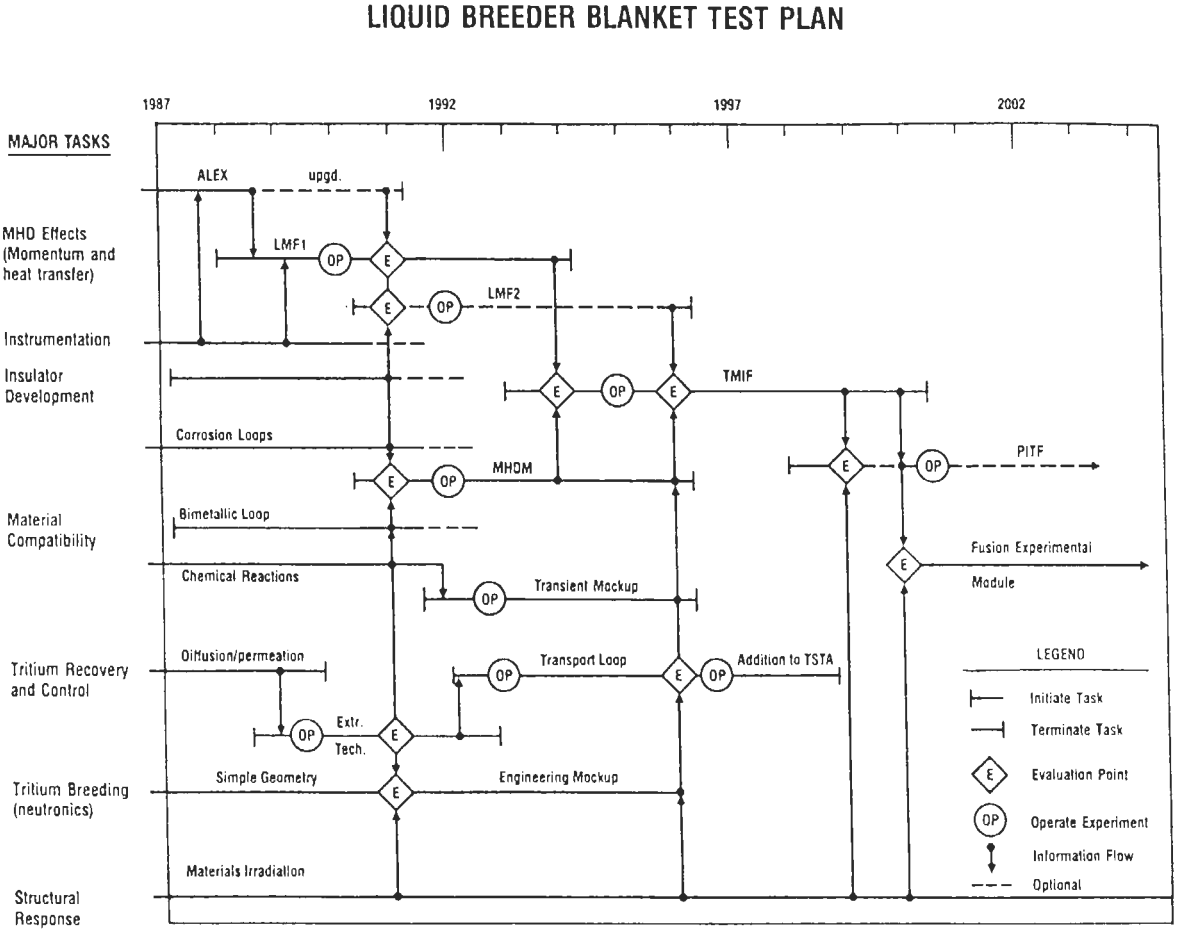

Fig. 2. Liquid breeder blanket test plan.

of solid breeder materials and configurations which need to be tested. The comparison also identifies material tests required to reduce important performance uncertainties.

Table 3 lists the seventeen solid breeder/multiplier material combinations considered in the context of a representative blanket design and compared on the basis of selected performance parameters. Except for Li_2O and Li_7Pb_2, those solid breeders are ternary ceramics. Beryllium is used as the neutron multiplier in combination with those solid breeders which may require better neutronics performance. Other multipliers (Pb and Zr_5Pb_3) have been proposed [11,12] but are not considered here. Preliminary analysis indicates that they are considerably inferior to beryllium with regard to enhancing tritium production, power multiplication and design simplicity. The low melting point of lead, the relatively poor thermophysical properties of Pb and Zr_5Pb_3, and the high energy threshold of the (n, 2n) reaction in Pb and Zr make these neutron multipliers less desirable for reactors with high neutron wall loads (> 2 MW/m^2).

Table 3
Solid breeder materials considered

Without a multiplier	Homogeneous solid breeder/multiplier mixture	With a separate Be multiplier region
(1) Li_2O	(6) $LiAlO_2$/Be	(10) Li_2O
(2) Li_2ZrO_3	(7) $LiAlO_2$/BcO	(11) $LiAlO_2$
(3) Li_8ZrO_6	(8) Li_2O/Be	(12) Li_5AlO_4
(4) $Li_2Be_2O_3$	(9) Li_2O/BeO	(13) Li_2SiO_3
(5) Li_7Pb_2		(14) Li_4SiO_4
		(15) Li_2ZrO_3
		(16) Li_8ZrO_6
		(17) Li_2TiO_3

Two configurations have been considered for incorporating the beryllium neutron multiplier in the blanket. In the first configuration, the multiplier is placed in a separate region in front of the breeder region. In the second configuration, the solid breeder and multiplier are mixed homogeneously. Analysis for the second configuration was limited to Li_2O and $LiAlO_2$. Since Be will chemically reduce the solid breeder materials (although the rate might be acceptably slow once an initial BeO layer forms), BeO is also included as an alternative for the homogeneous mixture cases.

The BCSS (Blanket Comparison and Selection Study) [13] $LiAlO_2$/He/FS/Be outboard blanket design is adopted here as a reference blanket configuration. This

Table 4
Blanket concept parameters

Parameter	Comment
Solid breeder material	As shown in table 3
Multiplier	None or beryllium or berylliumoxide
Structural material	HT9
Coolant and purge gas	Helium
Module width	0.3 m
Module length	2.0 m
Blanket depth	0.7 m to coolant plenum
Coolant plenum depth	0.2 m
Shield depth	0.3 m Fe1422
Breeder plate geometry	Wire-wrap clad plates Radial depth = 0.32 m for cases for separate multiplier cases = 0.57 m for cases without a multiplier and for homogeneous SB/M cases Plate thickness is SB-specific
Clad geometry	0.5 mm thick plate; ≃10 cm wire-wrap spacing, with 1 mm OD wires Accommodation of swelling/thermal expansion unspecified, possibly as in BCSS
Multiplier geometry	Unclad axial pins. Multiplier region radial depth is SB-specific
Coolant channel geometry	1 mm channel between solid breeder plates. Coolant flows through module perimeter and first wall, and then enters multiplier/breeder region
First wall geometry	Lobed first wall with surface grooving and internal cooled channels: total thickness = 9 mm; first wall thickness = 1.5 mm; second wall thickness = 0.5 mm; groove dimension = 7×1 mm^2; channel dimension = 7×1 mm^2
Coolant thermal-hydraulics	5.1 MPa and 275 °C inlet conditions to first wall 5.1 MPa and 332 °C at entrance to multiplier of breeder zone from first wall. Exit conditions are SB-specific Coolant flow rate 1.12 m^3/s per module (275 °C)
Breeder/multiplier thermal-hydraulics	Minimum and maximum temperature are materialspecific
Neutronics	Multiplier region thickness is SB-specific ^{6}Li enrichment is SB-specific Tritium breeding, energy multiplication rate, activation and heating profile are SB-specific
Tritium recovery	Purge flow pressure = 1 MPa Purge flow rate = 0.01 m^3/s per module (300 °C) Composition: He with 1% added H_2 Tritium inventory is SB-specific Tritium permeation rate is SB-specific
Blanket lifetime	15 MW yr/m^2, or 4 years at 75% availability

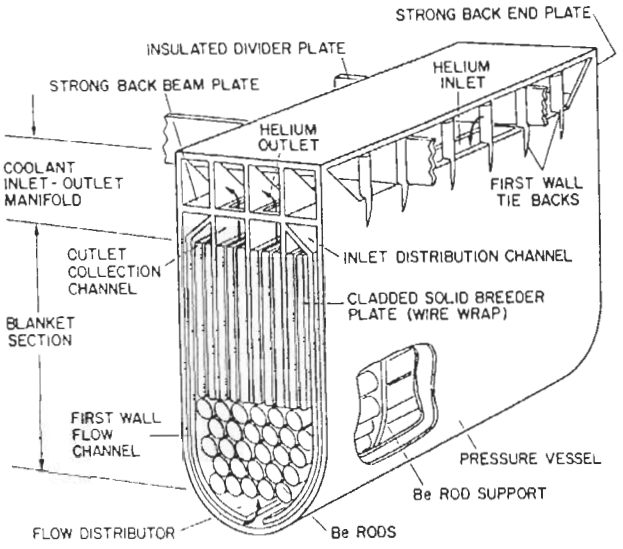

Fig. 3. Reference blanket design.

minimizes unnecessary analysis and provides a consistent blanket framework for the material comparison. However, design parameters that are affected by the choice of solid breeder (such as the plate thickness) are optimized for each particular case. The reference blanket module parameters are listed in table 4.

Table 5
Performance parameters

Neutronics
Tritium breeding ratio
Power multiplication (power generated in first wall and blanket, divided by the 14-MeV-neutron power)
Maximum Li burnup at 15 MW yr/m^2 [3 Full Power Years (FPY)]
Thermo-mechanics
Clad stress and deflection
Thermal stress in breeder
Tritium
Tritium inventory
Tritium permeation
Activation
Waste disposal rating (relative to Class C limits at 3 FPY)
Biological hazard potential (relative to maximum permissible concentration at 3 FPY)
Recycling hazard
Afterheat
Economics
Material cost (including Be)
Net thermal efficiency (including pressure drop in blanket)
Power leakage from blanket to shield

The reference blanket consists of 1125 modules with a 5 MW/m^2 neutron load at the first wall. A typical module is shown in fig. 3. The solid breeder or homogeneous solid breeder/multiplier mixture is placed in plates with a thin ferritic steel (HT9) cladding on each side. The pressure of the helium purge flow inside the plates is set at 1.0 MPa. The clad plates are wire-wrapped to provide a gap between adjacent plates for the main helium coolant flow which enters through the first wall and exists between the solid breeder plates. For the cases with a separate multiplier region, an array of multiplier rods is placed in front of the breeder plates. The thickness of the breeder plates is determined from the maximum heating rate, breeder thermal conductivity and maximum attributable breeder temperature. Since the volume fractions (and, hence, the plate thicknesses) are required for the neutronics calculations, a few iterations between the temperature and neutronics calculations are needed in each case. The ^{6}Li enrichment, the multiplier region radial thickness (for the cases with a separate multiplier region), and the ratio of solid breeder to multiplier volume fraction (for the homogeneous mixture cases), are chosen based on optimizing the tritium breeding ratio.

Blanket performance parameters were selected as a basis for the solid breeder comparison. They fall in the five general categories of neutronics, thermo-mechanics, tritium, activation, and economics, and are listed in table 5. The calculations performed for the different parameters are described in detail in ref. [9].

The results for each of these categories are summarized in table 6 and discussed below. Because of the particular importance of the tritium breeding ratio (for tritium self-sufficiency) and of the blanket tritium inventory (for safety), the results for these two parameters are discussed in more detail.

2.1.1.2. Results

Tritium breeding ratio

The tritium breeding ratio (TBR) was calculated from a one-dimensional (1-D) neutronics computer code. These 1-D neutronics calculations typically over-estimate the actual TBR by about 15–20% because of the assumptions of full coverage, fully homogeneous regions, and equal inboard and outboard blanket thickness [14]. For that reason, effective TBR values (which are assumed to be 15% lower than the 1-D TBR values) are considered in this section.

The TBR was first calculated for different values of the neutron multiplier thickness and a 60% ^{6}Li enrichment (as an initial estimate) for the separate Be multi-

Table 6
Blanket performance summary

Solid breeder	Effective TBR [a]	Power mult.	q (W/cm^3) [b]	Peak Li burnup (at%)	Gross η_{th} (%)	Power leakage (MW)	Blanket SB & M cost ($M)	Breeder total T inventory (g)	Breeder permeation rate (g T/d)	Pumping power ratio (%)	Dose rate at 1 m [c] (rem/hr g)	Afterheat time to reach T_{max} (h)
Cases without a multiplier												
Li_2O	1.08 (nat)	1.22	41.8	2.9	39.4	5.6	28	5.6	1.4	5.4	0.0029	183
Li_2ZrO_3	0.93 (29)	1.02	35.5	6.1	37.8	4.1	90	85.8	1.8	6.0	24.1	0.048
Li_8ZrO_6	0.98 (nat)	1.12	41.4	3.7	38.6	4.2	54	85.2	2.0	5.3	24.1	0.047
$Li_2Be_2O_3$	1.09 (nat)	1.31	47.6	5.4	39.7	3.4	135	552,000	2.4	4.1	0.031	56
Li_7Pb_2	1.22 (29)	1.18	33.7	5.0	39.1	14.9	110	1,590	2.9	5.6	2.64	0.024
Cases with a homogeneous SB/M mixture												
$LiAlO_2$/Be	1.51 (36)	1.51	43.9	46.8	41.4	7.1	104	230	2.2	3.1	1.86	5.4
$LiAlO_2$/BeO	1.09 (40)	1.36	43.5	35.3	40.3	6.1	96	76.5	1.3	3.6	1.27	20
Li_2O/Be	1.57 (nat)	1.52	45.9	19.5	41.2	4.7	73	8.1	2.3	3.1	0.0033	420
Li_2O/BeO	1.14 (14)	1.36	43.7	14.3	40.3	3.8	81	9.5	1.6	3.7	0.027	940
Cases with a separate Be multiplier region												
Li_2O	1.24 (20)	1.42	81.6	15.8	40.7	1.2	68	43.9	1.2	3.5	0.0029	130
$LiAlO_2$	1.09 (62)	1.39	64.9	37.8	40.4	2.5	75	36.4	1.1	3.6	7.1	2.6
Li_5AlO_4	1.17 (30)	1.40	72.6	23.2	40.6	2.5	68	23	1.9	3.3	7.1	0.51
Li_2SiO_3	1.10 (50)	1.37	68.5	31.2	40.4	2.6	78	9.6	1.7	3.4	0.14	21
Li_4SiO_4	1.14 (33)	1.38	70.0	24.9	40.5	2.5	71	9.2	1.5	3.5	0.14	2.5
Li_2ZrO_3	1.17 (58)	1.27	67.1	31.8	39.7	2.4	97	47	1.3	3.9	24.1	0.041
Li_8ZrO_6	1.22 (26)	1.34	74.6	21.2	40.3	2.1	91	45.4	1.6	3.5	24.1	0.036
Li_2TiO_3	1.12 (51)	1.39	65.5	32.9	40.6	3.2	77	4.1	1.1	3.6	5.6	5

[a] % ^{6}Li enrichment corresponding to optimum TBR is shown in parentheses; (nat) is for natural lithium (7.25% ^{6}Li).

[b] At 0.5 cm from tip of breeder plate.

[c] After 3-year irradiation and 10-hour cooling. For the separate multiplier cases, the dose rate for Be is 0.0034 rem/h g and is due entirely to impurities. For the homogeneous SB/M mixture cases, the dose rate for the multiplier (0.0034 rem/h g for Be and $\simeq$ 0.03 rem/h g for BeO) has been included in these figures.

plier cases. The general trend is that the TBR increases as the neutron multiplier thickness is increased, until saturation is reached. Consideration of the TBR incremental rate of change with increased Be thickness led to the selection of a 12-cm multiplier zone thickness (with a 0.54 volume fraction of Be at 80% theoretical density) as a reference thickness. This choice provided an optimized TBR for all the cases. For this multiplier thickness, the TBR was then calculated for different values of ^{6}Li enrichment and the results are shown in fig. 4. The TBR increases as the ^{6}Li enrichment is increased and reaches saturation at different ^{6}Li enrichment depending on the solid breeder.

Table 7 shows the ^{6}Li enrichment and the Li atom density at saturation (assumed here to correspond to 99% of the maximum TBR) for the different breeder materials. Saturation tends to occur at lower ^{6}Li enrichment as the lithium atom density of the material increases. The ^{6}Li atom densities at saturation is very close to 1.0×10^{22}/cm^3 for all the materials considered. Note that although the ^{6}Li atom density is about the same at saturation for the different cases, the TBR is different, tending to vary directly with the total Li atom density. This is mainly due to the difference in the tritium production from ^{7}Li between the different cases, and to the differences in the neutronics characteristics (e.g., slowing-down power, absorption) of nonlithium atoms present (e.g., O, Zr, Si).

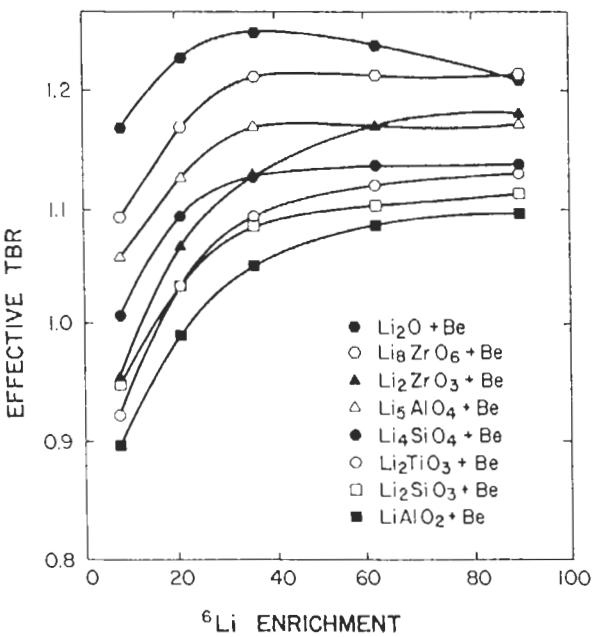

Fig. 4. Effective tritium breeding ratio as a function of ^{6}Li enrichment for the cases with a separate 12-cm thick Be multiplier region.

Table 7
^{6}Li enrichment and atom density at TBR saturation (99% of maximum TBR) for cases with a separate Be multiplier region

	Li atom density at 100% T.D. (10^{22}/cm^3)	Optimum ^{6}Li enrichment (%)	^{6}Li atom density at optimum enrichment (10^{22}/cm^3) [a]
Li_2O	8.07	20	1.02
Li_8ZrO_6	5.87	26	0.93
Li_5AlO_4	5.30	30	0.94
Li_4SiO_4	4.56	33	0.90
Li_2ZrO_3	3.25	58	1.17
Li_2SiO_3	3.36	50	1.00
Li_2TiO_3	2.84	51	0.92
$LiAlO_2$	2.33	62	0.90

[a] Based on the corresponding breeder volume fraction and 80% breeder theoretical density.

The TBR of Li_2ZrO_3 peaks later than the other materials when varying with ^{6}Li enrichment (and earlier than the other cases when varying with Be thickness). This is due to the high physical density (4.15 g/cm^3) of Li_2ZrO_3, and hence, to its relatively high Zr atom density which acts as an additional neutron multiplier.

For the cases without a multiplier, the neutron spectrum has more high energy neutrons than for the cases with a multiplier. The ^{7}Li(n, n'α)T reaction is significant at high neutron energy. Therefore, as the ^{6}Li enrichment is increased, the tritium production by ^{7}Li is decreased, which tends to have a stronger reducing effect on the total tritium production than the corresponding increase in tritium production through ^{6}Li.

For the four homogeneous breeder/multiplier mixture cases, increasing the breeder volume fraction in the mixture beyond 20% decreases the TBR. This indicates that only a small amount of breeder is required to achieve maximum tritium production. Furthermore, only a slight increase in TBR is observed when the ^{6}Li enrichment is increased, with saturation occurring fairly rapidly at about a 30% ^{6}Li enrichment. The Li_2O cases (Li_2O/Be and Li_2O/BeO) have a higher tritium production than the $LiAlO_2$ cases because the lithium atom density of Li_2O is larger than that of $LiAlO_2$. Also, the Be mixtures (Li_2O/Be and $LiAlO_2$/Be) show much larger values of TBR than the BeO mixtures (Li_2O/BeO and $LiAlO_2$/BeO) because the atom density of beryllium is 1.7 times larger than that of beryllium oxide. The 20% breeder and 80% multiplier mixture case was selected as reference because the TBR values were al-

ready high enough in all cases. Notice, however, that the high multiplier proportion in the mixture is only needed in the blanket region closest to the first wall; at deeper regions, it can be substantially reduced without significantly affecting the TBR.

The TBR results are summarized in fig. 5, which shows the optimum effective TBR for each case. To satisfy the tritium self-sufficiency criterion within the given uncertainties, the effective TBR can be ranked in different categories. Table 8 shows the risk associated with each TBR category and classifies the different solid breeder cases based on their effective TBR. Note that since the homogeneous $LiAlO_2$/Be case is in the low risk category, it is anticipated that all homogeneous mixtures of ternary ceramics (which usually have higher Li atom densities than $LiAlO_2$) with beryllium would be in the same category.

Table 8
Classification of the different solid breeder cases based on the effective tritium breeding ratio

Effective TBR range	Risk category	Cases
< 1.05	Unacceptable	Li_2ZrO_3, Li_8ZrO_6, all ternary ceramics without a multiplier element
1.05–1.10	High risk	Li_2O, $Li_2Be_2O_3$, $LiAlO_2$ + Be, $LiAlO_2$/BeO
1.10–1.20	Medium risk	Li_7Pb_2, Li_2SiO_3 + Be, Li_2TiO_3 + Be, Li_4SiO_4 + Be, Li_5AlO_4 + Be, Li_2ZrO_3 + Be, Li_2O/BeO
> 1.20	Low risk	Li_8ZrO_6 + Be, Li_2O + Be, all solid breeder/Be homogeneous mixtures

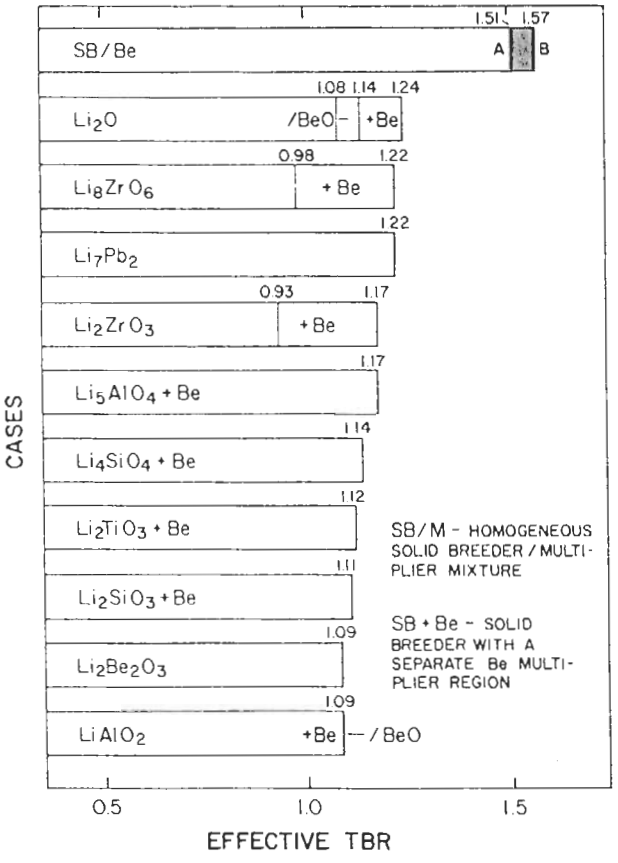

Fig. 5. Effective tritium breeding ratio for the different cases. For the cases with the solid breeder/beryllium homogeneous mixture, A and B are the lower and upper limits represented by the $LiAlO_2$/Be and Li_2O/Be cases, respectively.

The general conclusions that can be made from the TBR results are that:

(1) all solid breeders require a separate neutron multiplier except for Li_7Pb_2 and possibly Li_2O and $Li_2Be_2O_3$;
(2) the homogeneous SB/Be cases show exceptional neutronics performance;
(3) Be exhibits a much superior performance than BeO as a neutron multiplier; and
(4) Li_2O is the most attractive solid breeder candidate, showing the highest TBR for the unmultiplied, separate multiplier and homogeneous SB/M cases.

These particular results are based on one assumed blanket configuration, but it is not expected that different designs (e.g., solid breeder pins rather than plates or breeder out of tube) would significantly affect the relative solid breeder TBR performance. Similarly, the choice of coolant is not expected to affect the relative rankings. One particular configuration, however, might be an exception. It involves placement of a thin layer of breeder in front of the multiplier to absorb backscattered neutrons in ^6Li (and also reduce first wall activation). Calculations were done for two cases, one exhibiting a high TBR (Li_8ZrO_6) and the other a low TBR ($LiAlO_2$), to determine if the neutronics results were design-dependent, favoring a particular solid breeder material over another. The TBR was calculated for different values of the front breeder region thickness, ranging from 0.2 cm to 4 cm (with a 0.54 volume fraction of 80% dense solid breeder). The back breeder

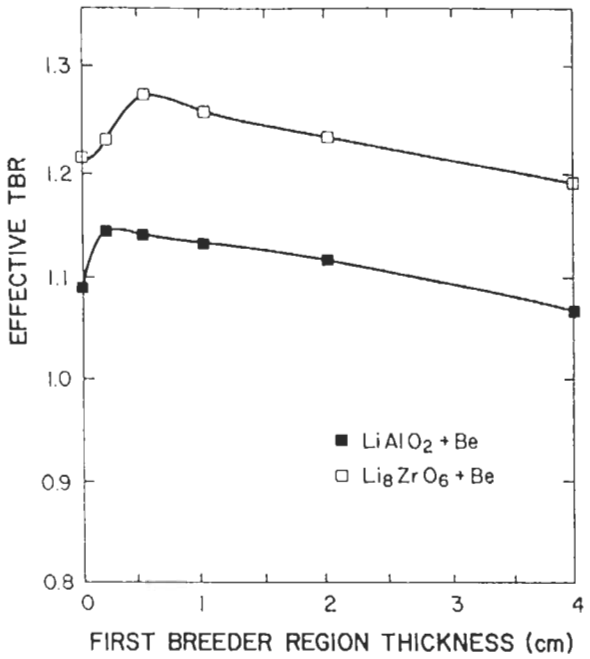

Fig. 6. Effective tritium breeding ratio as a function of the first breeder region thickness for two sandwich cases (both with 60% ^{6}Li enrichment).

region thickness was adjusted to keep the total breeder thickness the same as before and the ^{5}Li enrichment was set at 60%.

As shown in fig. 6, adding a thin breeder zone in front of the multiplier zone increases the tritium breeding in a similar way up to a certain thickness for both $LiAlO_2$ and Li_8ZrO_6. Qualitatively, too little front breeder does not capture the reflected neutrons, while too much scatters the incident neutrons and reduces the Be (n,2n) reaction rate, which explains the shape of the TBR curve in the figure. The maximum increase in TBR is about 0.05, corresponding to an equivalent 100% dense breeder region thickness of 0.13 to 0.2 cm. However, the corresponding peak heating rate in the breeder front region is very high – of the order of 150 MW/m^3. The other solid breeder materials are expected to show similar behavior and, thus, this choice of configuration does not affect the relative TBR solid breeder rankings.

Power multiplication

The power multiplication, M, corresponding to each optimum TBR case, is shown in table 6. The M results for different cases with the same configuration and multiplier (if present) tend to fall in the same range. The notable exceptions are the cases with Li_2ZrO_3, Li_8ZrO_6 and Li_7Pb_2 which exhibit lower power multiplications mainly due to the endothermic (n, 2n) reactions associated with their multiplier elements (Zr and Pb).

Note that the TBR and M results are rather insensitive to small changes in the volume fractions. For example, changing the breeder volume fraction from 0.70 to 0.75 in the case of Li_4SiO_4 + Be does not change the power multiplication (1.37) and only decreases the 1-D TBR from 1.35 to 1.34. Again, this indicates that the relative solid breeder behavior is fairly independent of the specific design configuration.

Peak heating

Table 6 shows that the separate-multiplier cases have higher peak heating values (q) than the other cases. For example, Li_2O with a separate multiplier has a 81.6 W/cm^3 peak heating value, while Li_2O/Be in the homogeneous mixture case and unmultiplied Li_2O only show 45.9 and 41.9 W/cm^3 values, respectively. It is interesting to note that the peak heating rate tends to increase with the Li atom density, as is indicated in particular in the cases with a separate multiplier. These peak heating rates constrain the size of the breeder plates, and hence the breeder volume fraction. However, as noted earlier, the TBR and M results are not strongly affected by small changes in the breeder volume fraction. Consequently, the heating rates are not expected to strongly affect the solid breeder comparison.

Peak lithium burnup

The peak lithium burnup due to tritium-producing reactions (which constitute 99% or more of lithium burnup), was calculated at 0.5 cm from the tip of the solid breeder plate and is shown in table 6 for each case. The peak burnup is high for the three cases involving $LiAlO_2$ with a multiplier, with the homogeneous $LiAlO_2$/Be case exhibiting the highest burnup (46.8 at%). This is due to the high volume fraction of Be needed at the front of the SB/M region, which means that the amount of Li is small and the burnup fraction is high.

The cases without a multiplier have lower values of burnup, with Li_2O showing the lowest value (2.9 at%). This difference is due to the lower-energy secondary neutrons produced by the multiplier which react with ^{6}Li in the front section of the breeder to produce high burnups. It can also be observed that the burnup fraction is generally higher for the cases with lower lithium atom density. Consequently, a breeder material ranking based on the least burnup tends to be the same as the ranking based on the highest TBR, since both are directly dependent on the Li atom density. Although concern exists about the possibility of high burnups affecting the material chemical composition and compa-

tibility at the tip of the breeder section, it is not clear yet how important this is as a criterion for comparing solid breeder materials. In general, it seems reasonable to assume that lower values of peak burnup are more attractive than higher values. The average burnup, which has not been calculated for this study, could also be an important factor, particularly in connection with its effect on tritium inventory.

Clad stress and deflection

As part of the thermo-mechanics calculations, the stresses in the clad and the clad deflection caused by the breeder total volumetric expansion (thermal expansion + swelling) were estimated for four cases for which swelling data after fast irradiation to 10^{27} captures/m^3 were available: Li_2O, $LiAlO_2$, Li_2ZrO_3 and Li_4SiO_4. The expansion was assumed to be fully relieved by deflection of the clad side walls. This may be most applicable to the spherepac form. It was found that the stresses in the clad were well within the clad maximum allowable stress. However, the clad deflection tended to be large relative to the 1 mm thickness of the gap (coolant channel) between adjacent solid breeder plates. For example, for the Li_2O case which exhibits the largest total volume expansion (about 13%), the clad deflection is on the order of 1.5 mm for each plate. In this respect, Li_2O is unattractive, Li_4SiO_4 (6.7% total volumetric expansion) is marginal, and $LiAlO_2$ and Li_2ZrO_3 (3.6% and 2.6% total volumetric expansion, respectively) are acceptable. However, if a means for expansion is provided, such as a bellow-type arrangement at the plate ends or extra porosity, then the importance of this expansion for differentiating between the different solid breeder materials will be diminished.

Note that the corresponding stresses on the solid breeder sphere-pac material were also calculated and found to be significantly lower than the solid breeder fracture stress.

Breeder thermal stress

The thermal stresses for the solid breeder in sintered block form were also estimated. The plate temperature distribution was first calculated by solving the 2-D heat conduction equation (with the neutron heat generation as source term) by means of a finite difference technique. The stresses were found to be several times higher than the allowable fracture strength (which is on the order of 50 MPa and 70 MPa for Li_2O and $LiAlO_2$, respectively). In order for the thermal stress not to exceed the fracture stress, 2-D calculations show that the maximum plate thickness needs to be less than 0.5 mm for $LiAlO_2$ and Li_2O. This shows the disadvantage of using the sintered block form, as extensive stress-induced cracking will occur affecting the temperature distribution and the tritium inventory. Consequently, the test program should investigate conditions with substantial temperature gradients to reproduce this cracking, and/or consider sphere-pac material.

Tritium inventory

The tritium inventory in the solid breeder and multiplier was calculated as the sum of diffusion, solubility and surface adsorption components. Details about the property data (which have uncertainties ranging from a factor of 2 to a factor of 100) and about the calculations can be found in ref. [9]. In general, swamping the purge flow with hydrogen will drastically reduce the adsorbed and dissolved tritium [15]. Here, it is assumed that the tritium solubility and surface adsorption inventories are reduced to 1% of the possible inventory due to the inclusion of hydrogen in the purge flow at a ratio of 100 : 1 relative to the tritium.

The three components of the tritium inventory are strongly dependent on temperature. Consequently, the tritium diffusive, solubility and surface adsorption inventories were determined based on numerically integrating the inventories over the 2-D temperature and tritium generation rate profiles in the plate. The total inventory for each material is shown in table 6 (based on average property values).

The tritium inventory results should be interpreted carefully because of the huge ranges of uncertainty, which clearly points to the need for obtaining more precise experimental property data. $Li_2Be_2O_3$, with an average diffusive inventory of 550 kg per blanket, is evidently unattractive, assuming the BeO-like tritium diffusion used in the absence of any data is correct. Li_7Pb_2 also has a high inventory (due to tritium solubility) and so does $LiAlO_2$/Be (due to diffusion). Apart from these, it is hard to differentiate between the other cases within the uncertainty range. Except for the $LiAlO_2$ cases, where the diffusive inventory is significant, and for the Li_7Pb_2 and Li_2O cases, where the solubility inventory is dominant, the total inventory for all the other cases consists mainly of the surface adsorption component. By further increasing the isotope swamping of the purge flow, these surface adsorption inventories could be further reduced beyond the 0.01 factor already used. This indicates the need for further experimental data related to the adsorption mechanism and to the effect of isotope swamping. The effect of large protium additions on tritium permeation and tritium recovery must also be considered in a blanket design context.

There are many uncertainties in the properties and design that can affect the tritium inventory indirectly. Analyses were performed to determine the effect on the tritium inventory of: (1) using a temperature dependent instead of constant thermal conductivity; (2) including the size variation of the breeder grains; and (3) inserting a helium-filled gap near the tip of the plate, assuming a sintered block form. It was found that the tritium inventory was increased in the three cases (by up to about 25%, 12% and 50%, respectively), but the magnitude of the increase is small compared to the uncertainties in the solid breeder tritium-related property data.

The diffusive inventory in the multiplier was also estimated. For Be, the inventory is very low both for the separate region case and for the homogeneous case (about 10^{-8} g per blanket). For BeO, however, the inventory is high (about 8 kg per blanket) and does not reach equilibrium during the blanket life.

Tritium permeation

The permeation rate of tritium from the solid breeder to the coolant is a function of the tritium form and partial pressure, and the cladding area, thickness and temperature. Furthermore, H_2 addition to the purge effectively forces the released tritium into the HT form, and the addition of H_2 at 100 : 1 (H : T) is assumed here for the reference blanket. The permeability estimated for HT9 clad material and an oxide barrier factor of 100 is uncertain by about an order of magnitude, primarily because of the uncertainty in the surface conditions and associated barrier factor.

From table 6, the resulting permeation rates from the solid breeder into the helium coolant are about 1–3 g/d for a 1.6 GWe reactor, similar to the 2 g/d estimated for the BCSS $LiAlO_2$/He/Be blanket [13]. Thus, the effect of solid breeder choice is roughly a factor of three (due to differences in the breeder temperature limits and thermal conductivity) which, given the uncertainties in the permeation coefficient and barrier factor (a factor of ten), is probably not significant. Tritium is also produced in the multiplier at about 1% of its production rate in the solid breeder, or 7.5 g T/d in a 5.4 GWth reactor. For mixed breeder/multiplier materials, the additional tritium would not affect the tritium permeation. If the multiplier is separate and unclad, however, this tritium will eventually permeate into the coolant and would dominate over any tritium permeating through the breeder cladding, regardless of the solid breeder material. Such a permeation rate into the coolant may be unacceptably large, and require cladding on the multiplier.

Activation

The activation of different solid breeder materials (including presumed impurities listed in ref. [9]) was calculated for two different spectra, one with a beryllium multiplier and one without. Also calculated for the former case was the activation of the beryllium multiplier. The fluxes used in the calculation correspond to the front of the breeder region (near the first wall). It was found that the results were approximately similar for both spectra.

The results include the dose rate (which gives an indication of the recycling hazard), the Biological Hazard Potential after 3-year irradiation and 10-hour cooling (as a measure of accidental release hazard) and the Class C waste disposal limit after 3-year irradiation and 10-year cooling (as an indication of waste disposal hazard). The dose rate is chosen to represent activation because it is least dependent on impurities, and impurities can, in principle, be removed (at a cost). The dose rates for the different solid breeder cases are shown in table 6. The zirconates and Li_7Pb_2 are the least attractive based on this criterion, the aluminates are marginal, while the oxide, beryllate and silicates (to a lesser extent) are attractive.

Afterheat

Decay heat values, one hour after shutdown, were calculated by assuming that the only contributions were from products of the primary elements. Contributions from products of impurity elements were ignored. They were then used in combination with the average steady-state temperature at the tip of the solid breeder plate, the maximum allowable temperature (usually based on the sintering limit) of the solid breeder and the solid breeder heat capacity to obtain the time to reach the maximum allowable temperature after shutdown under adiabatic conditions.

The results, shown in table 6, indicate that Li_2O and $Li_2Be_2O_3$ are very attractive (with times of 7.6 and 2.3 days, respectively) and, to a lesser extent, so are the silicates (with times of the order of 1 day). Li_2TiO_3, $LiAlO_2$, and possibly Li_5AlO_4 are adequate (with times of 5, 2.5 and 0.5 hours, respectively). However, the two zirconates and Li_7Pb_2 show times of about 1.5–3 minutes to reach the maximum temperature. If a loss of coolant accident occurs, this leaves very little time for corrective action before the solid breeder is irreversibly damaged. Again, these results are based on activation of the primary constituents, and are not determined by assumed impurities. The time parameter considered here is important in developing inherently safe blankets, particularly as it relates to protection of investment.

Material costs

Material unit costs were estimated to compare the fabrication costs for blankets containing the various breeder and multiplier materials [9]. The highest unit costs are for beryllium and for ^{6}Li enrichment at \$400/kg Be and \$1500/kg ^{6}Li. Table 6 lists the cost per blanket (1125 modules) for each case.

For the four homogeneous (20/80) breeder/multiplier mixture cases, the homogeneous mixture is assumed to be contained in the first 20 cm of breeder region, with breeder only in a second 37 cm breeder region. This reduces the amount of expensive beryllium while the decrease in TBR is acceptable (the effective tritium breeding ratio is reduced from 1.59 to 1.49 for the Li_2O/Be case and from 1.53 to 1.35 for $LiAlO_2$/Be).

The highest costs are for $Li_2Be_2O_3$ and Li_7Pb_2, with most of the other cases showing multiplier and breeder material costs between about \$67.5 million to \$107 million for the blanket module. The cost for the unmultiplied Li_2O case, however, is appreciably lower than those of all the other cases (\$28 million for the blanket), making unmultiplied Li_2O quite attractive on this basis. Note, however, that the solid breeder and multiplier costs are typically only about $< 5\%$ of the total commercial reactor cost.

Thermal efficiency and pumping power

The thermal efficiency, η_{th}, of the steam cycle was calculated from the helium main flow bulk temperature at the exit of the blanket (obtained from the mass flow rate, fusion power and multiplication factor). The steam cycle was based on the one described in ref. [16] with a temperature of 311 K in the condenser. For this cycle, η_{th} was found to be 68% of the ideal Carnot efficiency.

For the pumping power calculations, both the pressure drop across the multiplier region (if applicable) and the pressure drop across the breeder plates were considered. Estimates for the pressure drop in the helium circuit outside the breeder were obtained from ref. [13]. The other components include the inlet manifold, distribution channel, the side flow path, the grooved first wall, the collection channel, and the outlet manifold, with a combined 48 kPa pressure drop.

The pressure drop across the breeder region and multiplier regions were calculated from expressions for the relevant geometry and flow rates given in ref. [17]. The pressure drop calculations were made under the assumption of constant mass flow rate for all the different solid breeder cases. This maintained the same first wall conditions for this particular blanket design. However, one should be cautious not to generalize these results to other designs.

The cycle thermal efficiency and pressure drop results are summarized in table 6. The total pressure drop has been converted to a pumping power ratio (PPR), which is equivalent to the pumping power required divided by the electric power generated by the heat transported out of the blanket by the helium. The gross thermal efficiency can be seen to vary from 37.8% for the unmultiplied Li_2ZrO_3 case to 41.3% for the $LiAlO_2$ homogeneous mixture case. Apart from the unmultiplied Li_2ZrO_3 case, all the cases have thermal efficiencies within 3 percentage points. The main coolant pumping power ratio tends to vary inversely to the thermal efficiency, and shows a maximum of 6% for the unmultiplied Li_2ZrO_3 case and a minimum of 3.1% for the $LiAlO_2$ homogeneous case. However, the variation is mostly due to the number of plates in the design; the fewer the plates, the fewer the channels and the larger the pumping power for a given mass flow rate. The mass flow rate here is fixed by the first wall design. For blankets where the coolant does not initially flow through the first wall, the PPR could be changed. Also, since the neutronics are rather insensitive to small changes in the breeder volume fraction, it is conceivable that a fixed number of plates of the same size be used for all the cases, which will then have essentially the same pumping power requirements.

Power leakage

From the neutron flux spectrum and the neutron energy at the back of the 30-cm reflector, the power leakage was calculated. This criterion can be important for space-limited reactors since higher power leakage implies the need for additional shielding, leading to larger reactor size and cost. A factor of 2 to 3 increase in power leakage typically requires about an additional 5 cm shield thickness. However, the importance of the power leakage can be minimized in a tokamak-type reactor by limiting this additional shield increase to the outboard region where space is less restricted. On the inboard region, where space is critical, the blanket thickness can be reduced by a few centimeters without a serious reduction in the tritium breeding ratio. From the results shown in table 6, Li_7Pb_2, with the highest leakage power (about 14.9 MW for the whole blanket), is certainly less attractive than the other solid breeders. The values for the other cases all fall within the range 1.2 to 7.1 MW for the whole blanket, with Li_2O showing the lowest value.

2.1.1.3. Conclusions and R&D priorities

The performance parameters considered are not of equal importance. TBR is the most important parame-

ter since tritium self-sufficiency is a requirement. Safety concerns dictate that the tritium inventory is also of high importance. However, the magnitude of the uncertainties in the tritium related property data tends to make a comparison between the different cases difficult. Other important parameters include activation, afterheat, power multiplication and material cost. The dose rate after 3-year irradiation and 10-hour cooling, which gives an indication of the recycling hazard, is the activation parameter considered here. The time to reach the maximum allowable temperature after shutdown with no coolant flow (calculated from the decay heat) is also an important parameter. It indicates how much time is available to restart the cooling system in case of accidental shutdown, without damaging and having to replace the solid breeder and/or multiplier. Power multiplication and material cost are included here as the key power and economic parameters. Note that the relative (and even absolute in some cases) values of these parameters for the different solid breeder materials tend to be independent of the geometric details of the design. An important performance parameter not considered here is the compatibility of the breeder with the structure.

These six major parameters of importance can be classified in pairs based on the indications that they give about tritium (TBR and tritium inventory), economics (power multiplication and material cost), and safety (dose rate and afterheat time to reach the maximum allowable breeder temperature). Graphical representations of the comparison of the various cases based on these three pairs of major parameters are illustrated in the point graphs shown in figs. 7 (effective TBR and reciprocal of the tritium inventory), 8 (reciprocal of material cost and power multiplication), and 9 (after heat time to attain the maximum allowable material temperature and reciprocal of dose rate). The reciprocal form for specific variables is chosen such that the more attractive cases will appear in the top right hand corner of each figure.

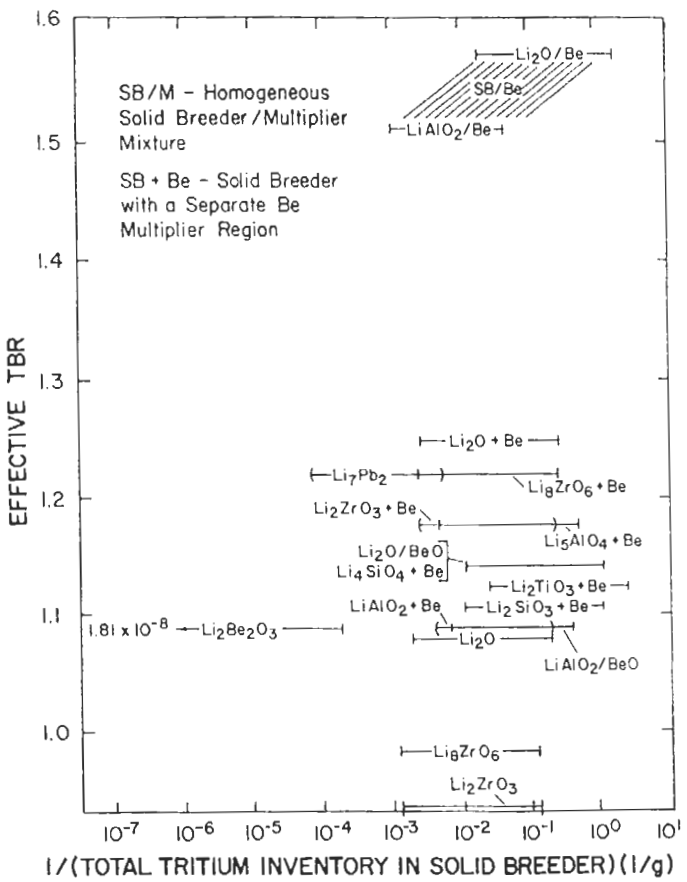

Fig. 7. Point graph of the effective tritium breeding ratio and of the reciprocal of the total tritium inventory for the different cases.

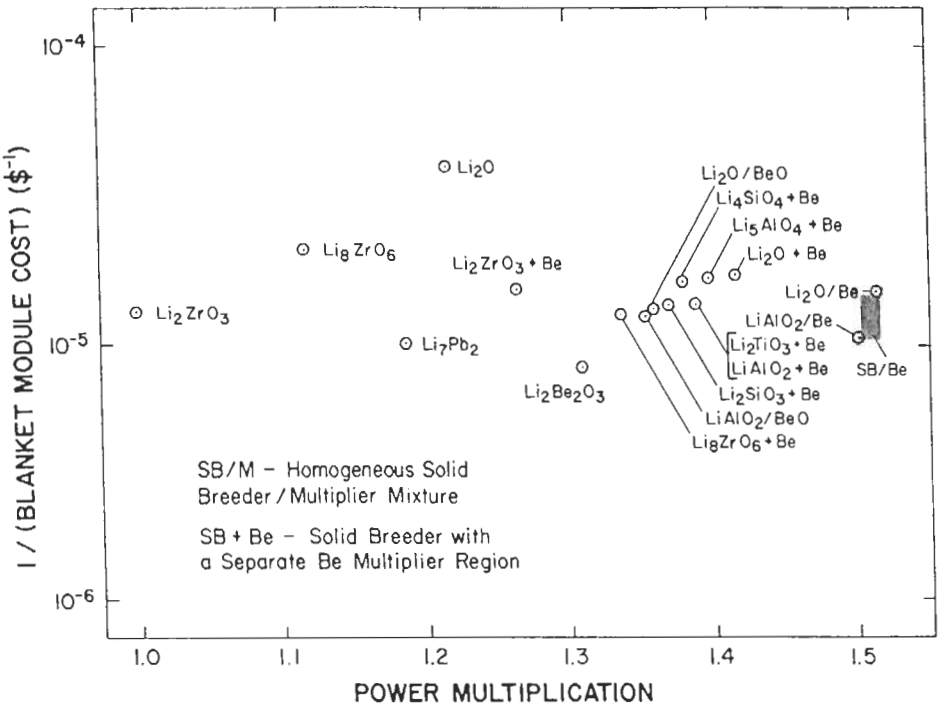

Fig. 8. Point graph of the reciprocal of material cost and of power multiplication for the different cases.

Based on the study and, in particular, on the results illustrated in figs. 7–9, the following general conclusions can be made:

(1) A neutron multiplier is needed for all solid breeders, except possibly for Li_2O, which has a marginal chance of satisfying the tritium self-sufficiency criterion without a multiplier. (Note that Li_7Pb_2 and $Li_2Be_2O_3$ are considered as multiplied here because of their neutron multiplier components, lead and beryllium, respectively).

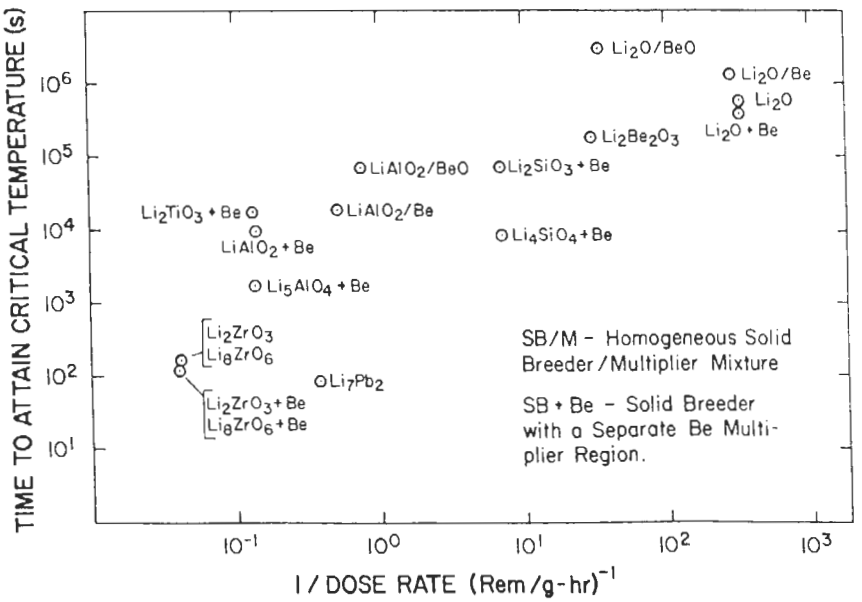

Fig. 9. Point graph of the afterheat time to reach the maximum allowable temperature and of the reciprocal of the dose rate after 3-year irradiation and 10-hour cooling for the different cases.

(2) Based on optimized neutronics performance, a homogeneous mixture of beryllium and solid breeder is superior to separate beryllium and solid breeder regions.
(3) Beryllium is superior to BeO in terms of improvement of tritium breeding and energy production. BeO is also unattractive based on its high tritium diffusive inventory.
(4) Even if Li_2O requires the use of a multiplier, the Li_2O and beryllium combination remains more attractive than all ternary ceramic and beryllium combinations in terms of achievable tritium breeding ratio and power multiplication.
(5) Among the ternary ceramics, the Li_4SiO_4 and Li_2SiO_3 (to a lesser extent) appear to be the most attractive. They result in the least activation and their tritium breeding ratio and energy multiplication are virtually as good or better than other ternary ceramics.
(6) $Li_2Be_2O_3$ does not appear attractive because of its relatively high tritium diffusive inventory (assuming BeO-like tritium diffusion) and its marginal tritium breeding ratio. While Li_7Pb_2 shows reasonable tritium breeding, it results in lower energy multiplication and higher tritium inventory, which, combined with its limited operating temperature range, does not make it particularly attractive.

With regard to the near-term experimental program for solid breeders, it is recommended that the following be emphasized:

(1) *Materials*: Li_2O without a neutron multiplier, and Li_2O, Li_4SiO_4, and Li_2SiO_3 with beryllium. $LiAlO_2$ should also be considered because of its attractiveness in the material stability and compatibility areas, which have not been considered in this study.
(2) *Configurations*: Homogeneous mixtures of beryllium and solid breeder, and sphere-pac solid breeder are seen as attractive. Since the homogeneous mixture is attractive from many aspects, problems related to such a configuration, e.g., chemical stability and tritium release, should be experimentally investigated. In addition, neutronics integral experiments should include homogeneous configurations. These tests should be done in addition to the tests on the more conventional configuration with separate breeder and multiplier regions.
(3) *Properties*: The uncertainties in tritium-related properties are particularly large and important for designs as well as breeder comparisons.
(4) *Test conditions*: A better understanding of lithium burnup is needed to clarify its importance and to accurately define the maximum allowable burnup limits. Tests should also include temperature gradients to determine the importance of cracking and/or breeder mass transfer.

2.1.2. Fission reactor evaluation for advanced solid breeder testing

2.1.2.1. Objectives

The major advantage of fission reactor testing is the ability to provide a neutron flux over a moderately large test volume prior to the availability of a higher power DT fusion device. In earlier work, specific requirements were identified for fission reactor facilities used for advanced solid breeder testing: sufficient flux, suitable spectrum, on-line instrumentation capability, and adequate test volume [18,19].

The ability of fission reactor testing to match anticipated fusion-relevant conditions has been evaluated, based on a comparison of tritium production and heat generation rates from microscopic calculations [2,20]. Here, the objective is to explore and compare the testing capability of various fission reactors to match these tritium production and temperature profiles which are anticipated in test elements with sufficient size to address advanced solid breeder performance issues. These include cracking under thermal stress, differential swelling, global tritium transport, internal mass transfer, purge flow distribution and temperature predictability. To accomplish this, representative reactors with significantly different neutron spectra were considered. Selected solid breeder cylindrical geometries and sizes were considered, as were various ^6Li enrichments. Results were calculated for Li_2O, but could be extrapolated to other breeder materials. Tritium production and neutron heating rate profiles, temperature gradients, and time dependent tritium production rate distributions were calculated.

2.1.2.2. Representative reactor conditions

Three test fission reactors were chosen for investigation: The Fast Flux Test Facility (FFTF) at Hanford, the High Flux Isotope Reactor (HFIR) at Oak Ridge, and the National Reactor Universal (NRU) at Chalk River, Canada. These reactors have different neutron spectra, as shown in table 9 and fig. 10 (where the relative neutron energy spectra are normalized by the total neutron flux).

The FFTF reactor is a fast neutron spectrum source. Other reactors in this class include: EBR-II (USA), JOYO (Japan), Phenix/SuperPhenix (France), and KNK (Germany). The FFTF was designed for testing and has in-core instrumentation capabilities. It runs

Table 9
Fission reactor capabilities and characteristics

Reactor	Reactor power (MWth)	Flux ($\times 10^{15}$ n/cm^2 s)		Core materials (structure/fuel/coolant)
		Thermal	Fast	
FFTF	300–400	small	4.3	316-SS/UO_2/Na
HFIR	100	2.3	1.5	SS/UO_2/H_2O
NRU	125	0.24	0.04	Zr/UO_2/D_2O

with typical cycle lengths of 60–150 days. The largest available position for instrumented testing is a hexagonal position measuring 12 cm flat-to-flat. The axial length of the core region is 91.4 cm. The space above the core region could also be utilized for testing if desired. The flux and energy spectrum chosen are for a row four position at the core midplane.

HFIR is a water-cooled reactor which has a softer neutron energy spectrum when compared to the liquid metal reactors. It is presently having its instrumentation capabilities increased through refitting. The HFIR runs with typical cycle lengths of 21–23 days. The largest available position for instrumented testing at present is a circular position measuring 3.7 cm in diameter. The axial length of the core region is 51 cm.

The NRU reactor is a water-cooled thermal reactor with a relatively modest non-thermal component of its neutron flux. Other reactors of this class include: ATR (USA), JMTR (Japan), and SILOE (France). The NRU reactor can accommodate instrumented in-core tests. It runs with typical cycle lengths of 14–30 days. The largest available position for instrumented testing would be a cylindrical position with a diameter of 10 cm. The axial length of the core is 300 cm. The selected flux and energy spectra are for a spectrally tailored position within the core chosen to optimize the relative fast component of the neutron energy spectrum from NRU.

2.1.2.3. Calculations and results

Details of the cylindrical test assembly model are shown in fig. 11. Specifically, each cylindrical test specimen consists of a solid or annular pellet which is surrounded by a stainless steel jacket. A gas gap (for temperature control) is included between this first stainless steel jacket and the second jacket which serves as a boundary between the reactor environment and the test configuration. The calculational models for FFTF, HFIR and NRU are described in table 10. The Li_2O regions were divided into five equal volume zones to enable spatial distributions through the pins to be computed using the MCNP Monte Carlo program. The calculations were done for a neutron source applied at the outer boundary of each model.

The model has several limitations. The calculations do not consider the incident photon flux. Therefore, the total heating rates in the test specimen will be somewhat higher (by about 10%) than reported here, and the

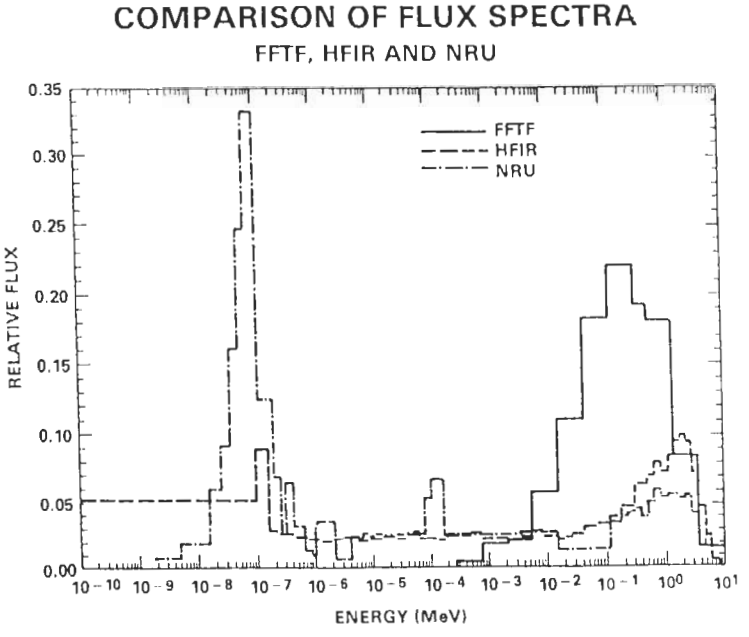

Fig. 10. Comparison of neutron flux spectra for the FFTF, NRU and HFIR reactors normalized to their total flux.

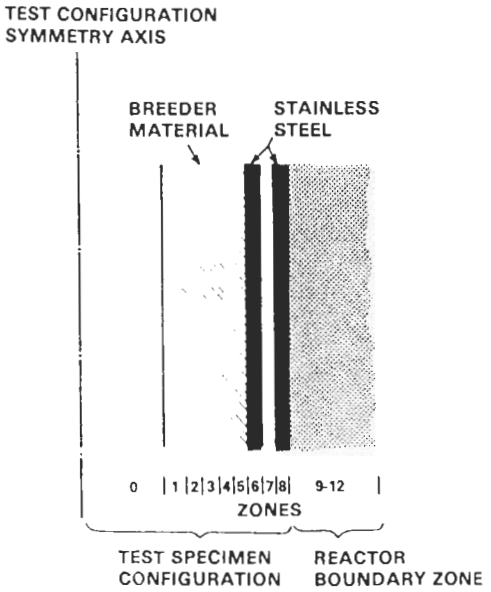

Fig. 11. Schematic of one-dimensional model used to calculate tritium production and heat generation rates in fission reactors. The zones in the figure are for an annular test specimen in the FFTF reactor.

spatial distribution of this component will be different from the neutron heating profile. The model assumes that the incident flux and spectrum at the boundary of the test specimen are not perturbed by the presence of the solid breeder material. Thus, the comparison of the absolute values for the calculated parameters between the different reactor types should be viewed as approximate. Finally, the model cannot address the impact of the solid breeder test upon the reactivity of the reactor. This could limit the quantity of ^{6}Li in a given test reactor. The effect on reactor reactivity was considered in earlier FINESSE effort [1].

Results for the FFTF reactor show that the total flux decreases by ~15% at the center of the test specimen configuration when the ^{6}Li-enrichment is increased from 7.5% to 80%. The integrated neutron heating rate within the Li_2O increases from 158 to 891 W/cm of axial length. Also, the integral tritium production rate increases from 1.3×10^{14} to 1.05×10^{15} T/s/cm of axial length. Note that the tritium production rate increases when the ^{6}Li-enrichment is increased from 7.5% to 80% but the increase is 27% lower than anticipated by linearly interpolating from the 7.5% ^{6}Li-enrichment value. This result suggests that while the total neutron flux suppression was only ~15%, the larger suppression in the tritium production rate is due to the preferential absorption of the lower energy neutrons (self shielding) at the outer region of the highly enriched Li_2O. The radial gradients for both the tritium production and heating rates within the solid breeder material were very modest, even for the 2.54 cm diameter pellet for FFTF testing.

Table 10
Calculational models for HFIR and NRU and FFTF

Zone	Outer radius (cm)	FFTF	HFIR	NRU
0–8	1.487	Li_2O Test Specimen		
9	2.120	36% SS/64% Na	H_2O	H_2O
10	2.730	36% SS/64% Na	H_2O	Zr
11	3.240	36% SS/64% Na	H_2O	H_2O
12	6.335	36% SS/64% Na		

The HFIR results indicate that the neutron heating and tritium production rates are almost an order of magnitude higher than FFTF for a given enrichment although the absolute incident flux at the specimen boundary (source) is comparable to the FFTF case, as shown in table 9. The NRU results, however, show rates comparable to FFTF although, from table 9, the NRU absolute flux is an order of magnitude lower than that of FFTF. Apart from this, the HFIR and NRU results show similar behavior. In both cases, neither the neutron heating nor the tritium production rates increase linearly with ^{6}Li-enrichment. This is due to the self-shielding occurring in test specimens of this size. The ratio of the neutron heating to the tritium production rates are fairly constant in both cases, which implies that the neutron heating contribution from elastic and inelastic scattering is relatively small. Also, the radial gradients for both heating and tritium production rates become quite large for ^{6}Li-enrichments greater than 0.5%. The same behavior is found for the annular pellet test geometry, with the integrated neutron heating and tritium production rates being only slightly smaller than for the solid pellet.

The neutron heating rates were transformed into temperature profiles based on the following test assumptions: (1) the temperature of the outer radius of the Li_2O pellet was maintained at 400 °C; (2) the center temperature for the pellet, or inner radius temperature, reached steady state; (3) all heat transfer occurred radially; and (4) the heat transfer coefficient was independent of temperature. The temperature profiles were then calculated using curves interpolated through the calculated heat generation rates for each of the five zones in the solid pellet cases. The results show that both the NRU and FFTF have an acceptable peak temperature for a 2.54 cm diameter pellet, with maximum tempera-

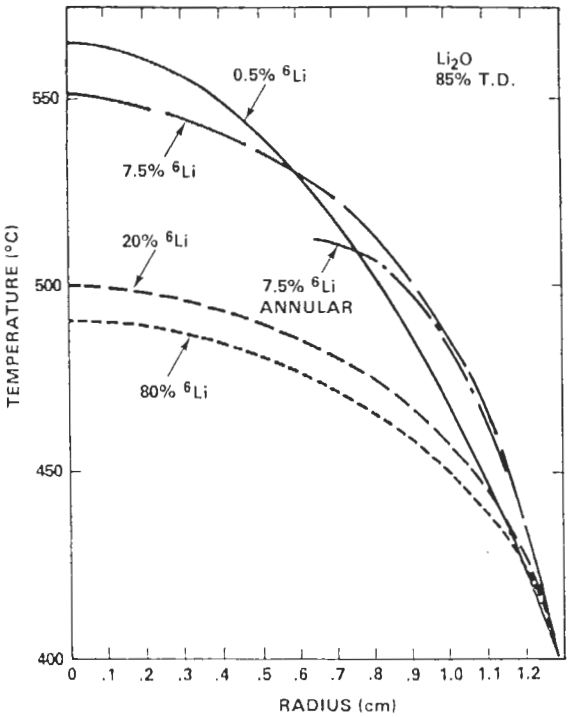

Fig. 12. Influence of lithium-6 enrichment on temperature profile in Li_2O pellet in the NRU reactor.

tures of about 550 °C and 700 °C, respectively. However, testing of such a pellet size in the HFIR reactor would lead to unacceptable temperatures (above 2500 °C) in the center of the pellet. The impact of lithium enrichment on the temperature profile achieved in a one inch diameter pellet is summarized in fig. 12 for the NRU reactor. The centerline temperature decreases with increasing ^6Li enrichment due to the significant self-shielding which occurs when testing in this reactor. Similar results were obtained for HFIR.

Finally, the impact of testing time and the associated lithium burnup are considered. For FFTF, the ^6Li absorption rate is fairly independent of radius, even at 80% ^6Li-enrichment. Therefore, the lithium burnup profile remains fairly uniform with time within the entire volume of the breeder material. However, for HFIR and NRU, the large ^6Li absorption rate leads to changes in the radial tritium production rate profiles with time. The time-dependent tritium production profiles in HFIR, shown in fig. 13, were estimated by assuming that the structural integrity of the pellet remains the same as ^6Li burnup occurs and the self-shielding does not change with time. As anticipated, the region of peak tritium production moves radially inward as a function of test time. The calculations for the HFIR reactor for this ^6Li-enrichment extend only to eight weeks, since at that point the total tritium production within the sample has dropped by ~15%. A similar behavior is observed in the NRU testing of a similar test specimen configuration and ^6Li-enrichment over a much longer period of three years (because of the lower neutron flux in the NRU reactor).

2.1.2.4. Conclusions

The spatial gradients for both the heat generation and tritium production rates are more favorable in a

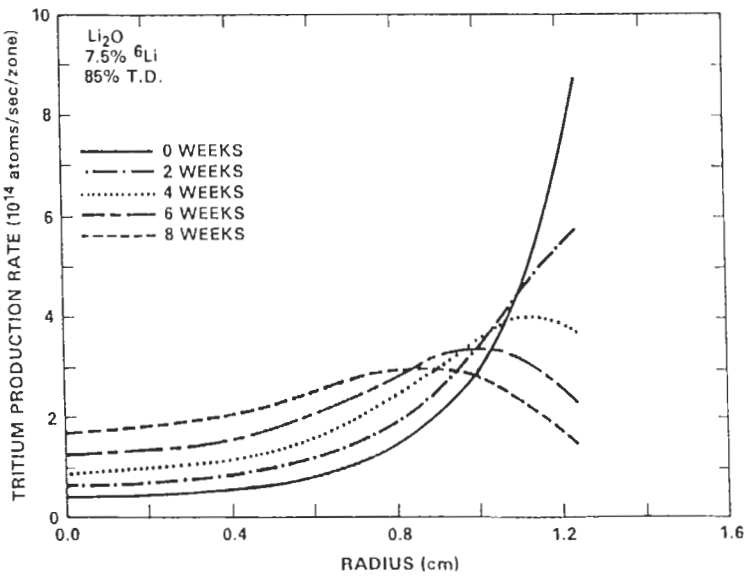

Fig. 13. Variation of tritium production rates with time in the HFIR reactor.

fast flux spectrum (FFTF) when compared to the steeper gradients obtained in the thermal or modified thermal spectra such as those for HFIR and NRU. Although the spectra for the HFIR and NRU reactors are different, the calculated heat generation and tritium production rates are quite similar if the differences in flux between the two reactors are used to normalize the results. This is not surprising since these rates depend predominantly upon the thermal portion of the spectrum. The temperature differences across the breeder pellet for either a 2.5 cm diameter cylindrical or 1.2 cm thick annulus become too large, even in the FFTF, if the enrichment is much higher than 20% ^{6}Li. For both the NRU and HFIR reactor, these temperature differences are prohibitively high unless the lithium enrichment is kept below 1–2% and the specimen width is small.

The peak tritium production rates in both HFIR and NRU move radially inward with test time due to lithium burnup in the outer zones for ^{6}Li-enrichments greater than ~7%. For FFTF the tritium production rate is relatively insensitive to enrichment up to 80% and, therefore, the burnup is apparently uniform with test time.

The analysis suggests the following general conclusions regarding the different capabilities offered by the spectra of existing fission reactors for solid breeder testing. For basic material property testing, fission reactors with either predominantly fast or mixed energy neutron spectra can be utilized. Care must be taken to choose the appropriate ^{6}Li enrichment and specimen size to achieve the desired test environment in a given test reactor. For "prototypic" solid breeder testing with relevant temperature and tritium production gradients, the choice of an appropriate reactor for testing becomes more difficult. Fission reactors with significant thermal neutron flux are limited to small test specimen dimensions or low reaction rates primarily due to self-shielding effects. Reasonable gradients for the initial tritium production and temperature within the test specimens can be obtained only for small test specimens with ^{6}Li enrichments of less than 2–3%. Also, the selective ^{6}Li burnup within the sample is quite severe and leads to a change in the tritium production gradient within the specimen as a function of the test time. Fission reactors with fast neutron spectra are less susceptible to self-shielding issues and, therefore, larger specimen sizes and higher burnup rates can be explored. High tritium production rates and acceptable temperature gradients within the test specimens can be obtained for larger diameter specimens ($\geq$ 2.5 cm in diameter) and higher ^{6}Li enrichments (up to 20%) with minimal change in the tritium production gradients with test time. The major limitation of fast neutron reactors is that the inlet temperature of the liquid metal coolant is typically around 360 °C, which limits the lowest achievable test temperature in the specimen to about the same value. Lower temperatures (~ 260 °C) are possible only by incorporating additional cooling systems at significantly higher cost.

2.2. *Experiments and facilities for liquid metal cooled blankets*

The magnetic field in a fusion reactor strongly interacts with flowing liquid metals, such that the most important issues are all affected in some way by magnetohydrodynamic, or MHD, effects. The large body force substantially increases the pressure needed to drive the coolant through the blanket. It also indirectly affects the heat and mass transfer by suppressing turbulence and altering, in some cases dramatically, the flow distribution within the blanket. Understanding the nature and the consequences of the interaction of liquid metal flows with magnetic fields, and development of an appropriate experimental data base and predictive tools are necessary before detailed designs of liquid metal-cooled blankets can be developed. Table 11 summarizes the features and objectives of the major MHD-related experiments for liquid metal blanket testing. Other important issues remain for liquid metal cooled blankets, such as tritium transport and recovery, structural behavior, and others. More complete treatment of these issues can be found in ref. [2].

The experimental program, prior to integrated fusion testing, can be divided into three phases of increasing level of integration. The first phase involves analytical, experimental, and numerical investigations of the structure of flow in typical components of flow networks (ducts, manifolds, expansions, contractions, etc.). Heat transfer experiments are expected to be of a confirmatory nature in this phase, since temperature profiles should be fairly straightforward to calculate once the velocity profiles are known. The effect of MHD flow distribution on mass transfer may be much more difficult to assess due to the importance of loop chemistry. For this reason, in this phase, experimental investigation of MHD effects on corrosion should be preceded by thorough testing in ordinary forced convection loops (with no magnetic field) with controlled impurity levels. The ALEX facility in the U.S. [10], and similar facilities worldwide [21,22], are already contributing information on MHD fluid flow for Phase I. In addition, several small thermal and forced convection loops exist in various locations for exploring material interactions

Table 11
Features and objectives of major liquid breeder experiments

ALEX [a]/ALEX Upgrade	LMF [b]	MHDM [c]	TMIF [d]	PITF [e]
Features of experiments				
Testing of flow network components	Testing of segments of blanket modules	Basic elements of relevant geometry	Actual materials and geometry	Prototypic blanket module
Working fluid: NaK	Working fluid: NaK	Relevant materials combination		
Loop structural material: austenitic stainless steel	Loop structural material: austenitic stainless steel	Transport loop	Transport loop	Transport loop
Magnetic flux density: 2–2.5 T	Magnetic flux density: 4–6 T	Relevant T, ΔT, impurities, V	Relevant environmental and operating conditions	Prototype environmental and operating conditions
Available dimension in B-field direction: 15–30 cm	Available dimension in B-field direction: 120 cm	Long operating time per experiment		
Measurement of velocity, pressure, temperature, and e lectric potential distributions	Measurement of velocity, pressure, temperature, and e lectric potential distributions	Measurement of dissolution and deposition rates	Measurement of integral quantities (ΔP, T, corrosion, and deposition rates)	Measurement of integral quantities
Objectives				
Develop and test instrumentation for local measurements in NaK environment	Develop and test instrumentation in NaK environment	Develop and test instrumentation in relevant environments	Design data for blanket test module	Engineering design data
Validate MHD flow, pressure, and heat transfer predictive capability for individual flow network components	Validate MHD flow, pressure, and heat transfer predictive capability for segments of blanket modules	Design data on MHD heat and mass transfer	Confirm and refine configurations	Reliability data in non-fusion environment
Obtain design data for flow network components	Obtain design data for segments of blanket modules	Verify techniques to reduce corrosion and corrosion effects		
	Explore techniques to reduce pressure drop and enhance heat transfer			

[a] ALEX exists at ANL; the other facilities were defined in FINESSE [2]
[b] Liquid Metal Flow Facility
[c] MHD Mass Transfer Facility
[d] ThermoMechanical Integration Facility
[e] Partially Integrated Test Facility (may be upgrade of TMIF)

without magnetic fields [7,23]. Much more data is needed in both of these areas.

The second phase of MHD experiments will be carried out in test modules simulating more complex features of leading blanket designs. Because of the electrical coupling between individual ducts in the blanket, the use of test modules of representative size and complexity is nccessary. More powerful magnets with increased magnetic field volume will be needed to achieve test parameters approaching those in a reactor blanket. Data obtained during this second phase will be used to validate predictive capability for pressure drop and heat transfer, and to obtain design data for blanket configuration screening and further development. The experiments will include exploration of techniques for MHD pressure drop reduction and/or heat transfer enhancement at parameter ranges close to those of the blanket environment. The second phase also includes MHD mass transfer (corrosion and deposition) testing. Corrosion tests, which involve measurement of dissolution and deposition rates, require long operating times per experiment in loops of prototypic temperatures, temperature differences, structural and coolant materials, and impurity levels. A separate facility called MHDM (MHD Mass Transfer Facility) has been identified because of the unique features of the facility and the experimental program.

The third phase involves experiments on modules with actual materials and geometry and with operating conditions as close to prototypic as possible. Engineering design data of the overall thermomechanical performance of the blanket modules and their corrosion characteristics will be obtained as well as information pertaining to design reliability in a non-neutron environment. Additional details on elements of the liquid breeder test program can be found in ref. [2].

A facility called LMF (Liquid Metal Flow Facility) has been identified as a critical near-term experiment which provides data during both the first and second phases of testing. The characteristics of LMF have been explored in detail, including both the physical aspects of the facility and the experimental program. Ref. [9] contains a more detailed description of LMF.

The purpose of LMF is to carry out both isothermal and heat transfer tests on elements of future blanket designs for which there are unresolved MHD-related issues. The quantities to be measured include velocities, pressures, and voltages at selected locations. During heat transfer tests, temperature distributions will also be obtained. Heat transfer measurements fall into two categories. In the first category, heat transfer is used as a diagnostic tool for the study of flow distribution for those cases in which direct measurement of flow structure is not practical or requires confirmation. In the

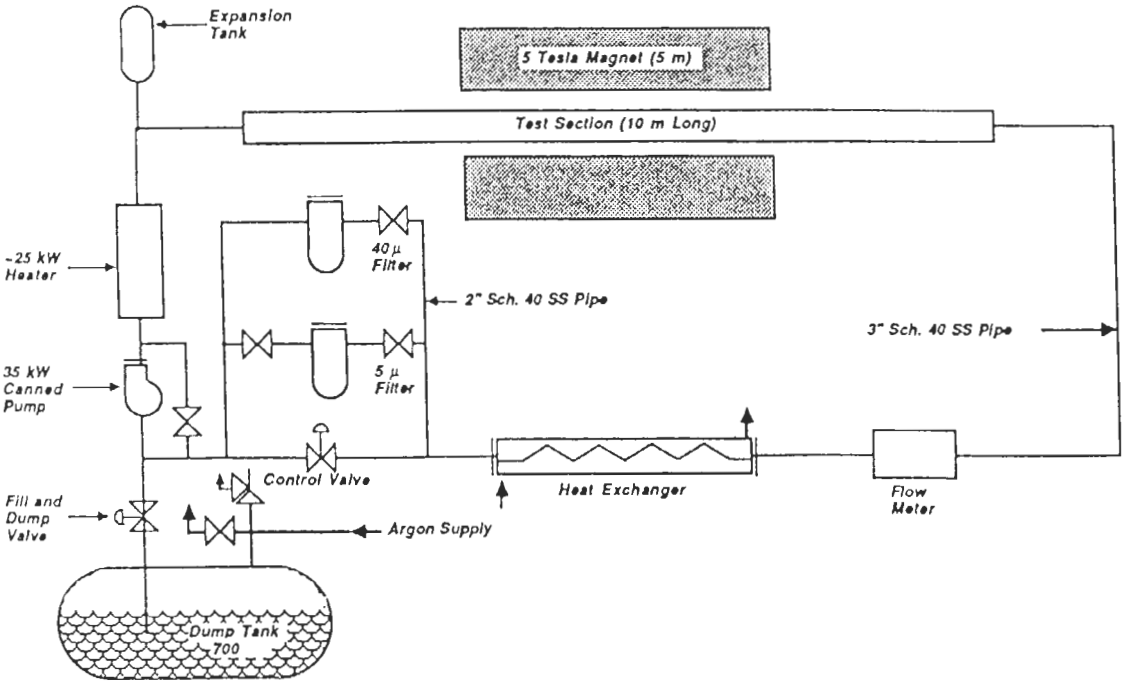

Fig. 14. Schematic of LMF loop.

second category, heat transfer parameters at or near prototypic conditions are obtained for direct validation of predictive calculational tools and/or for the creation of an empirical data base.

The major components of LMF are shown schematically in fig. 14. They include: (a) the test article, (b) the flow loop, (c) the magnet system, and (d) the instrumentation and data acquisition system.

2.2.1. Test article

The test articles largely determine the design and functional requirements of the facility. Blanket simulation submodules must have sufficiently large dimensions to achieve prototypical thermal and flow behavior. Long development lengths parallel to the magnetic field impose the most difficult requirements on test volume. This necessitates magnets with considerably larger pole face separation than ALEX or ALEX Upgrade. For a dipole-type magnet, the required pole face separation is about 1 m.

The facility also should be able to accommodate a variety of other test articles, each of which is designed to address a particular design issue related to MHD. Such testing may be necessary if there is reason to believe that the higher values of Hartmann number (M) and interaction parameter (N) in LMF will reveal additional information of engineering relevance. It is desirable that the facility be able to accept the identical test articles previously tested at lower M and N. Test articles, incorporating the most important geometric

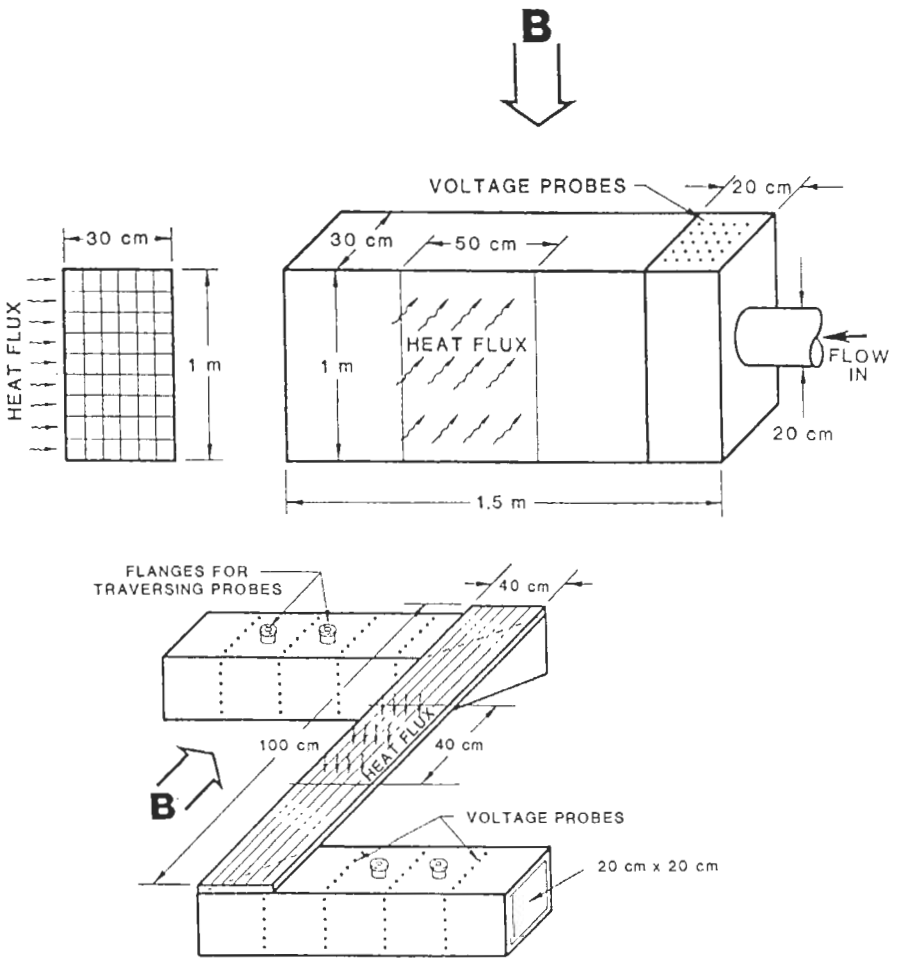

Fig. 15a. Conceptual design of a test section simulating the inlet (or outlet) manifold of the TPSS design. Flows in each of the individual ducts fed from the manifold can be measured with individual EM flow meters.

Fig. 15b. Conceptual design of a test section simulating the salient features of the BCSS liquid-metal-cooled blanket design.

features of the BCSS [13] and TPSS (Tokamak Power System Studies [24]) blankets, are shown in figs. 15a and 15b.

2.2.2. Flow loop

The recommended flow loop for testing lithium blanket designs uses NaK in stainless steel at low temperature. Low temperature operation with NaK simplifies the loop design and greatly facilitates operations. (LiPb eutectic has significantly different MHD properties as compared with elemental lithium; therefore, testing of a LiPb blanket might be better achieved using a fluid with more similar properties, such as mercury or Wood's metal).

The possible negative effects of low temperature operation in NaK have been determined to be acceptable. Corrosion obviously requires high temperature and correct materials, but the LMF facility is not intended for corrosion studies. Heat transfer depends primarily on temperature differences, rather than absolute temperature, except for a secondary effect on material properties. The only remaining advantage of lithium over NaK for heat transfer/fluid flow experiments is that, at identical test conditions, the Hartmann number with lithium is 50% higher than that of NaK, and the interaction parameter is 100% higher (although this can be compensated by reducing the bulk flow rate). The disadvantage in Hartmann number is not high enough to balance the expected reduction in the quality and variety of test data brought about by high temperature operation in lithium.

The size of the loop can be much smaller than a reactor primary cooling system and still maintain prototypical values of M and N. Some estimated loop parameters are shown in table 12. Loops operating at high temperature or loops made of different materials for corrosion studies will be considerably more expensive. This estimate includes all loop hardware and engineering, excluding the magnet. It is assumed that the loop will be sited in an existing building with existing cranes and other support hardware, utility hookups, exhaust stacks, etc.

2.2.3. Magnet system

The magnet system for LMF is the largest and most expensive element of the facility. The characteristics of the magnet will control to a large extent the scale and cost of the entire facility. Two major options exist for the magnet system: iron core versus superconducting, and dipole versus solenoid.

Although design and fabrication of a superconducting magnet such as the one envisioned for the LMF facility is a challenging task, the required technology and expertise exist and have been demonstrated. A superconducting magnet has advantages in power consumption, but requires a higher level of supervision and frequent helium replenishment. A conventional iron core electromagnet, as opposed to a superconducting magnet, requires less maintenance and supervision between tests, can be energized in a much shorter time, and its design, operation, modification, or repair is much more straightforward. On the other hand, the power supply and cooling water requirements are so demanding that, for the size and magnetic flux density magnitude envisioned for the LMF, the use of conventional iron core magnets is all but precluded.

Solenoid magnets are generally less costly than dipoles; however, a larger solenoid volume is required for the same testing capability as in a dipole magnet. Costs have been estimated for dipole and solenoid magnets and are given in table 12 together with the major parameters. The dimension of 1 m is in the direction parallel to the field. For the same type of magnet, the cost scales roughly with the magnetic flux density and the magnet volume.

Although a solenoid magnet may, at first, appear to be preferable because it simulates geometrically a segment of a tokamak torus, the solenoid magnet has severe test volume access limitations for testing in pre-

Table 12
LMF Facility Parameters

Loop parameters	
Working fluid	NaK Eutectic
Inventory of working fluid	700 liters
Loop materials	Predominantly 300 Series S/S
Volumetric flow rate through test articles	1–25 liters/s
Pump outlet pressure	1 MPa
Pump outlet temperature	$\leq 100\,^{\circ}$C
Test article conditioning temperature (at low pressure and flow rate)	300 °C
Overall length of test article (between flanges for test section replacement)	~10 m
Cost (excluding cost of test articles)	$1M
Magnet parameters	
Peak field	5 T
Warm bore	1.2 m
Uniform field volume	1 m × 0.3 m × 3 m
Field uniformity	±5%
Dipole magnet cost	$12M
Solenoid magnet cost	$15M

dominantly transverse fields. Radial access to the test volume can only be allowed at a very limited number of windows. This limits the type and variety of test articles that can be tested. Although additional attention must be paid to this question, as well as to the final cost differential between the two magnet types, it appears that a dipole magnet is preferable.

2.2.4. Instrumentation

Measurements of direct engineering importance are those of velocity, pressure, and temperature distributions. Although of limited engineering importance by themselves, voltage distributions can, under certain conditions, be directly related to the velocity profiles.

Measurements of the pressure drop and heat transfer coefficient are fairly straightforward, as these are integral parameters. Relatively standard pressure transducers can be used to measure pressure drop. Heat transfer coefficients can be obtained by measuring temperatures with standard thermocouples. Electric potential measurements are also relatively simple, since they can be accomplished by attaching wires directly to the channel walls.

The measurement of velocity distributions, on the other hand, is much more complicated, but is also very important. Common instruments for measuring velocities are Pitot probes and hot film anemometers. The former are of very limited use for the low velocities relevant to MHD testing. Hot film anemometry has been used successfully in the past for liquid metal MHD studies. However, calibration shift due to sensor contamination and reduced sensitivity due to reduced heat transfer in the magnetic field make such measurements extremely tedious. The shortcoming of reduced sensitivity is experienced by all heat transfer-based measuring instruments.

For flow conditions in which the product of the current density and the electrical conductivity is much smaller than the voltage gradient, a very attractive measuring instrument is the LEVI probe (Liquid Metal Electromagnetic Velocimeter Instrument). LEVI measures the emf generated locally in the flow, analogous to an electromagnetic flow meter which measures the global voltage drop across a channel. This technique has been shown to give excellent sensitivity and temporal response without the need for calibration [10]. The primary limitation of LEVI relates to its dependence on the local magnetic field. It can only be used in the presence of a transverse magnetic field and its sensitivity decreases as the magnetic field strength decreases. In addition, its accuracy diminishes as the wall conductance ratio approaches unity.

There would undoubtedly be cases where, because of the small sizes of the ducts, reliable detailed velocity profiles would be exceedingly difficult to obtain. In such cases, the flow structure can be deduced indirectly by carefully designed heat transfer experiments. In such experiments, information about the flow distribution can be obtained by measuring the temperature distribution with thermocouples strategically placed on the surface of the test article and within the flow ducts. In fact, heat transfer experiments should be viewed as much as a means for obtaining information about the flow structure and distribution as for measuring overall heat transfer parameters.

Because of the complexities of the velocity distribution measurements, it is unrealistic to expect that the flow field within a complex test article would be completely mapped. It is important, therefore, to apply pre-experimental analysis to the maximum extent possible to carefully select the locations for velocity profile measurements that provide the most important information.

3. Fusion testing issues

Integrated testing is essential for concept verification and demonstration of fusion nuclear components. It has been shown previously in the FINESSE study that only a fusion facility can provide the proper combination of environmental conditions for integrated testing [1].

Major initiatives are already underway in Europe (NET) [5], Japan (FER) [6], USA (TIBER/ETR) [7], USSR (OTR) [25], and internationally (INTOR) [26] to plan and design a fusion engineering test facility. These programs vary in the degree to which nuclear technologies are emphasized, but a primary objective for all of them is testing of fusion nuclear components.

A fusion engineering test facility will be a central and relatively expensive step in the fusion program. Fusion nuclear technology issues must be weighed together with other issues in the fusion program, including physics, engineering, and system integration concerns, in order to define the optimum design and operating characteristics of the facility.

Earlier effort in FINESSE [1,27] has addressed many of the fusion nuclear technology testing requirements on the major parameters and features of a fusion test facility. Issues related to tritium supply and the reliability of a tritium-producing blanket also have been addressed. Subsequent examination of the impact of the FINESSE results on the cost and design of a fusion test facility have identified a number of critical issues that

require further attention. An example is the requirements on the plasma burn time and the need for steady-state operation. These issues are examined in this section. Because of the renewed strong interest in a fusion engineering testing facility, this section also reviews the influence of fusion nuclear technology objectives on the fusion test facility characteristics and design, and on fusion testing in general. The section is organized into three topics: (1) Requirements for Nuclear Technology Testing, (2) Tritium Supply, and (3) Blanket Reliability and Device Availability.

3.1. Requirements for nuclear technology testing

Successful testing requires that the physical and operating characteristics of the test facility meet certain conditions. The test program also impacts the facility design and operation outside the reactor core. For example, large and complicated ancillary equipment, such as heat transport and rejection, tritium extraction, chemistry control, and instrumentation systems, often accompanies component testing. The safety impact of the test program is another important consideration. For example, in NET, a tritium-producing blanket with liquid lithium has been ruled out for safety reasons [5]. Protection of the facility against mechanical failures and radiation hazards (including accidental tritium releases) must also be considered.

The most important test requirements are those related to the major parameters of the test facility. These are summarized in table 13. These requirements on the test facility parameters are related to the assumed reference conditions for a commercial reactor. The table also provides a set of reference conditions based on a survey of recent tokamak reactor and reactor blanket design studies [12,13,28,29]. Two categories of parameter values are given: minimum and recommended. The minimum values are based primarily on detailed analysis of the important blanket phenomena under altered test conditions. One can show that test device parameters below the minimum value in any category will seriously limit the usefulness of nuclear testing for at least one identifiable phenomenon. There is a high probability that results could not be extrapolated to reactor conditions under these circumstances. Future analysis of additional phenomena may result in more stringent minimum test requirements, due to an increased understanding of the complexities of blanket behavior. It is likely that the minimum parameter values will be reduced only if the reference device parameters are reduced.

While the minimum parameter estimates provide values *below* which there is confidence that results *cannot* be extrapolated to reactor conditions, the recommended parameter ranges provide values *above* which there is confidence that results *could be* extrapolated to reactor conditions. The recommended values are determined partly from analysis and partly from engineering judgment. While testing at prototypical values is clearly most beneficial, the large majority of nuclear issues can still be adequately addressed if the recommended parameters are achieved in the fusion test device. However, since we do not fully understand engineering phenomena under fusion reactor conditions, a judgment is required based on typical experience in

Table 13
Device parameters: reference conditions and recommended values

Parameter	Test facility		Reference reactor
	Minimum	Recommended	
Neutron wall load (MW/m^2)	1	2–3	5
Surface heat load on first wall (MW/m^2)	0.2	0.2–0.5	1
Fluence at test module [a] ($MW\ yr/m^2$)	2	3–6	15–20 [b]
Plasma burn time (s)	500	> 1000 [c]	steady state
Plasma dwell time (s)	< 100	< 50	–
Continuous operating time	days	weeks	months
Availability (%)	20	30–50	70
Test port size ($m^2 \times m$)	0.5×0.3	1×0.5	–
Total test surface area (m^2)	5	10–20	–
Magnetic field strength (T)	3	5	7

[a] Fluence at test module. Required test device lifetime is greater (by about a factor of two).
[b] Blanket lifetime.
[c] Steady state is preferred.

scaling from other technologies in addition to the analysis of known behavior. Note that operating at the recommended set of parameters gives no guarantee that the results will be fully valid at full reactor parameters.

For both the minimum and recommended values, future analysis will likely result in further refinement of the estimates in table 13. Precise specification of the requirements on test device parameters is difficult. In general, the physical behavior in nuclear components varies gradually with the device parameters, showing threshold effects only in a limited number of cases (such as the transition from laminar to turbulent flow and the transition from elastic to plastic strains). The determination of test requirements must be constructed from analyses of the many phenomena which are affected by varying device parameters, and from an informed engineering judgment on how far the conditions can be extrapolated in order to confidently predict behaviors under full reactor conditions.

Exact simulation of all the conditions in the blanket (including temperature profiles, tritium concentration profiles, geometric boundary conditions, etc.), is not possible with device parameters that are scaled down from the reference reactor conditions. Therefore, it is important to define the degree to which imperfect simulation of the reactor conditions can be tolerated, based on whether or not the needed data can still be obtained. In addition, modifications to the test modules themselves can be partially successful in recovering reactor relevant behavior under scaled conditions. The process of altering test module characteristics to enhance the value of testing is called Engineering Scaling.

Table 14 shows the relationships between the parameters of the fusion test device and the main categories of blanket performance. The test parameters from table 13 are grouped into four areas: (1) neutron wall loading, which is the primary device parameter in determining the heat sources (surface and bulk heating), nuclear reaction rates, and accumulated fluence; (2) plasma burn time and pulsing, which represents effects related to non-steady-state operation; (3) device geometry and test volume; and (4) magnetic field strength and geometry. Relationships also exist among the performance categories; for example, the thermal condition of the blanket strongly impacts structural, corrosion, and tritium behaviors. These indirect relationships are not explicitly defined in table 14.

In the remainder of this subsection, the device parameter areas are examined individually to define more clearly the important nuclear phenomena which contribute to the definition of test requirements for the blanket.

3.1.1. Heat source requirements

Heat sources provide the energy input which controls blanket temperatures, and thereby all processes and interactions activated by temperature levels and gradients. The two principal heat sources for the blanket/first wall are surface heating, caused by particle and radiation loads to the first wall, and bulk heating resulting from neutron and secondary gamma-ray radiation. For given materials and geometry, the bulk heating is linearly proportional to the neutron wall load. The surface heating on the first wall depends on the partitioning of energy loss from the plasma between radiation and particles, but the maximum (for an ignited plasma) is limited to 25% of the neutron wall load.

Nearly every important phenomenon in the blanket is in some way affected by temperature, from basic properties to complex thermomechanical and chemical interactions. Examples of the most important temperature-dependent thermophysical, thermochemical, and thermomechanical properties include thermal conductivity, chemical solubility and diffusivity, yield strength, creep rate, and radiation swelling rate. Simple processes, such as thermal expansion and heat conduction are dominated by temperature profiles. More complex interactions, such as mass transport/redeposition and tritium transport, are strongly dependent on temperature, sometimes in ways which are not fully understood. These more complex interactions provide the greatest uncertainties in our ability to perform testing under scaled conditions.

In general, both the absolute level of temperature as well as temperature profiles are important to maintain. Control over the average temperature in a component is usually easy to obtain by allowing the coolant temperature to rise. On the other hand, temperature gradients are proportional to the local heat flux. Changes in the heat flux will result in unavoidable changes in the temperature gradients. Temperature differences across an element can be adjusted by geometrical changes, but local temperature gradients can not be adjusted independent of the heat source. Therefore, even with careful test module design, there are limits on how far the heating rates can be lowered. Limits have been studied for: (1) total amount of heat input, (2) relative contributions of surface versus bulk heating, and (3) geometric constraints on the heat source.

A reduction in the heat source results in lower spatial temperature gradients. A common engineering scaling technique to enhance temperature differences across blanket elements is to increase their thicknesses. For structural similarity, aspect ratios should normally be maintained, although there are some structural effects

Table 14
General effects of fusion test device parameters on blanket performance

	Neutronics	Thermal	Structural	Flow/corrosion	Tritium
Neutron wall load					
– Heat source (surface and bulk heating)	nuclide density and geometric changes due to thermal expansion and cracking	temperature profiles, heat transfer coefficient, thermophysical properties	thermal stresses, material properties, thermal creep, temperature-dependent radiation damage profiles	mass transport/corrosion rates and profiles, coolant properties, wall electrical conductivity (LM)	diffusion and other transport processes, solubility and surface adsorption, mass transfer, grain growth, porosity changes (sintering)
– Reaction rates	R.R. [a]	R.R.	R.R.	R.R.	tritium production rate
– Fluence	transmutations, activation	thermophysical properties, gap conductance	material properties, swelling, ductility, creep	degradation of MHD insulators, radiation-enhanced corrosion	tritium generation, trapping, burn-up related thermochemistry changes (SB), effects on permeation barriers
Plasma burn time and pulsing	–	transient temperature profiles	fatigue, crack growth, ratchetting, creep/fatigue	corrosion equilibrium	inventory and recovery equilibrium; permeation rate and barrier characteristics
Device geometry and test volume	neutronic boundary conditions, extrapolation to full blanket coverage, deep penetrations	thermal boundary conditions, MHD heat transfer, thermal entrance effects	component sizes (especially aspect ratios)	MHD velocity profiles and pressure drop entrance effects, MHD mass transfer, spatial profiles of corrosion	tritium breeding and inventory
Magnetic field (strength and geometry)	–	MHD heat transfer	steady and transient forces, MHD pressure stresses	MHD fluid flow and corrosion	–

[a] R.R. denotes reaction rates.

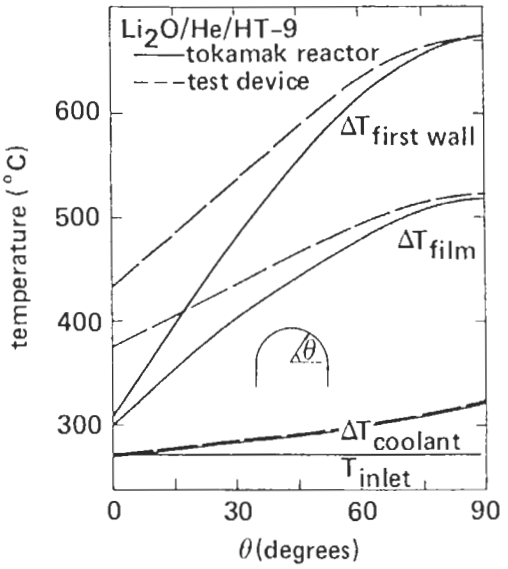

Fig. 16. Heat source effect on the Li_2O/He/HT-9 first wall temperature profile (reactor at 5 MW/m^2 neutron and 1 MW/m^2 surface heat load; scaled test module at 2.5 and 0.1 MW/m^2) [reprinted from ref. 1].

which are not linear in the dimensions (like fracture mechanics). Hard limits on the reduction in heat input come when space limitations prohibit increasing dimensions or when the dimensions are so altered from the reference case that new effects may occur, such as crack growth, axial conduction, and altered neutronics. These limits occur at roughly a factor of 3–5 reduction in the heat source.

A thermal analysis was performed on a plate-type, helium-cooled, solid breeder blanket module to demonstrate the extent to which temperature profiles can be affected by a reduction in wall loading [27]. Reactor conditions were assumed to be 5 MW/m^2 neutron wall load with 1 MW/m^2 surface heat flux, and the test device was assumed to provide only 2.5 MW/m^2 neutron wall load with 0.1 MW/m^2 surface heat flux. The blanket module design uses a lobed first wall, with coolant entering through first wall cooling channels at the rear of the module, passing toward the front ($\theta = \pi/2$), where an orifice redirects the flow through the interior of the blanket (see fig. 3). Scaling was applied to both the module dimensions and the coolant flow rate to maintain the bulk temperature rise in the coolant and the temperature drop across the first wall. Fig. 16 shows the results, which indicate that with a reduction in the wall load the temperatures can be matched only partially, even with careful engineering scaling. As mentioned above, incorrect temperature profiles in the first wall will affect many important phenomena activated by temperature.

The possibility for enhancing nuclear and surface heating by external means (e.g., resistive heaters or fissile materials) have been explored, but the methods proposed to date are awkward and/or add new uncertainties to data interpretation. For solid breeders, addition of uranium has been considered, but tritium and chemical behavior will almost certainly be affected.

The ratio of surface to bulk heating is important because the temperature profiles and heat transfer coefficients are affected. For example, it is well known that the temperature variation in a plate resulting from a surface heat flux is linear, as opposed to the parabolic distribution resulting from uniform bulk heating. Thermal stresses in first-wall and front-of-blanket elements are especially sensitive to these profile variations.

Liquid metal blankets have special difficulties with reduced heat sources because the magnetic field tends to couple the geometric features of the blanket with the heat transfer. Engineering scaling for the heat source must also account for the resulting effects on MHD phenomena, including entrance region velocity and temperature profile development. Temperature profile development lengths for laminated flow of liquid metals can be much longer than the channel length, which means that the entire blanket is in the thermal entry region, in which heat transfer strongly depends on location. As discussed in Section 4, the heat sources, velocity profiles, and geometry play a highly coupled role in determining the temperatures in liquid metal blankets. Geometric effects are treated in more detail below.

3.1.2. Neutron fluence requirements

A number of specific reactions result from neutron radiation, including tritium and helium production, atomic displacements, and transmutations. As a result of some of these reactions, neutrons are responsible for numerous changes in material properties and behavior. Material damage due to neutrons is an important factor in determining design limits for the blanket, including the anticipated lifetime. Many of the anticipated blanket failure modes are intimately related to neutron damage. Some of the effects include changes in thermophysical and thermomechanical properties, radiation swelling, embrittlement, creep, and solid breeder sintering.

In a test reactor with DT neutrons, these effects will depend primarily on the accumulated dose. They are not readily scaled to lower fluences. Test requirements can be identified based on achieving fluences at which significant changes in behavior occur or saturate. How-

ever, changes is behavior often result from interactions of different effects rather than single effects, for example, creep/swelling interactions and solid breeder/clad interactions. Therefore, a knowledge of material property changes alone is not sufficient to determine test requirements.

Table 15
Examples of important effects as a function of exposure

Exposure MW yr/m^2	Phenomena/effects
0–0.2	Thermophysical property changes (e.g., thermal conductivity) Solid breeder cracking Liquid metal embrittlement of structure Onset of Li_2O and multiplier swelling Insulator embrittlement and conductivity changes First wall erosion Initial operation stress effects Tritium permeation through first wall and clad Hydride formation and hydrogen embrittlement in structure Porosity in breeder may close off Radiation-induced-sintering and grain growth
0.2–1	Li_2O swelling dominates breeder/clad mechanical interaction Ductility changes (HT-9, 316 SS) Initiation of fatigue and creep/fatigue First wall erosion/redeposition and surface cracking Relaxation of thermal stress Radiation-induced trapping in structure (defect saturation) Reduction in fracture toughness (structure) Early transmutation effects (e.g., drop in conductivity of copper due to Ni production) Measurable radioisotope concentration
1–3	Changes in ductility start to saturate (HT-9, 316) Fracture toughness, Δ – DBTT saturates Thermal stress relaxation complete Burnup effects on chemistry, compatibility, breeding Breeder/clad corrosion Irradiation hardening ($< 450\,^\circ$C)/ softening ($> 450\,^\circ$C) saturates
3–5	Possible fatigue crack propagation Onset of irradiation creep/swelling interaction of austenitic alloy Clad swelling (316) dominates breeder/ clad interaction Possible fracture toughness degradation (HT-9)
5–10	Potential onset of irradiation creep/swelling interaction of HT-9 Possible fatigue failure Change in fracture mode Changes in toughness/strength/ductility and tearing modulus
10–20	End-of-life phenomena: Operational stress effects – First wall thinning – unstable deformation – Fatigue, creep fatigue – unstable cracking Unforseen high-fluence-material behavior

Table 15 shows some of the important phenomena which occur in fusion nuclear components as a function of neutron fluence. Engineering effects are emphasized in addition to basic property changes. These include interactive effects (such as breeder/clad mechanical interaction or radiation-enhanced corrosion) and behaviors which are not strictly related to material damage (such as tritium production and afterheat).

Radiation effects are extremely sensitive to material choices and operating conditions (primarily temperature). In addition, the lack of data results in large uncertainties. Therefore, the entries in table 15 are only approximate estimates. They represent the most important anticipated effects for the primary candidate materials and designs as they are currently understood. Exceptions to these guidelines will undoubtedly occur for particular materials or designs.

From these estimates of fluence effects, some general conclusions can be drawn. Radiation effects can be classified into roughly four categories (depending on many factors, including the specific material and design): beginning-of-life effects, occurring between 0–0.2 MW yr/m^2; early-life effects, occuring between 0.2–2 MW yr/m^2; middle-of-life effects, occurring between 2–10 MW yr/m^2; and lifetime effects, occurring between 10–20 MW yr/m^2. A minimum requirement has been defined based on matching the exposure required to active or saturate early-life engineering phenomena. It is very desirable to activate the middle-of-life effects. There are a very large number of phenomena which can

be explored without pushing to end-of-life fluences. Clearly higher levels of exposure are better if they can be attained at reasonable cost. It is desirable to test components to their full lifetime values or beyond in order to anticipate lifetime and long-exposure failure modes; however, in the first fusion facility, cost considerations and technology limits may preclude any testing beyond the middle-of-life effects.

It is extremely important to distinguish between the fluence attained at the test module and the test facility lifetime. The fluence values discussed above and in tables 13 and 15 are those that need to be achieved at the test module. The test facility lifetime should be longer for at least two key reasons. First, many of the important test modules are not exposed directly to the plasma, and the highest neutron flux at the module is generally a factor of two or more lower than that at the first wall. Providing an enclosure for the test module will enable the device to continue operation even in the event of a failure in the test module. Second, it is inconceivable for the first fusion test facility that a useful module can be irradiated for the entire life of the facility. Early modules may fail, and knowledge will be incorporated for testing better modules during the life of the facility.

3.1.3. Plasma burn time requirements and pulsing effects

Steady-state plasma operation is a generally accepted goal for the development of competitive commercial fusion reactors [12,28,29,30]. Given this, a key question now is whether the design basis for the first fusion engineering test reactor (ETR) should be steady state or pulsed and, if it is pulsed, how long of a burn time is needed.

Key reasons in favor of steady state (or, at least, long plasma burn time) as the design basis for ETR include:

(1) Demonstration of steady-state plasma operation is a necessary element in exploring the long-term reactor potential of the confinement concept [8,29,30].
(2) Steady-state operation should reduce the failure rate and improve the reliability of many of the basic ETR components. Reduced cycling will extend the achievable lifetime and fluence in the test facility.
(3) Steady-state operation will improve substantially the usefulness of nuclear technology testing in ETR.

This last item concerning the benefits of steady-state operation to nuclear technology testing is amply supported in previous work [1–4] and is the subject of further analysis in this subsection. Before summarizing this analysis, some general observations are worth noting. Adopting steady-state operation as the basis for ETR will require further development in plasma physics [8]. However, regardless of ETR needs, such development is required to demonstrate a key aspect of the long-term reactor potential of selected confinement concepts. Accelerating the current drive development for ETR operation is well justified in terms of the benefits of improved reliability and usefulness to nuclear technology testing. The use of some non-inductive current drive may not increase the cost of ETR; it may actually reduce the cost [7]. Key components such as the impurity control and exhaust system will not require any additional design features or increments in cost to achieve steady state beyond those required for burn times longer than hundreds of seconds. Many components, such as magnets, first wall and limiter/divertor, will have better reliability and probably lower cost in an experimental device if they are designed for steady state (the INTOR [26] design has identified many problems associated with the short plasma burn time). It is suggested that ETR studies carefully evaluate the impact of using non-inductive current drive on the cost of development, construction, and operation of ETR.

Steady-state operation is extremely important for successful nuclear technology testing. Plasma cycling means time-dependent changes in the major environmental conditions for nuclear testing: (1) nuclear (volumetric) heating, (2) surface heating, (3) poloidal magnetic field, and (4) tritium production rate. These time-dependent changes in the "source conditions" will result in time-dependent changes in the "response" of test elements such as blanket modules, heat and tritium transport loops, and sections of limiter/divertor plates. These time-dependent changes in the responses will introduce new effects and phenomena that: (1) can be, in some cases, more dominant than the steady-state effects for which testing is desired, or (2) will, in many cases, complicate the tests and make the results difficult to model, interpret and understand.

The remainder of this subsection is concerned with analysis of the effects of burn time on the usefulness of some key nuclear technology tests. Table 16 indicates a range of burn cycle times that may exist in an ETR. The burn cycle consists of periods of time for plasma start-up, burn, shutdown, and a dwell (or rejuvenation) time. Operating time requirements are based on analysis of the time dependent responses of all the important blanket phenomena. These include thermal, fluid flow, corrosion, structural, tritium, and neutronic performance.

The unsteady behavior of the blanket is generally very complex, but often the evaluation of burn cycle requirements can be related to relatively simple time constants for the processes involved. Many engineering

Table 16
Reference burn cycle times (in seconds)

Burn time	
< 200	Short burn
> 5000	Long burn
> 10000	Quasi-steady state
Plasma startup/shutdown	
15	
Dwell time	
20	Minimum time to evacuate
100	Relaxed requirements on vacuum pumps, ducts, etc.

processes can be described approximately with an exponential dependence on time, such as:

$$f = f_0(1 - e^{-t/\tau}),$$

where τ is a fundamental time constant. Time constants for more complex processes can be expressed in terms of the percentage achievement of the equilibrium value (for example, the time to reach 99% of the equilibrium value).

A partial list of estimated basic time constants is given in table 17. These time constants were evaluated using blanket characteristics from the reference designs described in ref. [1]. Three major classes of time constants which recur frequently are:

(1) Diffusive processes governed by a diffusivity and scale length, $\tau_c = L^2/D$. This includes primarily thermal and mass diffusion.
(2) Convective processes governed by a velocity and scale length, $\tau_c = L/v$. This applies primarily to various residence times.
(3) Changes in bulk quantities, such as tritium inventory or blanket bulk temperatures.

The time constants follow some general trends: flow processes are usually very fast, material interaction and tritium processes are usually very slow, and thermal processes are in between – of the order of minutes. To understand the relationship between unsteady responses and the test requirements, it is helpful to consider three possible situations for the time constant of a given process relative to the burn time:

(1) Time constant much shorter than the burn time. A good example of this is MHD velocity profiles, which have a time constant of the order of 1 s or less. In this case, the process reaches a true equilibrium within a single burn time. If the duty cycle (burn time divided by total time) of the machine is high, then the conditions in the blanket are prototypical most of the time.
(2) Time constant much longer than the burn time plus dwell time. A good example of this is corrosion, which normally takes weeks to months to become developed. In this case, the process eventually reaches a quasi-equilibrium after many cycles, with conditions changing very little during a single burn cycle. The higher the duty factor, the closer the quasi-equilibrium will be to the true equilibrium condition.

Table 17
Approximate characteristic time constants in representative blankets

Flow	
Solid breeder purge residence	6 s
Liquid breeder coolant residence	30 s
Liquid breeder cooling circuit transit	60 s
Thermal	
Structure conduction	4 s
Structure bulk temperature rise	20 s
Liquid breeder conduction (Li)	30 s
Solid breeder conduction ($\frac{1}{2}$-cm plate)	50–100 s
(1-cm plate)	200–400 s
Coolant bulk temperature rise (200 K at 4000 MW_t)	
Li	100 s
LiPb	1500 s
Solid breeder bulk temperature rise ($LiAlO_2$, 300–1000 °C)	
Front (near plasma)	120 s
Back (away from plasma)	1800 s
Material interactions	
Dissolution of Fe in Li (500 °C)	40 days
Tritium	
Diffusion through solid breeder ($LiAlO_2$, 0.2 μm grains)	
1250 K	8–200 s
750 K	13–300 h
Surface adsorption ($LiAlO_2$)	3–10 h
Diffusion through SS316 (1 cm)	
800 K	10 days
600 K	150 days
Inventory in solid breeder (water-cooled $LiAlO_2$, 0.2 μm grains)	
67% of equilibrium	6 months
99% of equilibrium	4 years
Inventory in liquid breeder	
LiPb	30 min
Li	30 days

(3) Time constant roughly equal to the burn or dwell time. A good example of this might be temperature responses, particularly in solid breeder blankets (which possess relatively low thermal conductivities). This condition is the most problematic, and requires detailed analysis to determine the nature of the responses that depend on temperature.

There are two situations which cannot be accommodated by this simplified classification: threshold effects and interrelated processes of different time constants. Structural responses provide good examples of important threshold effects. For example, irradiation of ferritic steels generally increases the ductile-to brittle transition temperature (DBTT). If the blanket temperature falls below the DBTT due to plasma cycling, then the structural response could be dominated by low temperature effects rather than the reference conditions. Another example is high cycle fatigue, which is a structural response that would not properly represent the conditions in a continuous burn reactor. Some of the known time-dependent threshold effects include, for example, temperature-dependent chemical reactions; high cycle fatigue and fracture mechanics; DBTT – low temperature embrittlement; solid breeder thermal fracture; and plastic deformations, especially ratchetting. In addition, table 15 contains a large number of fluence-related threshold effects.

Interrelated time constants also complicate the definition of test requirements. For example, even though corrosion is dominated by long time constant processes, it is also strongly affected by blanket temperatures, which have relatively short time constants. The cyclic effects on temperature could result in significantly different corrosion behavior, such as temperature-sensitive chemical reactions and redeposition. It is difficult to predict all of the effects of cycling because of the large number of important interrelationships between phenomena which exist in a blanket. These factors strongly support steady operation to match the conditions in the reference reactor.

Some of the time constants are strong functions of temperature and can vary over many orders of magnitude. Fig. 17 shows the large variation in tritium diffusion time constant for $LiAlO_2$ over the temperature range between 650° and 1250° C for a grain radius of 0.1 μm. There is a fairly large band of uncertainty indicated in the figure. For comparison, the thermal diffusion time constant for 0.5 cm of $LiAlO_2$ is also shown.

While the time constants provide a good general understanding of the time dependent behavior of the blanket, it is necessary in many cases to perform more detailed calculations. This is especially true when several processes are operating simultaneously, and possibly nonlinearly.

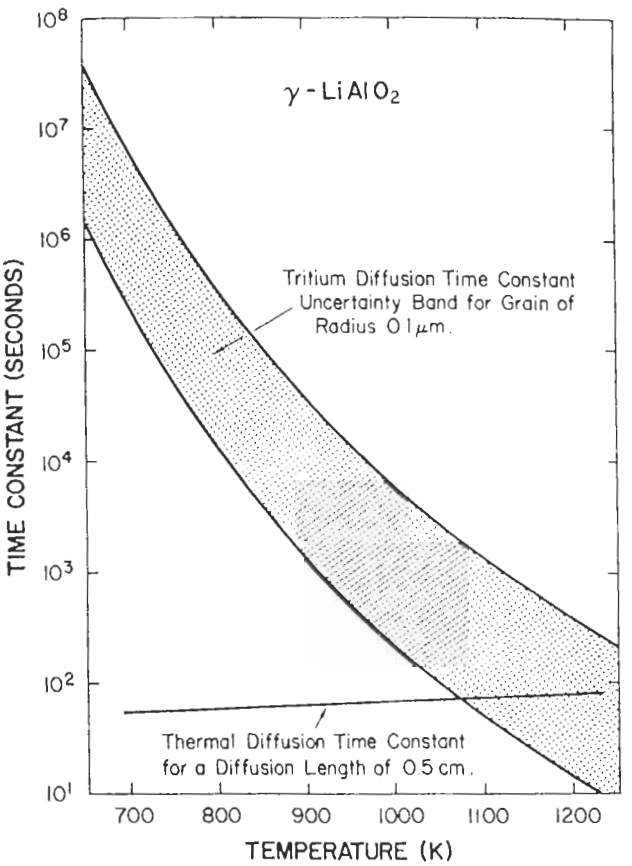

Fig. 17. Tritium and thermal diffusion time constants as a function of temperature (γ-$LiAlO_2$).

A calculation was performed to determine the transient tritium release rate from $LiAlO_2$ plates under pulsed conditions. Because of the larger temperature-dependence of the tritium behavior, a 2-D time-dependent temperature calculation was performed first to determine the breeder plate temperature. The tritium release calculation included intragranular diffusion, grain boundary diffusion, pore diffusion, surface adsorption, and solubility.

The tritium release model is one-dimensional in the tritium transport pathway. Three separate zones are included: the grain interior, the grain boundary, and the interconnected porosity. Distance from the grain center is measured in non-dimensional units, where 0–1 is the grain, 1–2 is the grain boundary, and 2–3 is the interconnected porosity. Fig. 18 shows an example of the diffusive tritium concentration as a function of time in the three zones for $LiAlO_2$. The tritium generation rate

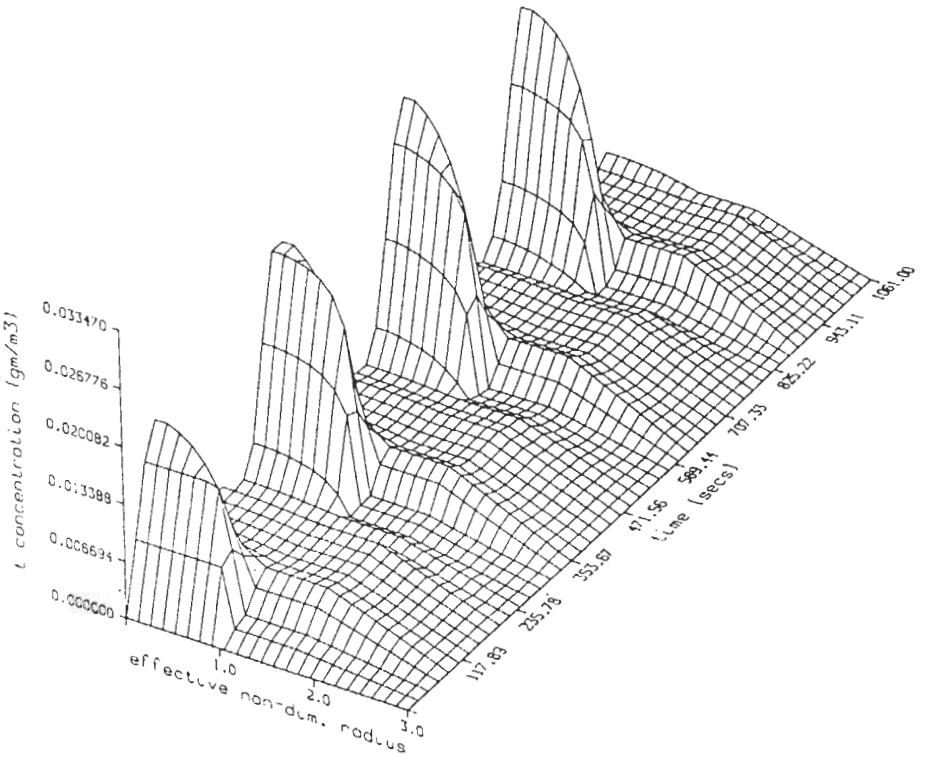

Fig. 18. $LiAlO_2$ diffusive tritium concentration profiles with 200-s burn, 50-s dwell, and 12-s ramp times (microscopic calculation).

is pulsed in accordance with the plasma burn scenario, with 200-second burn time, 50-second dwell time, and 12-second ramp times (during which the generation rate is assumed to increase or decrease linearly). The sharp increase of diffusive inventory during the initial part of the burn is due to the tritium production suddenly increasing while the temperature and, hence, the tritium diffusivity and solubility, remain relatively low. After the breeder heats up, the diffusive inventory quickly drops back down.

Fig. 19 shows an example of the tritium release rate from one $LiAlO_2$ grain to the purge flow (at an effective non-dimensional radius of 3.0) as a function of time from a location at the center of the breeder plate in the radial position nearest the plasma. The release rate is proportional to the gradient of the concentration (fig. 18) at the purge stream boundary. The tritium generation rate in the grain is also shown in the figure and illustrates the burn, dwell and ramp times considered for each cycle. For this example, the release rate takes about three cycles to reach its short-term maximum value. The tritium release rate per cycle is not equal to the tritium generation rate in the grain per cycle for the time period shown because of the assumed long surface adsorption response time. It is likely that at times of the order of the surface adsorption response time (1–10 h), the surface adsorption process will reach some type of quasi-steady state. The tritium released per cycle will then approach the tritium generated per cycle.

The release rate shows two peaks per cycle. This is an interesting behavior observed for the solubility data

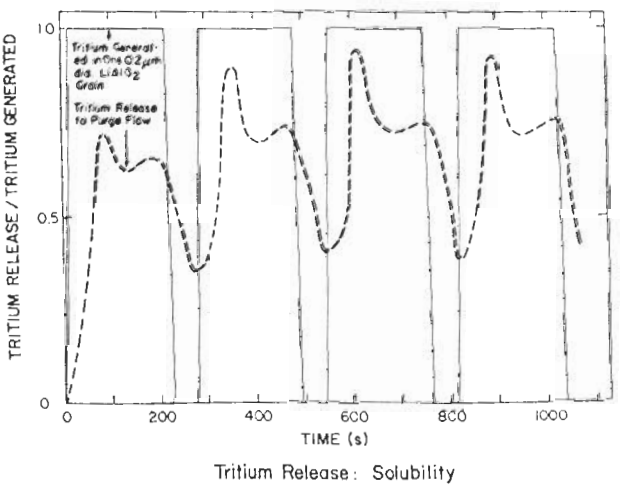

Fig. 19. Transient tritium release rate from 0.2 μm grain $LiAlO_2$ (for 200 s burn, 50 s dwell, and 12 s ramp times).

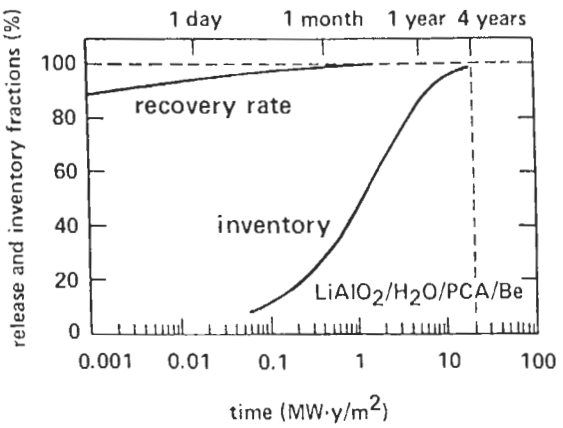

Fig. 20. Time-dependent of tritium recovery and inventory in $LiAlO_2/H_2O$/Be blanket [reprinted from ref. 1].

and time assumed in the calculations. The release rate increases initially as the generation rate increases, then the release rate begins to decrease due to dissolution. When the dissolution mechanism saturates, the release rate starts to increase again. Finally, during the ramp down and dwell times, the release rate decreases.

Figs. 18 and 19 show the large effect that pulsing has on tritium concentration profiles and release rates. This behavior is markedly different from that for steady-state operation. Experimental results with such short pulses may be difficult to interpret and extrapolate to reactor conditions.

The calculation above was performed at the front of the blanket where temperatures are the highest and diffusion is the fastest. The lower temperatures at the rear of the blanket lead to substantially longer time constants, which provide requirements on the total operating time as long as days, or even months. For example, fig. 20 shows the results of a calculation of the total, integrated blanket tritium release rate and inventory based on diffusion in a $LiAlO_2$ water-cooled blanket [13]. The release rate is relatively fast, provided the level of approximation to the equilibrium rate is not required to be too high. On the other hand, primarily due to the colder rear part of the blanket, the total inventory can take many months to reach an equilibrium. Important safety and fuel self-sufficiency issues will be difficult to assess without long total test times.

Analysis of the time-dependent thermal behavior of liquid breeder blankets was also performed. The importance of the velocity profiles in determining the magnitude on the steady state heat transfer coefficient has been clearly demonstrated in previous studies [1,31]. Here we have observed that the velocity profiles also play a major role in determining the time constant for temperature responses. Fig. 21 shows the wall temperature in a cooling channel several meters from the entrance. The first wall is subjected to a constant uniform heat flux of 0.5 MW/m^2 and no volumetric heating. Slug, parabolic, and skewed velocity profiles were assumed. The shape of the skewed profile is also shown in

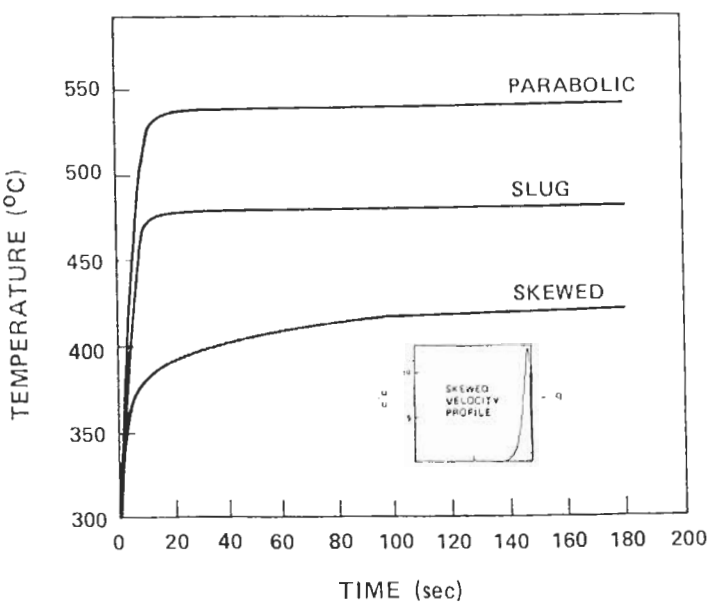

Fig. 21. Transient first wall temperatures of a liquid metal blanket cooling channel at 5 m from the inlet for different velocity profiles.

fig. 21. While the time to reach equilibrium for slug and parabolic profiles is roughly 10–20 s, the time for a skewed profile can be 100 s or longer.

2.1.4. Device geometry and test volume requirements

Testing of blanket components is assumed to occur at various test locations in the test device. Since the fusion engineering test facility will be the first accurate simulation of all reactor environmental conditions, a wide array of test types will be desired. Some of these tests will be oriented towards verification of overall component behavior, and some will focus on specific

Table 18
Examples of number and size of test articles required for fusion nuclear technology testing

Tests	Typical test article size (cm × cm × cm)	Number of test articles [a]
Specimen		
Structural material irradiated properties	1 × 1 × 2	30000
Solid breeder and multiplier irradiated properties	1 × 1 × 2	1200
Plasma interactive materials irradiated properties	1 × 1 × 5	900
Radiation damage indicator cross-sections	1 × 1 × 0.5	500
Long-lived isotope activation cross-sections	1 × 1 × 0.1	200
Element		
Structure thermomechanical response	10 × 10 × 10	50
Effects of bulk heating on heat transfer	10 × 10 × 100	5
Various element tests for solid breeder blankets	10 × 10 × 5	50
Weld behavior	10 × 10 × 5	50
Optical component radiation effects	2 × 2 × 2	20
Instrumentation transducer lifetime	1 × 1 × 2	70
Insulator/substrate seal integrity	1 × 1 × 2	20
Submodule		
Unit cell thermal and corrosion behavior	LB [b]: 100 × 50 × 30	5
	SB [b]: 10 × 50 × 30	5
Submodule mechanical responses		
Tritium behavior (e.g., permeation in coolant, response to thermal and flow transients)	10 × 50 × 10	3
Module		
Verification of neutronic predictions	50 × 50 × 100	4
- Tritium breeding, nuclear heating during operation, and induced activation		
Full module verification	LB [c]: 100 × 100 × 50	5
- Thermal and corrosion	SB: 100 × 100 × 50	5
- Module thermomechanical lifetime		
- Tritium recovery		
Shield effectiveness in complex geometries	50 × 50 × 100	50
Biological dose rate profile verification	DT device	1
Afterheat profile verification	DT device	1
Sector		
Blanket performance and lifetime verification	LB: 900 × 300 × 80	3
	SB: 300 × 100 × 80	3
Radiation effects on electronic components	1 × 1 × 1	20
Instrumentation performance and lifetime	5 × 5 × 5	100

[a] Test article defined as one physical entity tested at one set of conditions. Duplication of tests for statistical purposes, off-normal conditions, data at several time intervals, for high fluence tests, are *not* included in the number of test articles.

[b] LB = liquid breeder blankets, SB = solid breeder blankets.

[c] Some designs require larger test volume.

issues or elements of the design which can provide substantial information on the effects of the fusion environment. A proposed matrix of tests is provided in table 18, including five categories of increasing size and complexity: specimen, element, submodule, module and sector. The table characterizes the types of tests which are considered in each category and the approximate space requirements. Overall space requirements can be computed from this table if the use of parallel and sequential testing is properly considered. The total test surface area given earlier in table 13 does not include the "sector" testing indicated in table 18. Cost/benefit analysis needs to be performed prior to a decision on "sector" testing.

Besides space requirements, geometry can significantly impact the conditions in the test module. Important characteristics of the test locations and their relationship to the device include:

(1) the shape, volume, and surface area exposed to the plasma;
(2) the position of test parts relative to the device (e.g., inboard vs. outboard, proximity of other components); and
(3) the overall geometry of the device, including the plasma, magnetic field, and structure geometry.

These factors are grouped into the category of geometric test requirements.

In addition to determining test requirements, changes in the test module geometry can be intentionally utilized as a primary factor in engineering scaling. Engineering scaling in the test module can allow certain phenomena to be recovered if reduction in one of the device parameters results in an unacceptable loss of information.

Geometry influences most phenomena to some extent, but is a primary factor for neutronic, structural, and liquid metal MHD issues.

3.1.4.1. Geometric effects on neutronics responses

In a test device, it is desirable to maintain similar profiles of nuclear heating, tritium production, and radiation damage parameters in order to test the thermal and mechanical performance. The extent to which the profiles match the reference reactor defines the quality of the simulation. Tests to verify neutronics behavior are a special class, since the accuracy required in the measurements is much greater. Tritium production provides the most stringent requirements, because the required accuracy in predicting tritium self-sufficiency has been shown to be very high [14].

Extensive calculations were performed in previous FINESSE studies [1] to determine the effects of test module size, device size, plasma distribution, and test port geometry on the neutronics behavior of the blanket. The calculations were based on analysis of the helium-cooled Li_2O/HT9 plate-type breeder and the self-cooled lithium/vanadium-alloy designs; however, the results are expected to be generally applicable in other designs. The presence of a neutron multiplier of ^6Li enrichment will cause the most significant differences, since the contribution of low energy neutrons is greater in these cases.

Some of the largest effects occur due to altered boundary conditions, which result from factors such as partial coverage or non-prototypical reflector conditions. Changes in the volumetric tritium production rate due to partial coverage were explored using a two-dimensional neutron transport calculation [32]. Fig. 22 shows the geometrical arrangement assumed for the test module. The reference reactor blanket is assumed to provide full coverage in the poloidal angle, whereas the test module, in the partial coverage cases studied, occupies an angle of 2θ. The remainder is filled with a reflective filling material (stainless steel). Fig. 23 shows the ratio of the local volumetric tritium production rate

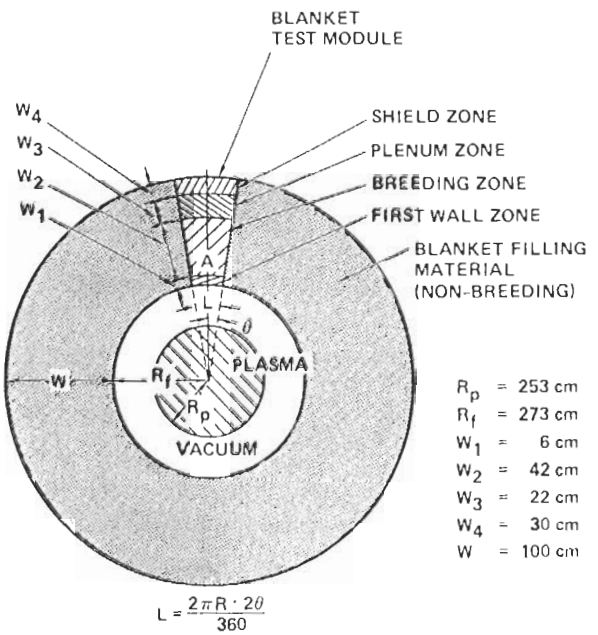

FIRST WALL ZONE:	PCA, 6.6% DENSE, BALANCE HELIUM
BREEDING ZONE:	6% PCA, 85% Li_2O (DENSITY FACTOR 0.8) BALANCE HELIUM
PLENUM ZONE:	PCA, 10% DENSE, BALANCE HELIUM
SHIELD ZONE:	100% STAINLESS STEEL

Fig. 22. Geometrical arrangement for the test module in a fusion test device [reprinted from ref. 31].

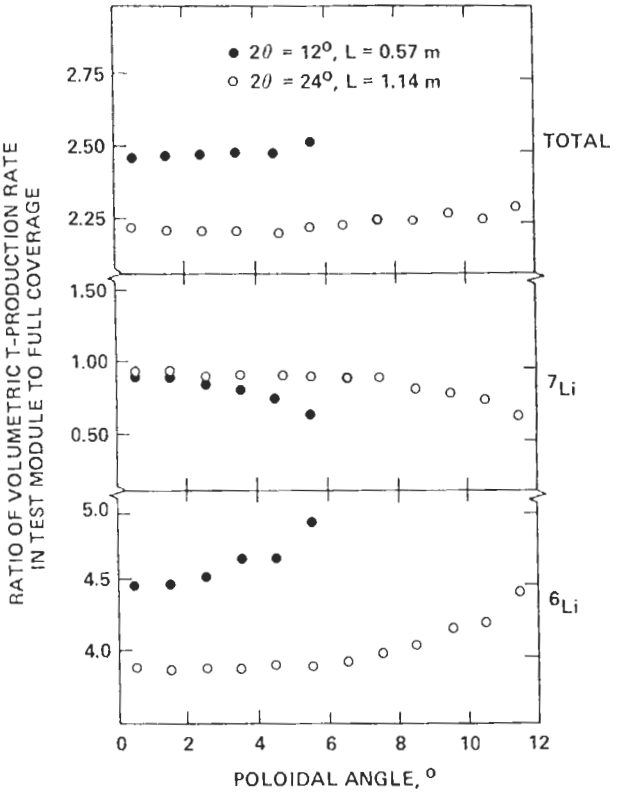

Fig. 23. Variation of the local tritium production rate in the poloidal θ direction for two test module sizes, $\theta = 6°$ and $\theta = 12°$ [reprinted from ref. 31].

as a function of the poloidal angle in the partial coverage case as compared to the full coverage case. Two test module sizes are shown: $2\theta = 12°$ and $2\theta = 24°$. A local increase in volumetric tritium production is observed, primarily due to the contribution from ^{6}Li.

Altering the absolute value of the tritium production rate adds significant uncertainty to the demonstration of tritium self-sufficiency. Altering the spatial gradients adds to this uncertainty, and also restricts the ability to perform accurate neutronic measurements.

Calculations of the effect of varying the device size and test module dimensions (including width, radial depth, and first wall thickness) indicate that the neutronic parameters in the test module usually can be maintained within 20–30% of reactor values, provided the boundary conditions are suitably maintained. The impact of scaling can be roughly judged from a knowledge of the neutron mean free paths in the blanket materials. The mean free path is roughly 5 cm in structural materials, 7.5 cm in solid breeder materials, and 15 cm in liquid lithium. If the first wall thickness is increased beyond 2–3 cm or the blanket radial depth is decreased to less than about 20 cm, then the neutronic profiles will be affected significantly (by 25% or more). These conclusions are supported by more detailed calculations [33].

In conclusion, adequate simulation of neutronics parameters in the test module should be feasible for testing most non-neutronics issues (e.g., thermomechanics and tritium recovery), provided the dimensions are not changed by more than a factor of 2–3 away from the reference reactor values. However, measurements of tritium breeding ratio and some other neutronics parameters require much higher accuracy, and may not be practical without full-size "look-alike" test modules (or full sectors). If modules are used, the surface area at the first wall should be no less than 1 m × 1 m. Further details on neutronics test requirements can be found in ref. [33].

3.1.4.2. Geometric effects on structural responses

Elastic stresses and strains can usually be preserved even if the test volume is limited, provided aspect ratios are maintained. The same is not true for inelastic strains. For example, structural effects due to radiation damage are difficult to scale because the damage profiles depend primarily on neutron reaction cross sections and kinematics, which are relatively independent of geometry. The impact of altered damage profiles can be very large.

Structural response is so dependent on the loading conditions, that a more important issue is how geometry affects thermal stresses, pressure stresses, and so on.

Aspect ratio scaling is an important option in test module design, but great care must be maintained in order to avoid altering the other phenomena in the test. For example, as discussed below, heat transfer in liquid metal blankets depends more on the channel length than the length-to-diameter ratio.

3.1.4.3. Geometric effects on MHD-related responses

The uncertainties in liquid metal MHD-related phenomena (discussed in more detail in the next subsection) arise almost entirely due to the complex influence of geometry. The velocity profiles not only depend on the channel dimensions and shape, but also on the wall thickness and the blanket configuration outside the channel. They are also strongly influenced by the details of the magnetic geometry. Because of these dependencies and because it is precisely these interactions which provide the largest uncertainties in blanket behavior, very careful attention must be given to geometric similarity for testing liquid metal blankets.

The test requirements on space can be very severe. The two primary reasons for this are the possibility of long entry lengths for the development of velocity, temperature, and mass concentration profiles, and the possibility of global (interchannel) eddy currents.

One possible method of scaling to allow testing in smaller modules involves the concept of residence time. For diffusive processes, including heat and mass transfer in laminar flow, profile development depends primarily on the amount of time the fluid is in the channel. Reducing the flow velocity in proportion to the reduction in channel length will result in approximately the same level of profile development. This is especially important because the heat and mass transfer coefficients are very strong functions of distance along the channel in the entrance region.

Another phenomenon which would require larger test modules is global eddy currents. Global eddy currents can arise when geometric perturbations cause voltage differences between channels. If the structure is electrically continuous (i.e., the channel walls are not insulated), interchannel currents can have a large influence on both velocity profiles and pressure drop. This occurs because the MHD-induced currents are no longer constrained to return through thin channel walls. If aspect ratios are maintained, then global eddy currents may be reproduced in smaller test modules; however, the smaller test modules must contain the relevant geometric details of the larger reference blanket.

Because of the large negative impact of global eddy currents, they should be eliminated in reactor designs. However, testing must confirm this. Even a small amount of interchannel current could have a significant effect.

3.1.5. Magnetic field requirements

Except for ferromagnetic forces (in ferritic steels) and transient magnetic field effects, the influence of the magnetic field is limited primarily to liquid metal blankets. Many liquid metal blanket phenomena are influenced by the magnetic field through its effects on the fluid dynamics. The interaction of magnetic fields with flowing liquid metals is generally referred to as liquid metal magnetohydrodynamics, or MHD. The most important effects are an increase in the pressure drop across the blanket, leading to high internal pressures and higher pumping power, and changes in heat and mass transfer resulting from fluid mechanics which bears little resemblance to that of ordinary fluid flow. For further details on liquid metal MHD and its effects in liquid metal blankets, see refs. [34–36].

Both self-cooled and separately cooled liquid metal blankets can be strongly affected by the magnetic field. The liquid metal flow rate in separately-cooled designs is determined primarily by tritium extraction requirements. In LiPb systems, with its extremely low tritium

Table 19
Definitions and evaluation of MHD parameters

Parameter	Definition	Typical reactor values	
		Li	17Li–83Pb
Hartmann number	$\mathrm{Ha} = aB\sqrt{\frac{\sigma}{\mu}}$	6.3×10^{4}	1.6×10^{4}
Reynolds number	$\mathrm{Re} = av\frac{\rho}{\mu}$	6.6×10^{4}	3.1×10^{5}
Interaction parameter	$N = \frac{aB^2}{v}\frac{\sigma}{\rho}$	6.0×10^{4}	825
Magnetic Reynolds number	$\mathrm{Re_m} = av\,\mu_0\sigma$	0.19	0.052
Wall conductance ratio	$C = \frac{\sigma_w t}{\sigma a}$	0.025	0.090
Property values: (all units mks)		$\sigma = 3\times10^{6}$ $\mu = 0.38\times10^{-3}$ $\rho = 495$	0.83×10^{6} 1.5×10^{-3} 9200
Reactor conditions assumed: (all units mks)	$a = 0.1$ $B = 7$ (at inboard) $v = 0.5$	$\sigma_w = 1.5\times10^{6}$ $t = 0.005$ $\mu_0 = 4\pi\times10^{-7}$	

solubility, the required flow rate could be nearly as high as the coolant flow rate in order to keep tritium permeation within acceptable limits. Even if separately-cooled blankets require very small flow rates, the magnetic field will still significantly alter pumping requirements, material interactions, and heat transfer (especially natural convection).

A small number of nondimensional parameters (defined in table 19) are typically used to described the MHD flow regimes. These include the Hartmann number (Ha), which represents the ratio of magnetic forces to viscous forces; the interaction parameter (N), which represents the ratio of magnetic forces to inertial forces; the magnetic Reynolds numbers (Re_m), which is the ratio of induced field strength to the applied field strength; and the wall conductance ratio (C), which determines the level of control that the walls exert over the flow conditions. Table 19 summarizes the important dimensionless parameters and evaluates them for representative reactor conditions using properties for both Li and 17Li–83Pb. In most fusion applications, the Hartmann number and interaction parameter are extremely large (order of 10^3–10^5), indicating that the magnetic field totally dominates the fluid flow characteristics (there are exceptions, such as reversed-field pinches, in which Ha and N are much lower). The magnetic Reynolds number is very small, which means that induced magnetic fields can be neglected, leading to substantial simplifications in modeling. And finally, the wall conductance ratio is small but finite.

Achieving values of these parameters in an experiment identical to those in the reference blanket ensures the experiment will be fully prototypical in MHD flow. Most test reactor designs provide magnetic field strengths very close to the value prescribed in the reference reactor. However, regions of high magnetic field in a fusion test facility, such as the tokamak inboard region, are generally not considered for test modules because of space, cost, and accessibility. Furthermore, the closely related parameters of magnetic field geometry and test module size are of equal or greater importance in determining the fluid flow characteristics, as discussed earlier in the subsection on geometry.

MHD effects are treated here in three parts: MHD velocity profile and pressure drop requirements, MHD heat transfer requirements, and MHD mass transfer requirements.

3.1.5.1. MHD velocity profile and pressure drop requirements

While preserving the exact values of the nondimensional parameters ensures prototypical operation, it may be possible to reduce the device parameters and still adequately test blanket components. The most difficult parameter to maintain is the Hartmann number, which is proportional to both the magnetic field strength and the test module dimension along the field line. While the magnetic field in the test reactor will probably be nearly the same as the reference conditions, the region available for testing on the outboard of a tokamak will most likely have a much lower field than the inboard region (typically a factor of 2). Furthermore, in these testing regions space is likely to be limited. The interaction parameter can be adjusted by varying the bulk velocity, but this technique is risky, because other phenomena (heat transfer in particular) may be strongly affected.

Operating at reduced parameters may be acceptable if the most important phenomena are adequately simulated. For the pressure drop and velocity profiles (ignoring the secondary effects on heat and mass transfer), the most important requirement is to maintain similar fluid flow regimes. In this case, the data should be easily extrapolated.

One important regime to maintain is suppression of turbulence. This is discussed below as part of the heat transfer requirements. In addition, different flow regimes can result when the balance of forces changes. For example, it is known that the characteristics of flow around bends turning parallel to the magnetic field depends on the competition of inertial and viscous effects. The requirement to maintain reactor prototypical regimes for this type of geometry is $Re \gg Ha^{1/2}$. More details on MHD flow regimes can be found in refs. [1] and [2].

A complication arises because the scaling of pressure drop and velocity profile as a function of the nondimensional parameters depends on geometric factors. Geometries have been identified in which fractional powers of the wall conductance or Hartmann number are involved. For example, boundary layers near magnetic field entrance regions might scale like $C^{1/6}$ [37]. Inertial terms which are normally neglected can become important if $C < N^{-3/5}$, which is a regime that is entirely possible in future blanket designs.

At the present time, there are many uncertainties in liquid metal MHD. The correct scaling of MHD fluid flow is known only for a small number of simple geometries. In this atmosphere of uncertainty, conservatism is necessary in establishing the test requirements. A magnetic field greater than 1–2 T is clearly needed. However, operation above 5 T in the region where the test modules are located would remove many uncertainties.

3.1.5.2. MHD heat transfer requirements

Because of its influence on the velocity profiles and suppression of turbulence, the magnetic field is also a dominant factor in determining the thermal and structural characteristics of liquid metal blankets. A determination of the minimum required magnetic field must take account of these effects as well as the basic fluid mechanics.

The fact that the flow is laminarized in a strong magnetic field has a huge effect on heat transfer, leading to a large reduction in the heat transfer coefficients and great increases in the thermal entry length. The transition from turbulent to laminar flow occurs at Hartmann numbers lower than those expected in any test reactor (Ha > Re/500 for magnetic field perpendicular to the flow and Ha > Re/60 for magnetic field parallel to the flow [34]). Magnetic field strengths greater than about 1 T are required.

Probably more constraining are restrictions due to the changes in heat transfer coefficient that accompany changes in the spatial variation of the velocity profiles. The velocity profiles in MHD flow can usually be separated into the core region and boundary regions for the purpose of analysis and discussion. The flow quantity in the boundary layers (such as Hartmann layers) is negligible in many cases of interest. If the hydrodynamic boundary layer is much thinner than the thermal boundary layer, then the hydrodynamic boundary layer is nearly transparent to heat transfer. The thermal boundary layer thickness depends on location in the blanket. At channel inlet regions, it can be extremely small; at the exit of a channel of length 1–10 m, it may be of the order of centimeters. Velocity boundary layer thicknesses tend to be inversely related to Ha and N. Although the Hartmann number and interaction parameter are usually very large, the layer thickness can be related to a fractional power of the nondimensional parameters. The requirements would then be much more stringent.

In some cases, the flow quantity in the layer is finite. For this type of flow, the effect on heat transfer can be very strong, and better simulation of the nondimensional parameters is required.

It is known that the heat transfer coefficient is altered by bulk heating when the velocity profiles are strongly nonuniform. As above, the requirement on magnetic field depends on the nature of the boundary layers.

In conclusion, the effect of the magnetic field on heat transfer is not simple to describe, but rather depends on the details of the geometry and wall conductivity. In many cases of interest, if the Hartmann number and interaction parameter are larger than 10^3, then the heat transfer coefficient should not be greatly affected by further increases. Cases in which higher field would probably be required include:

(1) nonconducting duct,
(2) geometric perturbations which lead to fractional scaling in B, and
(3) boundary layers with finite flow quantity.

More quantitative definition of the minimum field for heat transfer simulation will require further analysis.

3.1.5.3. MHD mass transfer requirements

Mass transfer is also affected by the magnetic field through the MHD velocity profiles. In this case, the thickness of mass diffusion boundary layers is much thinner than thermal boundary layers. Therefore, the core flow is relatively unimportant.

The details of the thin MHD velocity layers can affect mass transfer if they are not much thinner than the mass diffusion layer thickness and if mass transfer is determined primarily by convection in the liquid phase. Past studies have shown that for liquid-phase dominated mass transfer there can be an increase of as much as a factor of 5 in corrosion rate if the Hartmann number is increased from about 100 to about 10000 [1]. For Ha > 10000, the effect is largely saturated because the Hartmann layer thickness is smaller than the mass diffusion boundary layer thickness. The corresponding magnetic field strength depends on the channel dimensions: for a 10-cm channel, this corresponds to a field strength of about 1 T.

This estimate is very preliminary, since data about material interactions is limited, even outside the magnetic field. It is not at all clear that solid phase diffusion and interface reactions can be ignored in determining the corrosion rate. More analysis is clearly needed to determine test requirements due to liquid metal material interactions.

3.2. Tritium supply

Ensuring adequate supply of fuel is an absolute requirement for successful operation of a DT fusion test facility. The amount of tritium needed for the test facility is uncertain because the characteristics of the reactor and its operating scenario are not firmly fixed at this time. The amount of tritium available from external sources is limited. If the requirements for tritium cannot be economically met from external sources, then internal tritium production must be provided by tritium-producing blankets.

Table 20
Potential tritium sources [38–41]

Source	Supply rate (kg/yr)	Inventory (kg 1986)
Atmosphere/oceans		
Cosmic rays	0.2	4
Atmospheric bomb tests	0	145
Unmodified power reactors		
PWR/BWR (1 GWe)	0.002	0.006
CANDU (12 GWe)	2.5	8
Modified power reactors		
PWR/BWR (1 GWe)	0.1	0
CANDU (1 GWe)	0.5	0
Fuel reprocessing plant		
1000 Mg U/yr capacity	0.05–0.1	?
Military production reactors		
US/USSR/UK/France/China	30 –40(?)	?

Table 20 summarizes the potential external sources of tritium [38–41]. The most significant civilian source is existing fission reactors. CANDU reactors produce larger amounts of tritium than standard LWR's due to neutron absorption in deuterium in the heavy water moderator and coolant. Present CANDU reactors produce about 0.21 kg/yr of tritium per GWe. Both light-water and heavy-water fission reactors could be modified to produce more tritium by replacing fuel or absorber material with lithium. In CANDU reactors, this enhanced capacity has been estimated at 500 g/yr per GWe (for no change in power production).

Overall, there is a reasonably assured steady supply of 2–2.5 kg/yr from CANDU reactors, and there is a potential for an additional 1 kg/yr from modified power reactors and fuel reprocessing. The availability of tritium from military production reactors is very uncertain.

It is likely than an engineering test facility would operate in separate phases of increasing availability and, therefore, of increasing tritium consumption. During the initial phases of commissioning, plasma optimization, and short-duration engineering performance testing, the total tritium consumed would be small. A calculation for NET estimated 4 kg of tritium total needed to operate during these phases [42]. This amount is probably available from existing sources such as CANDU reactors.

During the high-availability testing phase, the tritium consumption rate at 25% availability and 600 MW fusion power will be 8.4 kg/yr (56 g/MW yr is the conversion constant). From the evaluation of possible external supplies given above, tritium to sustain a device with such power over long periods of time will be difficult to obtain. There are great incentives to design a test facility with lower fusion power to reduce capital costs, tritium and other operating costs. Fusion nuclear technology testing requires only about 20 MW of fusion power, but plasma physics and engineering considerations for tokamaks require fusion power greater than ~ 300 MW at reasonable wall loading.

Even if tritium could be made available from external sources, the financial burden might be prohibitively high. Using an estimated present cost of tritium of $10000/g, a consumption rate of 8.4 kg/yr translates into an annual operating cost of $84 million for tritium alone. Producing tritium within the test facility may be a financial necessity.

The operation of tritium-producing blankets as a part of the test facility has been considered in several previous studies [5,26]. There are a number of possible options for "internal" tritium production. For example, the NET team is considering water-cooled LiPb eutectic, water-cooled solid breeder, He-cooled solid breeder, and self-cooled liquid breeder blanket options [42]. The INTOR group, in its Phase II report chose water-cooled Li_2O as the primary option [26]. Water-cooled Li_2SiO_3 with Pb multiplier and water-cooled 17Li–83Pb were chosen as alternates. Recent studies have explored the use of aqueous lithium salt blankets [43–45].

Risk is an important concern in making a decision to implement a tritium-producing blanket in a test facility, and also in the choice of a specific blanket option. If a tritium-producing blanket must be implemented, several measures can be taken to reduce the risk. First, one can select the design which appears most feasible using existing technology to the maximum extent possible, and operate with temperatures and pressures as low as practical. It should be noted, however, that the fusion environment will be "new" to any type of blanket selected. Provisions must be made to cope with unanticipated problems or changes in behavior. In addition, a key problem with this type of blanket is that the information obtained through its operation will probably not provide the maximum benefit for extrapolation to commercial reactor blanket designs. Second, an aggressive pre-fusion test program must be implemented to eliminate as many potential failure modes as possible. Without fusion testing, it is difficult, if not impossible, to fully qualify a tritium-producing blanket of any design.

In this study, a clear distinction is made between the functions of a test blanket (or "blanket test module") and a tritium-producing blanket. The two functions

may be performed in a single component; however, the objectives of maximizing device availability and maximizing testing benefit may dictate separate components. In general, it is clear that many design options exist and there are no clearly superior choices. Much more effort and analysis are required in this area.

3.3. Blanket reliability and device availability

If tritium-producing blankets are used in ETR, then blanket components will require a program of pre-operational testing and development. Depending on the desired tritium breeding ratio, and hence the total number of breeding modules employed, the test time needed to confidently provide an acceptable impact on overall device availability may be very long (> 10 years).

The required pre-operational testing of blanket modules has been evaluated by performing parametric studies in three areas:

(1) Calculation of the minimum mean time between failure (MTBF) required to achieve a given availability goal for the blanket system.
(2) Calculation of the amount of pre-operational testing required to provide a given amount of confidence in meeting the MTBF requirement.
(3) Determination of the effect of parallel testing on the time required to reach a given level of confidence in the MTBF.

There is a trade-off between the amount of pre-testing of tritium breeding blanket modules (required to achieve some overall blanket availability goal) and the need for externally supplied tritium. If a smaller tritium breeding ratio is acceptable (and, therefore, a smaller number of breeding modules are employed), then the testing needed to obtain a given level of confidence in the overall blanket availability is reduced. At the same time, the presence of fewer breeding modules results in a greater need for externally-supplied tritium. Analysis is provided to compare the on-site tritium breeding cost savings and the blanket module testing time requirements.

For the purposes of this study, it is assumed that the ETR operation goal is an availability of 50% and that this requires a tritium breeding blanket availability goal of at least 80%. These and other assumptions are summarized in table 21. Operation with fewer than the full number of breeding modules is assumed to reduce the tritium breeding capability of the machine linearly.

Fig. 24 shows the three standard periods during component life. "Burn-in" and "wear-out" failures are not considered here. It has been assumed that pre-operational testing has been successful in eliminating design and fabrication problems which can result in early failures. The analytic model used in this analysis pertains to the useful life period and assumes that module failure occurs due to the randomly-occurring event, a process which can be described by an exponential distribution of failure times.

Table 21
Representative ETR parameters considered in the reliability analysis

Fusion power	300 MW
ETR availability goal	0.5
Blanket availability goal	0.8
Number of blanket sectors	12
Number of modules per sector	5
Total number of modules	60
Number of test modules	2 minimum [a]
Full coverage TBR	1.05
Tritium consumption rate	8.4 kg/FPY
Tritium cost	$84 M/FPY

[a] Two test modules are provided even for the "full coverage" case, resulting in a TBR of 1.05 with 58 tritium breeding modules. The number of test modules can be increased for lower coverage cases.

If the availability for an individual blanket module is given by a_m and there are n identical blanket modules, then the overall blanket system availability is:

$$A_b = a_m^n,$$

where a_m is the "availability" per module and is a function of the MTBF and the mean time to repair (MTTR):

$$a_m = \mathrm{MTBF}/(\mathrm{MTBF} + \mathrm{MTTR}).$$

If the MTTR, A_b, and n are specified, then the MTBF for a blanket module can be calculated directly. Fig. 25

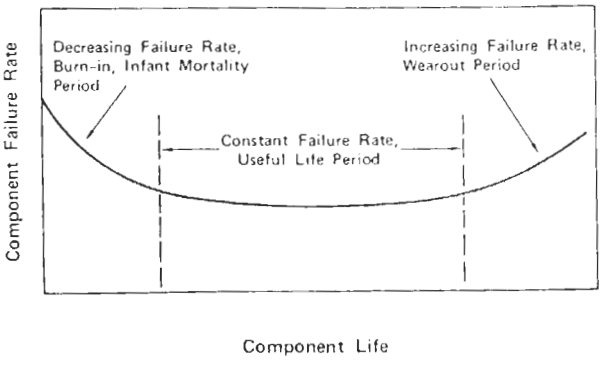

Fig. 24. Failure rate over component life.

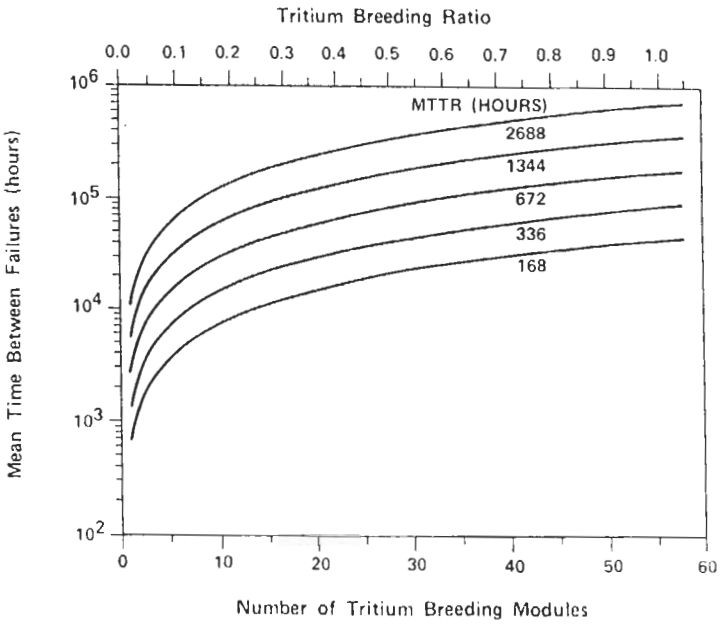

Fig. 25. The tritium breeding module MTBF (at various values of MTTR) necessary to achieve a blanket availability goal of 0.8 as a function of the number of tritium breeding modules (and tritium breeding ratio).

shows the MTBF for tritium breeding modules (at various values of MTTR) required to achieve an overall blanket availability of 0.8 as a function of the number of breeding modules and the breeding ratio.

If blanket module testing is viewed as a series of time-terminated trials, then the occurrence of module failures can be described as a Poisson process. A detailed derivation of the failure rate confidence level

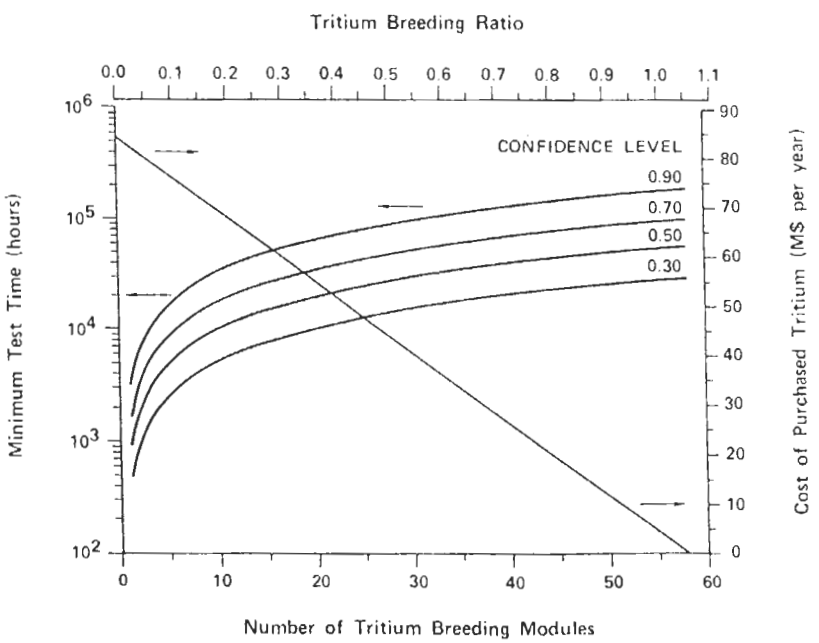

Fig. 26. Minimum required testing time (at various confidence levels) to achieve a blanket availability of 0.8 as a function of the number of tritium breeding modules and tritium breeding ratio. Also shown is the cost of external tritium supply as a function of the breeding ratio.

versus the expected failure rate, total testing time, and test failure occurrences is given in ref. [9]. Using Poisson statistics, fig. 26 shows the minimum test time to achieve a given confidence level in the availability goal. This test time increases with the number of tritium-breeding modules because the required MTBF per module increases. For all these cases, the MTTR was fixed at 336 h and the number of test failures was assumed to be zero. The confidence in a given MTBF is actually degraded by test failures, making this a best-case estimate.

Also shown in fig. 26 is the cost of tritium required from external sources if the number of breeding modules is less than 58. (A full-coverage TBR of 1.05 is achieved with two test modules and 58 tritium breeding modules). As stated above, the amount of make-up tritium is assumed to be linearly related to the number of breeding modules.

In conclusion, for a facility with 300 MW of fusion power and an availability goal of 50% (a tritium-producing blanket availability goal of 80%), the required MTBF may be 90000 h or more, depending on the module replacement time. High confidence (90%) in this level of performance will require testing times of at least several times the MTBF. Parallel testing can significantly reduce the actual calander time for testing, although more elaborate testing programs will be more expensive.

It is quite likely that such lengthy testing times will not be achieved prior to fusion testing. If significant tritium breeding is attempted in ETR without adequate testing, then confidence in the breeding modules, in a statistical sense, will be low. This means high risks for the fusion test facility. Such risks should be reduced by an aggressive development program prior to fusion testing. However, tradeoffs among increased costs and risks for the fusion facility must be carefully weighed in plans for a fusion engineering test facility.

4. Theory and modeling

4.1. Introduction

A fundamental objective of the R&D plan for fusion nuclear technology is the development of predictive capabilities, which are necessary to design, construct, and operate fusion nuclear components. This requires a highly interactive program of theory, modeling, and experiments. In the early stages of R&D, theory and models are used to anticipate scientific and engineering phenomena, to define performance parameter ranges of interest, and to characterize uncertainties. Thus, theory and modeling are necessary in planning and designing experiments to maximize their benefits. Results from experiments are then used to verify analytical and numerical models.

The coupling between experiments and modeling efforts in fusion nuclear technology is shown more clearly in fig. 27, developed previously in FINESSE. Whereas the ultimate goal of the experimental program is fusion integrated testing, the ultimate goal of the modeling program is an integrated set of design codes for overall predictions of the performance of fusion nuclear components. This design code may consist of a combination of analytical, numerical, and empirical parts.

The major components of interest in fusion nuclear technology are the blanket, tritium and vacuum system, plasma-interactive components, and radiation shielding. The present level of understanding and available methods to model each of these components vary considerably. In the liquid metal blanket, for example, the interaction between the magnetic field (necessary for plasma confinement) and the flow of the liquid metal coolant can be represented by Navier-Stokes and Maxwell's equations. Although these equations are well defined, they are extremely difficult to solve fully because of the non-linearity and the three-dimensional nature of the problem. Modeling of tritium transport systems in solid breeder blankets, on the other hand, is complicated due to the lack of understanding of the microscopic transport processes in the fusion environment.

The blanket has received the largest amount of attention, particularly liquid metal blankets. The emphasis on modeling liquid metal blankets has been motivated by two reasons: (1) the present ability to predict blanket thermomechanics, particularly MHD effects, is very

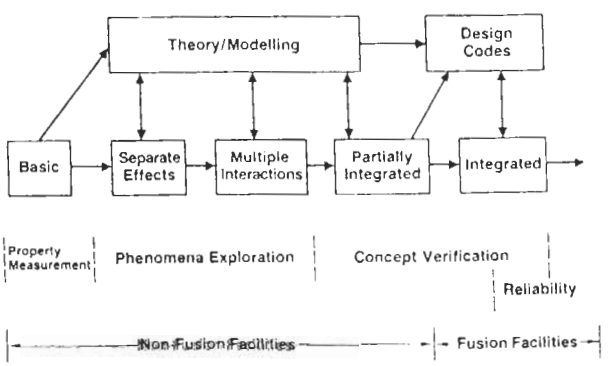

Fig. 27. Types and role of experiments and facilities for fusion nuclear technology (reprint from Phase I FINESSE report [2]).

limited; and (2) the potential for advancement in predictive capabilities and the planning of effective experiments through theory and model development is great.

Numerical analysis for several simple MHD fluid flow and heat transfer problems is described. The analysis uses both the finite element method for fully developed MHD flows and the finite difference method for developing flows. The examples described constitute initial attempts to treat the full set of MHD equations, including viscous and inertial effects. Extending the range of problems that can be solved using the full solution remains a considerable challenge. Approximate solutions which neglect inertial and viscous effects avoid many of the numerical problems associated with the full solution. These methods offer potential advantages for treating many important problems, and are currently under study. However, no further discussion is made here.

Theoretical and experimental studies of heat transfer in liquid metal blankets were carried out to explore the effects of bulk heating on heat transfer and to define the validity of probe measurements under the conditions of bulk heating.

Work on areas other than liquid metal blankets has also been performed. The development of a preliminary model for predicting tritium transport and inventory in solid breeders is described. Thermomechanical modeling of liquid metal cooling of limiters is discussed, in which thermal hydraulic and structural analysis are included.

4.2. Liquid metal MHD modeling

Fig. 28 shows a logic diagram for MHD model development that traces the primary elements in the modeling program and their relationships. Three primary modeling tasks are shown: theory and analytical method development, numerical methods, and analysis. The intimate ties with the experiments and the interaction with conceptual design studies are illustrated in the figure. The ultimate aim of the MHD modeling effort is a design code for liquid metal blankets. How-

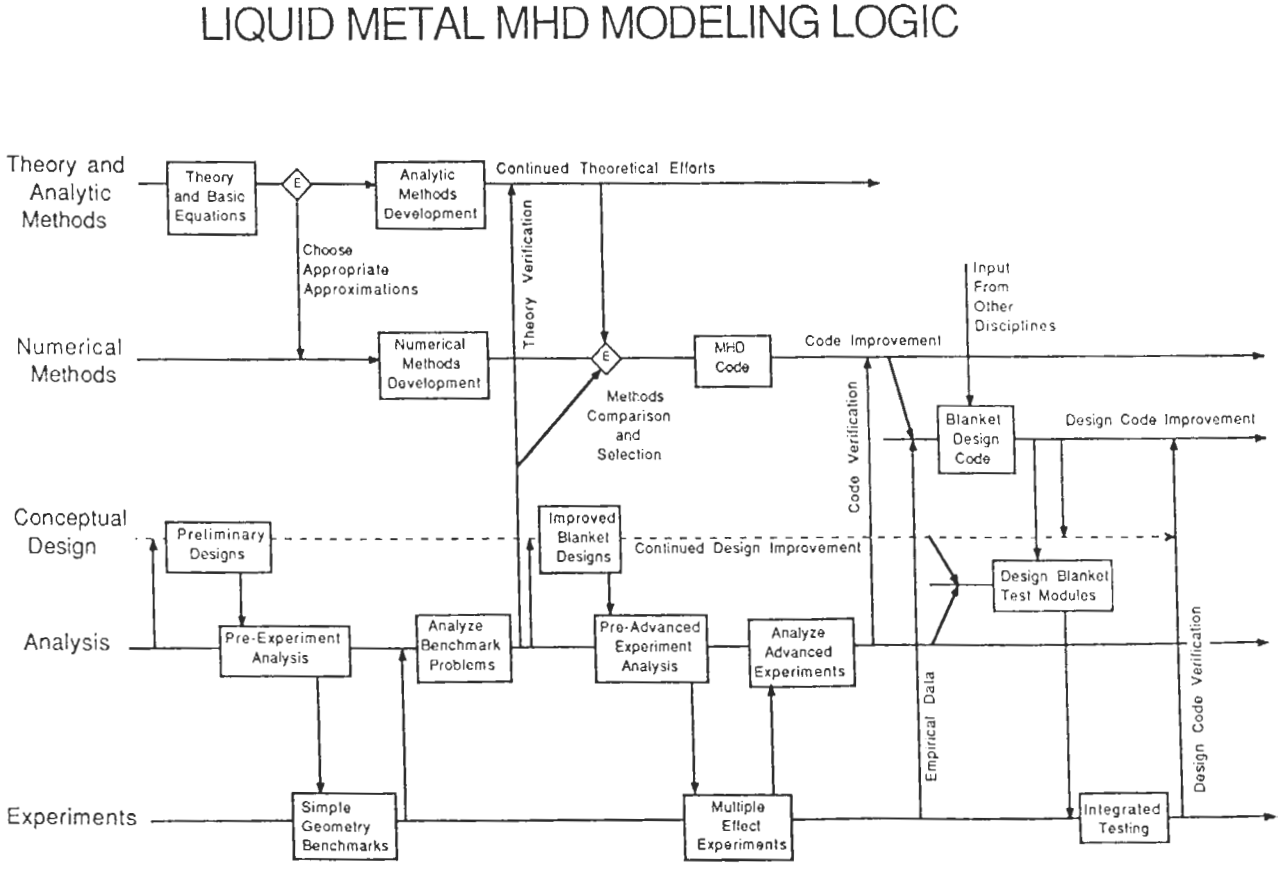

Fig. 28. Liquid metal MHD modeling logic.

ever, to achieve that goal, different stages of development will be encountered where modeling of simpler geometries will be performed in the early stages to validate and guide the improvement of the models.

Approximate analytical solutions to simplified sets of the MHD equations for flows at high hartmann numbers and interaction parameters can be found in the work of Hunt [46], Walker et al. [47], Walker and Ludford [48], Petrykowski and Walker [49], and many others. Asymptotic techniques to analyze large interaction parameter flows are employed. A separate solution is obtained for the inviscid core region, which is matched to the boundary layer solution. Analytical solutions provide important physical insights, but are very limited in the range of fusion-relevant problems which can be treated.

By using and modifying existing methods in computational fluid dynamics (CFD) to account for the magnetic forces, solutions to practical MHD problems may be obtained. These and other numerical techniques based on infinite Hartmann numbers and interaction parameters (which render the flow inertialess and inviscid) offer the potential to solve problems in geometries and parameter ranges for which purely analytical solutions are intractable.

MHD problems solved numerically in this work utilized the SIMPLE (Semi-Implicit Method of Pressure Linked Equations) [50] method to predict the flow development of a conducting fluid in simple two-dimensional geometries in the presence of a magnetic field. The finite element method was also used to solve the fully developed flow in rectangular ducts with a perpendicular field, where a mesh refinement technique was emphasized in the solution procedure to resolve the thin Hartmann layer near the walls.

Numerical problems arise in dealing with liquid metal flows under strong magnetic fields. These stem from the diminishing effect of inertia and viscosity, and the disparate scale lengths in the core region and boundary layers. For very high magnetic field, magnetic forces are larger than inertial and viscous forces that are used for correcting the pressure in CFD. Modifications to the pressure correction procedure are necessary to account for the electromagnetic forces, and future plans will be aimed in that direction, which might be termed as computational magnetohydrodynamics (CMHD). Improvements in the use of mesh refinement will also contribute to the accuracy of the solution.

These first attempts at numerical solutions to the MHD flow equations were performed primarily to develop and test certain solution techniques. The ultimate development of an MHD code for fusion applications will require years of concentrated effort and much work remains to be done.

4.2.1. Computational magnetohydrodynamics

The calculational procedure solves the equations of motion (Navier-Stokes equation) and Maxwell's equations, which describe the flow of a conducting fluid in the presence of a magnetic field. The flow is assumed steady, incompressible and laminar, and two-dimensional duct geometries are considered. The assumption of small magnetic Reynolds number decouples Maxwell's equations from the hydrodynamic ones. In this case, the induced magnetic field is neglected and the magnetic body force is linearly related to the velocity field through Ohm's Law.

The finite difference solution algorithm is based on the SIMPLE method [50] where an iterative process of pressure and velocity guess and correct operation is utilized to drive the residual mass errors to zero or small values. Because the magnetic Reynolds number is small, the magnetic body forces in the hydrodynamic equations can be directly related to the velocity field through Ohm's Law. The electromagnetic body force thus appears as a source term in the momentum equations. When the electromagnetic forces are very large compared to the viscous or inertial forces, divergence may result.

The general discretized equation of the differential equations can be written as:

$$A_P\phi_P = A_N\phi_N + A_S\phi_S + A_E\phi_E + A_W\phi_W + S_\phi, \qquad (1)$$

where ϕ stands for the dependent variable being solved, and A_P, A_N, A_S, A_E and A_W are the coefficients at nodes P, N, S, E and W, which characterize a control volume, and S_ϕ is the source term of the variable ϕ, which can represent external body forces, such as electromagnetic ones.

The problems analyzed numerically include developing flow in ducts with the magnetic field in the plane of the flow aligned with the main flow direction or perpendicular to it. The development of two-dimensional velocity and temperature profiles are explored for a conducting fluid in the entrance region of straight ducts in the presence of a magnetic field. The main effect of a magnetic field aligned with the flow direction is to delay flow development.

In a pipe flow, for example, the development of the centerline velocity along the pipe can be seen in fig. 29 for a range of values of N/Re, where N is the interaction parameter and Re is the Reynolds number. The centerline velocity (u_c) is normalized with respect to the

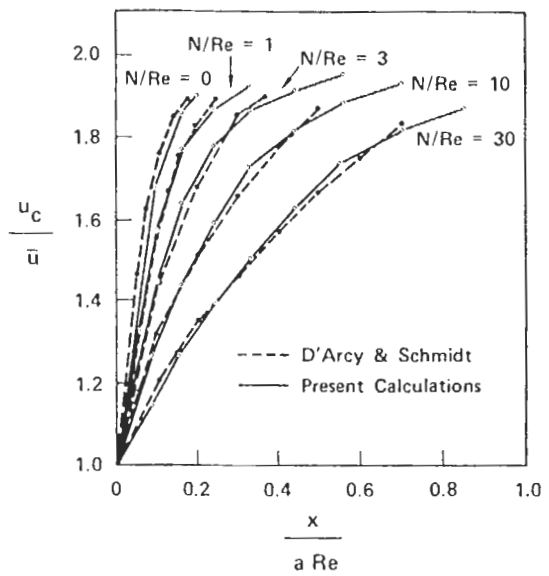

Fig. 29. Effect of an axial magnetic field on the development of centerline velocity along the axial distance (x) in a pipe of radius a.

average velocity across the pipe. The results compare favorably with the analytic solution of D'Arcy and Schmidt [51]. The electrical conductivity of the pipe walls remains arbitrary and has no effect on the dynamics of the flow. As can be seen from the figure, for $N/\mathrm{Re} = 30$, the entry length is about 3.5 times that of the non-magnetic case.

In a channel flow, the delay in flow development due to a parallel field can be clearly seen in fig. 30. The velocity at the entrance is either a slug or a skewed profile and the channel walls are assumed insulated. The channel half-width is a. The figure shows the development of the velocity profile along the channel for different values of Hartmann number (Ha). For $\mathrm{Ha} = 0$ and $\mathrm{Ha} = 100$, the velocity is fully developed at a distance of 50 channel widths for both the slug and the skewed inlet profiles, while at $\mathrm{Ha} = 1000$ the velocity profile is still developing. At higher Ha, the development of the velocity will be delayed further. This means that liquid metal coolants in a reactor blanket that flow parallel to a strong magnetic field will not reach full development in this configuration.

For a magnetic field applied perpendicular to the mean flow direction, the flow develops quickly in a few channel diameters to a flat Hartmann profile. Fig. 31 shows normalized velocity profiles at the channel exit across the channel, which is assumed fully insulated. For $\mathrm{Ha} = 100$ and $\mathrm{Re} = 200$, the velocity profile is fully developed Hartmann profile at the channel exit, which is at $3.3a$ from the inlet.

These effects of the magnetic field on the flow of liquid metal coolants in reactor blankets can influence the heat transfer from the first wall. Since there is no interaction between a parallel field and a fully developed laminar velocity field, no change in heat transfer is expected. However, for a developing laminar flow the interaction with a parallel field can enhance heat transfer slightly due to the suppression of velocity profile development.

In laminar flow perpendicular to the magnetic field, higher fields enhance heat transfer by increasing the flow rate near the wall. Fig. 32 shows how Nusselt number (Nu) changes along the channel with increasing Hartmann numbers.

In a real reactor blanket, liquid metal coolant flows through regions of varying geometry and/or varying magnetic field. Large velocity gradients can exist when the coolant flows through ducts of varying geometries, such as flow behind a sudden enlargement. Peculiar M-shaped profiles may exist when the coolant flows through a fringing magnetic field. All these variations can have a significant effect on the ability of the coolant to transfer heat from the first wall and, therefore, detailed analysis of the flow behavior is needed.

Numerical calculations of MHD laminar, viscous flow through an abrupt expansion of a circular channel clearly show the flow behavior when a magnetic field is applied in the direction of the main flow. The effects of this interaction on the recirculating eddy of a conducting fluid behind an orifice show that the body forces act in an opposite direction to the vortex eddy. This tends to weaken it, creating an almost stagnant region behind the orifice.

Macagno and Hung [52] studied the behavior of a captive eddy in a non-conducting flow both experimentally and numerically. They showed that at relatively small Reynold's numbers the re-attachment location moves downstream with increasing Reynolds number. McMichael and Deutsch [53] obtained an analytical solution using asymptotic expansion techniques for a conducting flow in slowly varying tubes in the presence of an axial magnetic field. They showed the appearance of flow separation along the wall in both converging and diverging regions of the tube. Their results, however, are limited to slowly varying tube radius.

Fig. 33 shows the arrangement of the problem considered. The flow pattern can be described as a main stream that has generated an annular eddy between itself and the walls. Fig. 34 shows the relative location of the re-attachment region and the eddy center as a

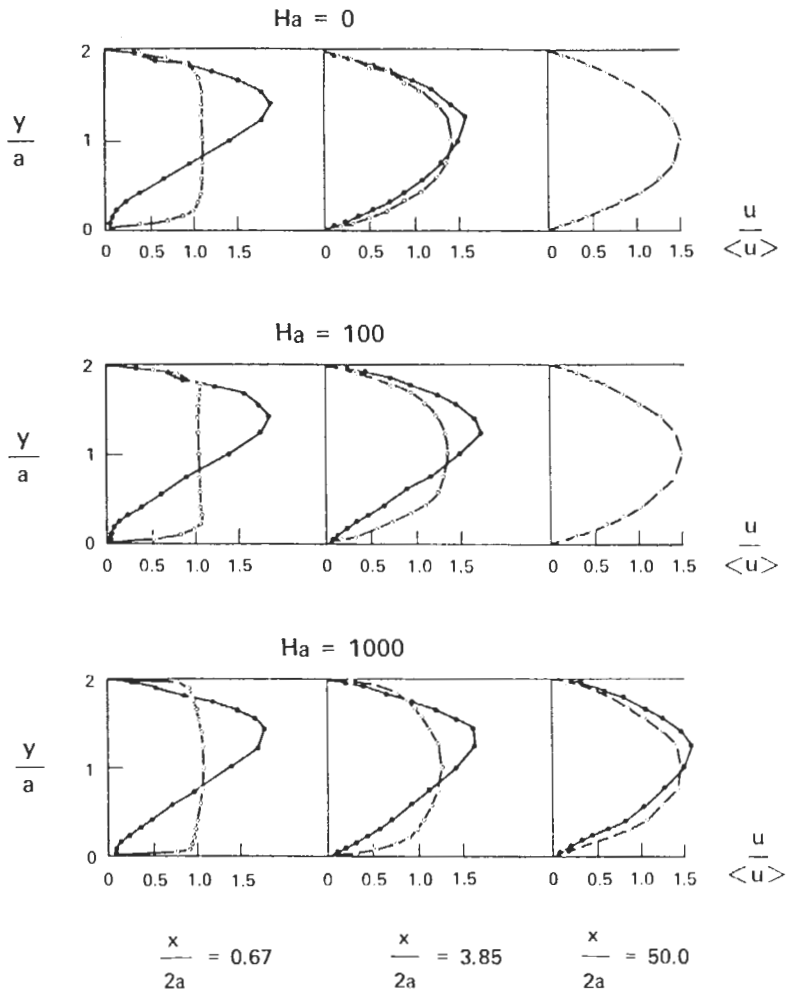

Fig. 30. Development of the velocity profile along an insulated channel of half-width a and axial magnetic field.

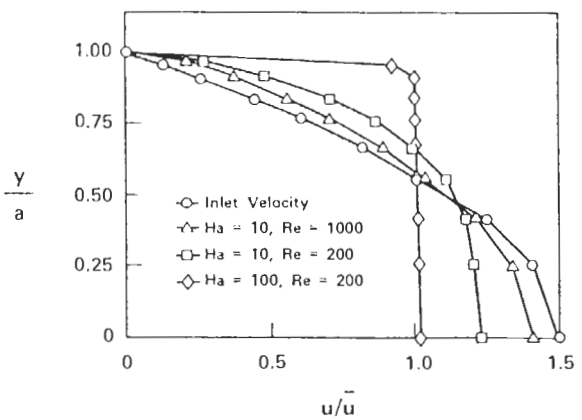

Fig. 31. Effect of a perpendicular magnetic field on the velocity profile at the exit of an insulated channel of half width (a) and insulated walls.

function of Reynolds and Hartmann numbers. When the applied magnetic field is zero, the results show good agreement with the experiments of Macagno and Hung [52]. When a horizontal magnetic field is applied, the re-attachment point moves downstream. Fig. 35 shows the effect of an axial magnetic field on the development of the velocity profile along the pipe. It can be seen from the figure that as Hartmann number increases, the length of the recirculating zone increases and the intensity of the eddy decreases. This creates an almost stagnant region behind the enlargement, which can have a great effect on heat transfer from the first wall in the presence of obstacles in liquid metal coolant ducts. Fig. 36 shows the wall pressure distribution along the pipe at different Hartmann numbers. In the non-magnetic case, large adverse pressure gradients develop downstream of

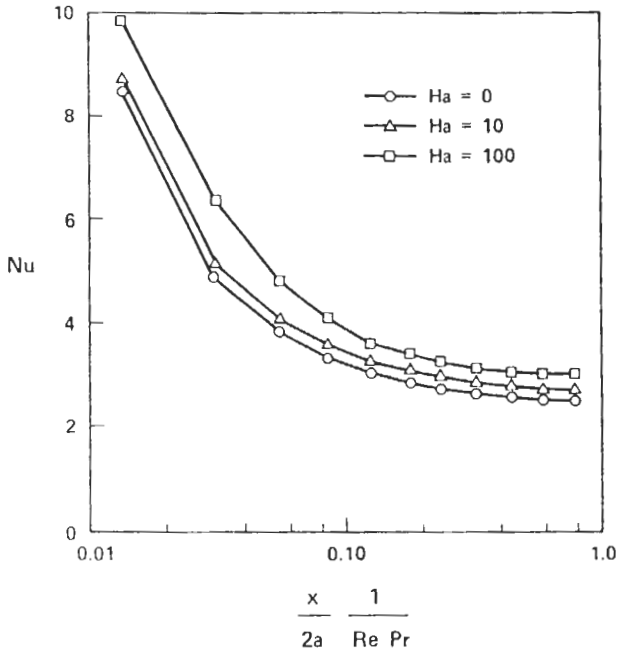

Fig. 32. Effect of a transverse magnetic field on entry length heat transfer in an insulated channel (parabolic inlet profile and constant wall temperature).

the enlargement. Magnetic forces, however, tend to decrease the maximum pressure gradients behind the enlargement and shift the maximum further downstream.

Convergence of eq. (1) may be impaired if the varia-

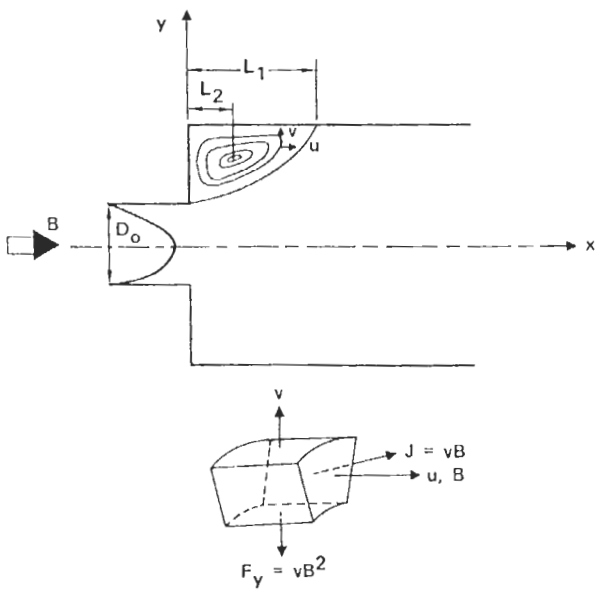

Fig. 33. Configuration of pipe expansion and a definition sketch.

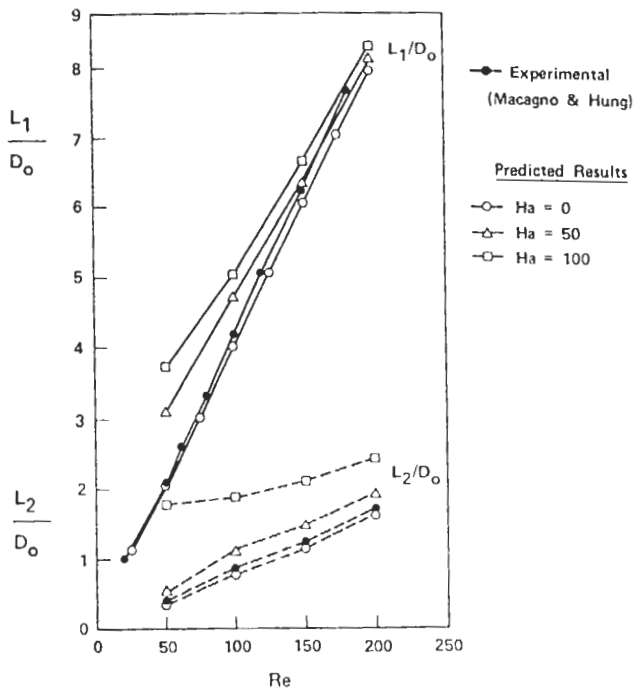

Fig. 34. Characteristics of the annular eddy as a function of Reynolds number at different Hartmann numbers (L_1/D_0, relative eddy length; L_2/D_0, relative location of eddy center).

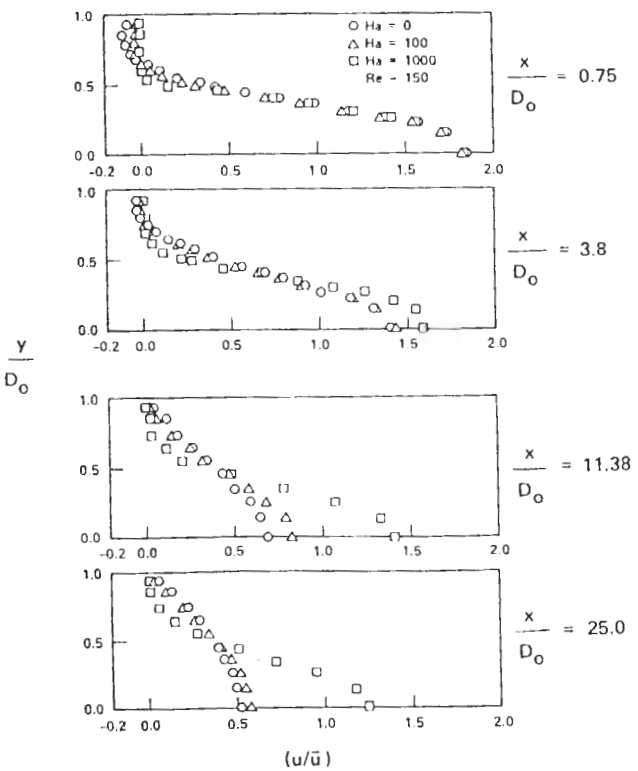

Fig. 35. Effect of axial magnetic field on the development of velocity profile along the pipe.

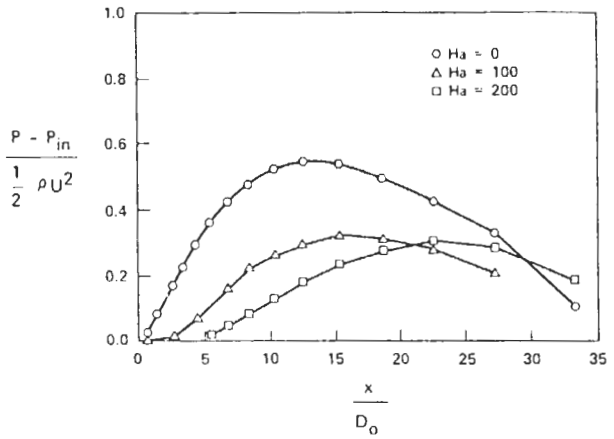

Fig. 36. Wall pressure distribution along the pipe at different Hartmann numbers.

tion between the coefficients and the source term is large. One possible remedy to this problem is to vary the variable ϕ slowly between iterations, i.e., use an underrelaxation method. If the variable ϕ, which was computed in the $(k-1)$th iteration, is denoted by $\phi^{(k-1)}$ and the value which would be computed in the normal way in the kth iteration is denoted by ϕ^k, then the value which would be actually used in iteration k is:

$$\phi = \alpha\phi^k + (1-\alpha)\phi^{k-1}, \tag{2}$$

where α is the under-relaxation parameter $(0 < \alpha < 1)$. In the present calculations, α was varied between 0.5 and 0.1 depending on the problem being considered. Another possible remedy which was not tried is to reduce variations in the source term S_ϕ at each iteration.

To obtain convergence at high Hartmann number flows, the electromagnetic forces must be included in the pressure and velocity iterative correction process. The coupled non-linear partial differential equations which govern the flow of a steady, constant property conducting fluid in a magnetic field can be written as:

$$\rho\frac{\partial}{\partial x_j}(u_i u_j) - \frac{1}{\mu_0}\frac{\partial}{\partial x_j}(b_i b_j) = -\frac{\partial}{\partial x_i}\left(P + \frac{|\boldsymbol{b}|^2}{2\mu_0}\right) + \mu\frac{\partial^2 u_i}{\partial x_j \partial x_j}, \tag{3}$$

where u_i and b_i are the velocity and magnetic field components in the x_i-space $(=1, 2, 3)$. P, ρ, μ and μ_0 are the fluid pressure, density, viscosity and magnetic permeability. The equation which governs the magnetic field can be written as:

$$\frac{\partial}{\partial x_j}(u_j b_i) - \frac{\partial}{\partial x_j}(u_i b_j) = \frac{1}{\mu_0\sigma}\frac{\partial^2 b_i}{\partial x_j \partial x_j}, \tag{4}$$

where σ is the electrical conductivity of the fluid. The velocity and magnetic field must satisfy

$$\frac{\partial u_i}{\partial x_i} = 0 \quad \text{and} \quad \frac{\partial b_i}{\partial x_i} = 0. \tag{5}$$

As can be seen from eq. (3), the term $(|\boldsymbol{b}|^2/2\mu_0)$ is added to the pressure. This must be included in any pressure correction scheme. A solution method would iterate between eqs. (3) and (4) to calculate intermediate values of u_i and b_i. Then, using the continuity equations (5), a pressure correction equation can be constructed which can correct the velocities and, hence, the induced magnetic field. The process is repeated until the residual errors in eq. (5) are made very small. This seems a preferred method of solving MHD flows and further work is being pursued in this direction.

Another important fact of high Hartmann number flows is the narrow boundary and free shear layers which have to be resolved accurately by increasing the number of grid nodes. This, however, will increase the number of iterations required for convergence. In the present calculations, variable grid spacing was used to improve spatial resolution in regions of high velocity gradients.

Mesh refinement can be an efficient method to improve the accuracy of MHD calculations while minimizing the amount of computational effort (storage spaces as well as time). However, it is not possible, in general, to predict the size and location of areas which require a refined mesh. One way to improve the mesh is by using the errors calculated from an initial coarse-grid calculation to indicate regions which require a finer mesh. Increasingly finer meshes can be iteratively determined until the desired level of accuracy is obtained.

To test the effectiveness of this technique, a finite element solution for 2-D fully developed duct flow is under development. Initial results have been obtained with pre-defined meshes of various sizes, and residual errors have been calculated. While self-adaptive solutions have been obtained successfully in 1-D problems, results are not yet available for the 2-D duct geometry.

Fig. 37 shows the geometry of the duct in the x–y plane with a fully developed velocity in the z-direction. A uniform magnetic field is applied in the y-direction perpendicular to perfectly conducting walls and parallel

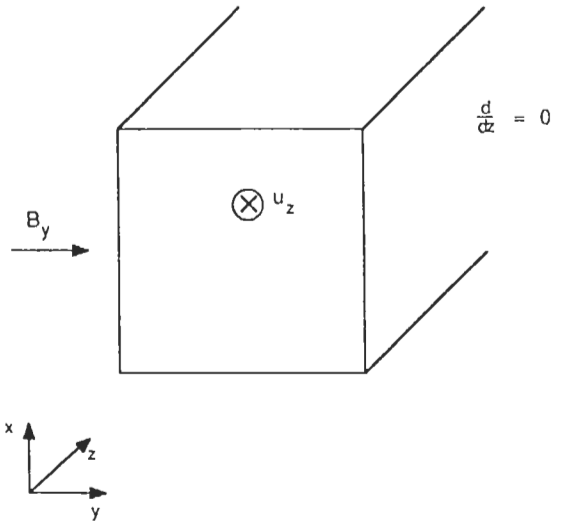

Fig. 37. Geometry for the fully developed 2-D channel flow problem.

to the non-conducting walls. Fig. 38 shows the finite element solutions of the velocity using 5×5, 10×10, and 20×20 meshes, as compared to Hunt's [46] analytical solution for the velocity along the axis $y = 0$. The velocity in the figure is normalized with respect to the channel average velocity. Increasingly finer meshes show the trend towards approaching the analytical solution.

Numerical methods to model MHD flows were emphasized in the present work. The two approaches used (namely, the finite difference and finite element methods) have helped to highlight the main difficulties and limitations to the numerical approach. The FEM seems potentially attractive especially when used with an irregular grid or complicated geometry. Although this potential has been recognized, certain difficulties may arise in trying to model the full non-linear fluid flow in MHD problems. Since the FWHM is rather well developed for fluid flow and heat transfer, and given the limited resources available, further work will concentrate on the FDM. Numerical techniques, such as pressure correction based on the SIMPLE method, will be utilized and improved. The method proved useful for MHD calculations at low and intermediate Ha and N parameters. Further work is proceeding on improvements to the numerical scheme to account for the electromagnetic forces in the pressure correction procedure. This is expected to extend the ability to model MHD flows at higher Ha and N parameters.

4.3. Heat transfer in flows over a wedge or a cylinder with volumetric heat generation

The importance of volumetric heat generation in liquid metals presents a unique and interesting heat transfer problem; in addition to causing the bulk temperature of the coolant to rise, it can alter the temperature profile and, hence, the heat transfer coefficient. It has been found [31] that volumetric heat generation can decrease the heat transfer coefficient and, as a result, cause an increase in the wall temperature. One of the primary purposes of this work was to determine the effects of heat generation in the coolant on hot film probes used to measure velocity profiles in the liquid metal. However, it also has general relevance to flows over plates and wedges. Both analytical and experimental work have been performed.

The analytical work utilized a similarity transformation similar to Chambre [54] to convert the partial

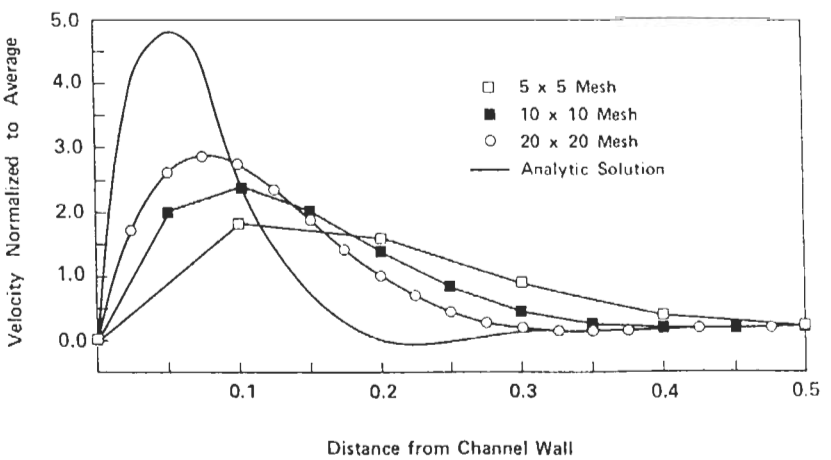

Fig. 38. Comparison of finite element solution with analytic solution.

differential equations governing the velocity and temperature into ordinary differential equations. The equations are then solved numerically. The analysis considers flows over wedges and over circular cylinders. For flow over a flat plate (wedge angle equals zero), an abnormal temperature overshoot in the temperature profiles is observed. Fig. 39 shows the boundary layer temperature profiles for flow over a flat plate at different Prandtl numbers. The figure indicates that the temperature of the flow near the wall is greater than the wall and free stream temperatures. For liquid metal coolants (Pr ~ 0.01), no temperature overshoot is expected. However, it is more pronounced for high Prandtl number flows.

The analysis has also been extended to flows over a circular cylinder, where an equivalent wedge method is used for performing the analysis. The average change of Nusselt number for the unseparated flow region of the cylinder due to heat generation for Pr → 0 is:

$$\Delta\overline{\mathrm{Nu}}_{\mathrm{d}} = 1.23\lambda_{\mathrm{d}}\,\mathrm{Re}_{\mathrm{d}}^{-1/2}\,\mathrm{Pr}^{-1/2}, \qquad (6)$$

where λ_{d} is a heat generation parameter based on the hot film diameter (d) defined as:

$$\lambda_{\mathrm{d}} = Q_{\mathrm{v}} d^2/K(T_{\mathrm{s}} - T_{\mathrm{in}}),$$

where Q_{v} is the volumetric heat generation, T_{in} is the inlet flow temperature, and T_{s} is the surface temperature.

To obtain the actual Nusselt number for flows over a cylinder, first the average Nusselt number without heat generation, $\overline{\mathrm{Nu}}_0$, is obtained from literature. Then the change ($\overline{\Delta\mathrm{Nu}}$) is obtained from eq. (6), and the actual Nusselt number ($\overline{\mathrm{Nu}}$) is obtained from $\overline{\mathrm{Nu}} = \overline{\mathrm{Nu}}_0 - \overline{\Delta\mathrm{Nu}}$.

To obtain an approximate estimate of the effect of heat generation on the heat transfer coefficient for flow over a hot film anemometer, the change in Nusselt number relative to the Nusselt number for the case of no heat generation can be written as:

$$\frac{\Delta\mathrm{Nu}_x}{\mathrm{Nu}_{0x}} = \frac{2\lambda_x}{\mathrm{Re}_x\,\mathrm{Pr}}, \quad \mathrm{Pr} \to 0, \qquad (7)$$

where x is for a flat plate when $x = \pi d/4$. This value of x corresponds to the top location of the cylinder if the cylinder is cut open and transformed to a flat plate.

Eq. (7) indicates that the change is proportional to the heat generation parameter (λ_x), and inversely proportional to the Reynolds and Prandtl numbers. Therefore, the change is largest for higher heat generation, lower velocity, and low Prandtl number fluids. Table 22 shows the results of the comparison for various Reynolds numbers and heat generation parameters. For small hot film diameters, the effect of heat generation on the Nusselt number is negligible. However, the effect is large for larger cylinders.

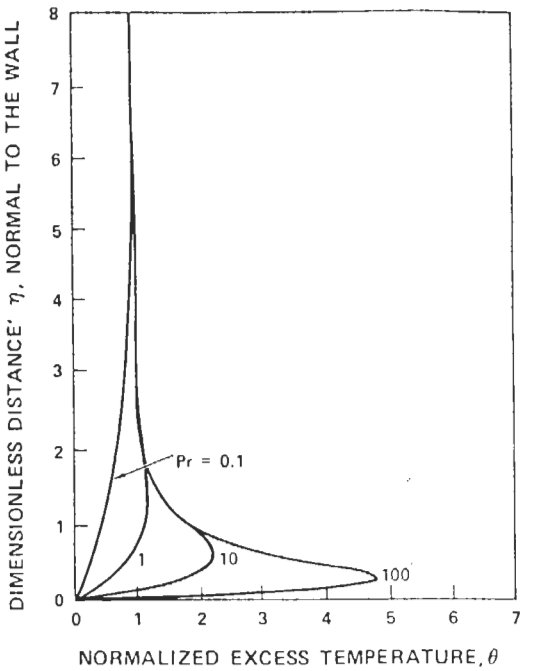

Fig. 39. Boundary layer temperature profile for flow over flat plate.

For a hot film anemometer placed in a liquid metal flow with volumetric heat generation, no appreciable change in Nusselt number is expected due to the small diameters of the hot film. This conclusion was verified in this study using a small scale experiment where a liquid metal loop was built and the few experiments

Table 22
Change in Nusselt number due to heat generation for a Pr = 0 flow over a cylinder [a]

Diameter d (m)	Heat generation rate Q_{v} (W/m^3)	Velocity V (m/s)	$\Delta\mathrm{Nu}_x/\mathrm{Nu}_x^0$ (%)
152×10^{-6}	33×10^5	0.14	0.04
10×10^{-3}	33×10^5	0.14	0.3
5×10^{-2}	33×10^5	0.14	13
152×10^{-6}	50×10^6	1	0.08
10×10^{-3}	50×10^6	1	0.5
5×10^{-2}	50×10^6	1	26

[a] The cylinder is approximated by a flat plate with the length of $x = \pi d/4$.

performed confirm the prediction that the change in Nusselt number is small [9].

4.4. Tritium transport modeling

The feasibility of a fusion reactor depends on the development of economical and safe methods to extract tritium from the blanket breeding material at a rate equal to the breeding rate. It is important, therefore, to predict the tritium inventory and to understand quantitatively the movement of tritium in the blanket and tritium processing systems. A comprehensive model of the total tritium transport is needed to provide this understanding. Such a model also would be a useful tool to provide input to experiment planning and to analyze and interpret experimental results.

The effort in this area has been directed mainly toward transient modeling of the tritium transport in solid breeder blankets. The model focuses on the different mechanisms transporting the tritium generated in the solid breeder grain to the purge flow. These mechanisms include diffusion through the grain, grain boundary and open porosity. Surface adsorption/desorption is also included as an effective source term in the pore diffusion equation. It is intended to eventually include solubility in the model. All these processes are temperature dependent, so the temperature distribution must also be calculated. The tritium generation rate in the breeder grain can be obtained from neutronics calculations.

The preliminary results included calculating the transient tritium release with a step change in tritium generation at time = 0 s. Fig. 40 illustrates the variation of the tritium release with time for such a case with $LiAlO_2$ as the solid breeder. Four cases are considered: one with no adsorption/desorption taking place and three with adsorption/desorption taking place but with different volume fractions of hydrogen in the purge flow. The effect of adding a significant amount of hydrogen to the purge flow can be seen. Essentially, with 1% or even 0.1% of hydrogen in the purge flow, little tritium is adsorbed and the tritium release curve is similar to the diffusion-controlled case (with no adsorption/desorption). However, with only 0.0001% of hydrogen in the purge flow, tritium adsorption occurs appreciably and there is a long time before any tritium release occurs and the attainment of steady state is delayed.

These early results are encouraging in that they reproduce the expected tritium release behavior based on experimental results. However, the model needs to be developed further and tested before being used as a tool for interpreting experimental data and/or design studies.

4.5. Modeling of plasma-interactive components

Successful operation of the impurity control system depends on the thermomechanical behavior of its components. If liquid metal blankets are used, safety considerations dictate the use of coolants other than water in the in-vessel components. The present research considers the viability of using liquid metal as a coolant for in-vessel components such as limiters and diverter plates. Detailed thermal and mechanical stress analysis of the limiter is also considered, and a three-dimensional finite element code was developed for stress analysis.

4.5.1. Design window for liquid-metal-cooled limiters

The purpose of this work is to investigate the feasibility and attractiveness of liquid metals as coolants for in-vessel components. In detailed calculations, a pumped limiter in a tokamak reactor was used as an example. A technique used extensively in this work is that of defining the possibility of a design using a design window. A design window can be explained as a permissible region of operation defined by various limits.

Considerable effort has been devoted to developing a geometrical configuration for the limiter that minimizes the problems associated with liquid metal coolants. Key factors are: (a) minimizing the coolant flow path length inside the limiter in order to reduce the required flow speed for a given temperature and surface heat flux; (b)

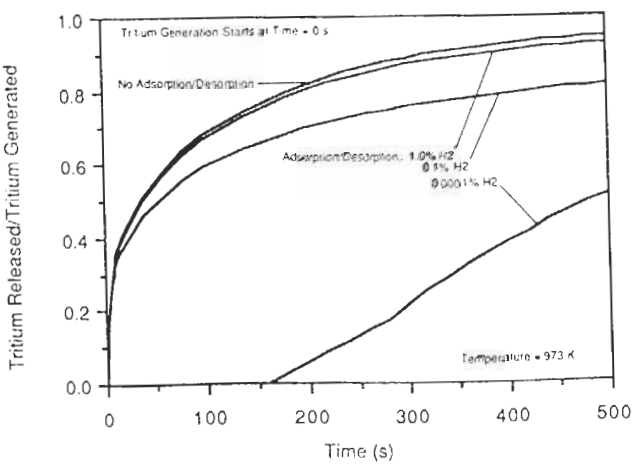

Fig. 40. Calculated tritium released over time after step change in tritium generation for no adsorption/desorption and for adsorption/desorption with different H_2 volume fractions in the purge flow.

optimizing flow direction relative to the magnetic field; and (c) flow mixing and other techniques to enhance heat transfer inside coolant channels. The purpose of the first two items is to reduce MHD pressure drop. Enhancing heat transfer reduces the temperature at the coolant/structure interface and reduces the maximum temperature in the structure.

An example of the results is found in fig. 41, which shows the "design window" under some of the most favorable conditions for a lithium-cooled limiter with insulated feed pipes. The limiter is double-edged and is shaped to make the incident heat flux uniform. The flow in the inlet and outlet manifolds is perpendicular to the toroidal field, while it is parallel to the field inside the small cooling channels within the limiter. The poloidal width of the limiter is 2.1 m and the cooling channel length is 30 cm in the toroidal direction. The lithium inlet temperature is 230°C. The maximum thickness of the vanadium wall is 1.5 mm. The maximum temperature for the structure is about 700°. The results in fig. 41 show that a design window exists at a heat flux of 4 MW/m^2, but the window is not sufficiently wide to compensate for the many present uncertainties.

Fig. 42 is similar to fig. 41, except that the surface heat flux is increased to 5 MW/m^2. The use of insulated walls is necessary in this case. The results are also found to be sensitive to the fluid velocity profile (slug flow as assumed in figs. 41 and 42).

These calculations were performed for an uncoated limiter with vanadium as the structural material. The use of beryllium as a coating, which may be required from a plasma contamination and/or erosion lifetime standpoint, imposes additional thermal stresses on the vanadium structure and narrows the design window further.

4.5.2. Thermal and stress analysis of limiters

Detailed thermal and primary stress analysis for double-edged limiters was carried out. Additional details on these calculations can be found in ref. [9]. The thermal analysis considers the temperature distribution in an elemental section of the limiter for a given wall heat flux. A three-dimensional stress analysis code was developed to calculate both thermal stresses caused by wall heat flux, and primary stresses caused by the coolant pressure. Copper limiters with water coolants, and vanadium alloy limiters with lithium coolant were considered.

Assuming a uniform heat flux on the surface of the limiter, the temperature distribution was calculated by solving the energy equation. These temperatures are then used to calculate the stress intensity in the limiter. Fig. 43 shows the geometry of the limiter specimen and the rectangular finite element mesh. The plane EFE′F′ faces the plasma. The results obtained consider only the central portion of the limiter where the heat flux is

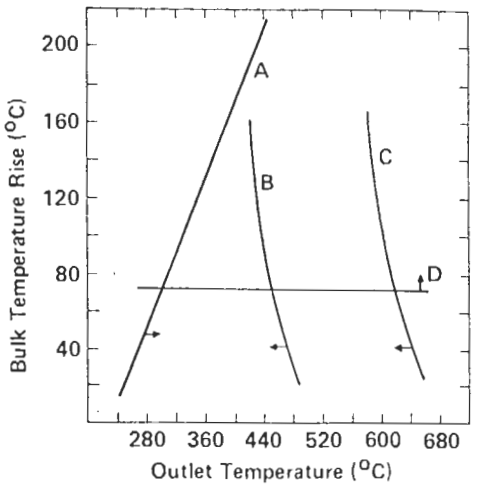

A - Minimum inlet temperature limit
B - Maximum structure temperature limit
C - Maximum interface temperature limit
D - Maximum primary stress limit

Fig. 41. Design window for lithium-cooled vanadium limiter with insulated conduits at 4 MW/m^2 heat flux.

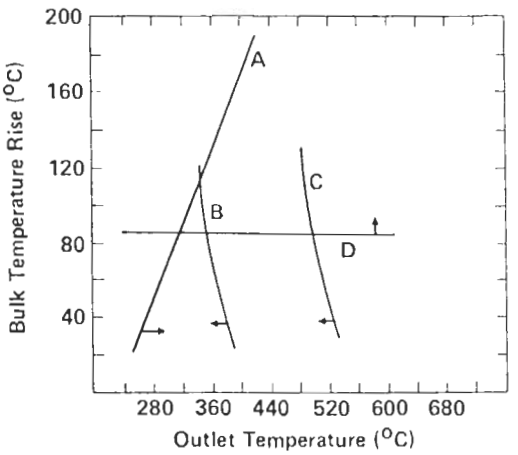

A - Minimum inlet temperature limit
B - Maximum structure temperature limit
C - Maximum interface temperature limit
D - Maximum primary stress limit

Fig. 42. Design window for lithium-cooled vanadium limiter with insulated conduits at 5 MW/m^2 heat flux.

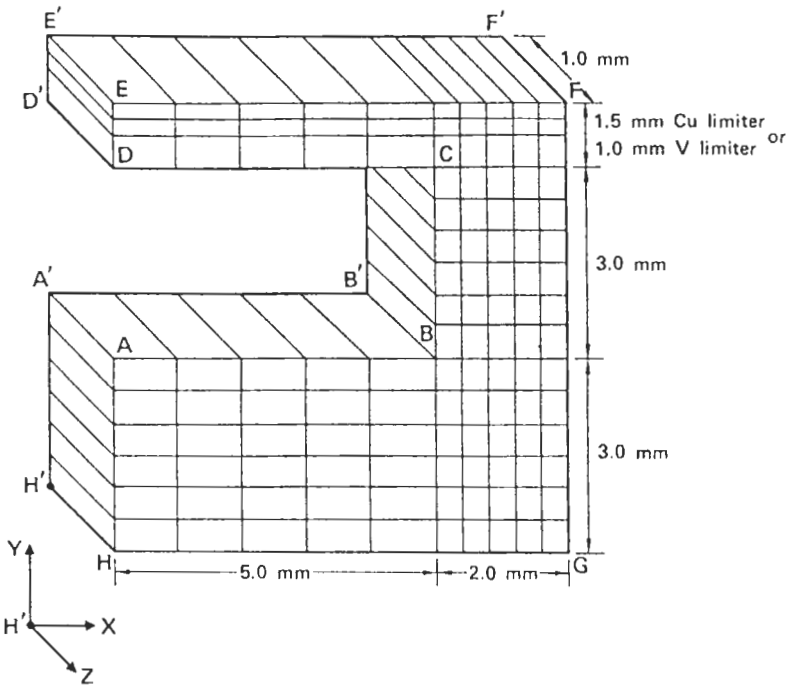

Fig. 43. Three-dimensional finite element mesh geometry.

assumed uniform. However, plans to model the curved leading edge of the limiter are under consideration.

Fig. 44 shows the temperature distribution in $x-y$ plane for a vanadium limiter with a wall heat flux of 6 MW/m^2 and a coolant Nusselt number of 7.0.

The results show that for water-cooled copper limiters

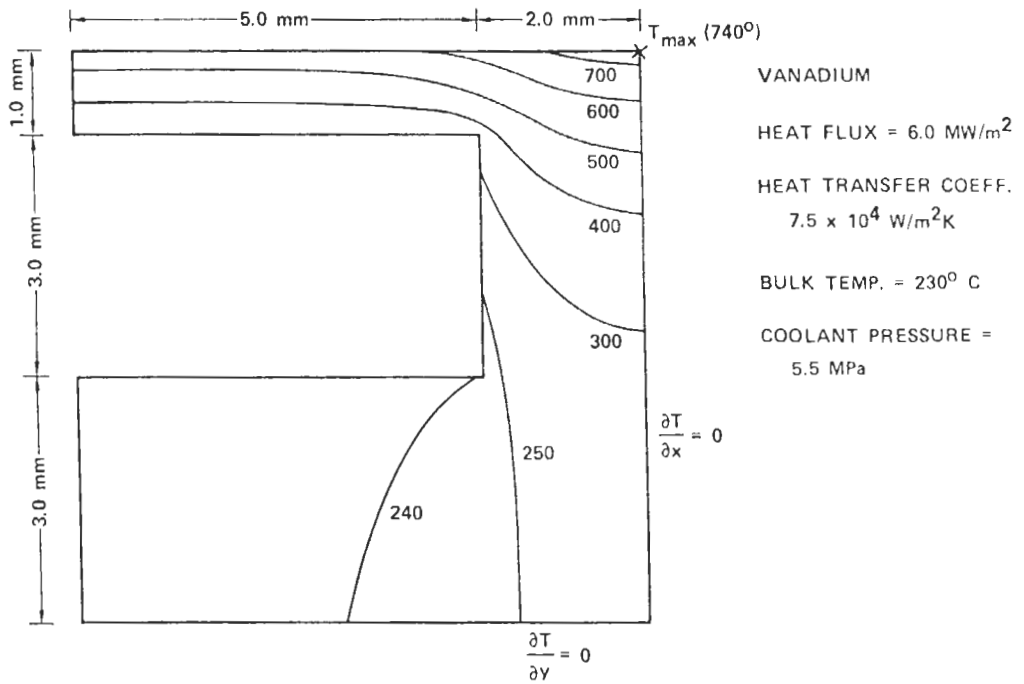

Fig. 44. Temperature distribution in a vanadium limiter. Results are shown for the $X-Y$ plane of fig. 43.

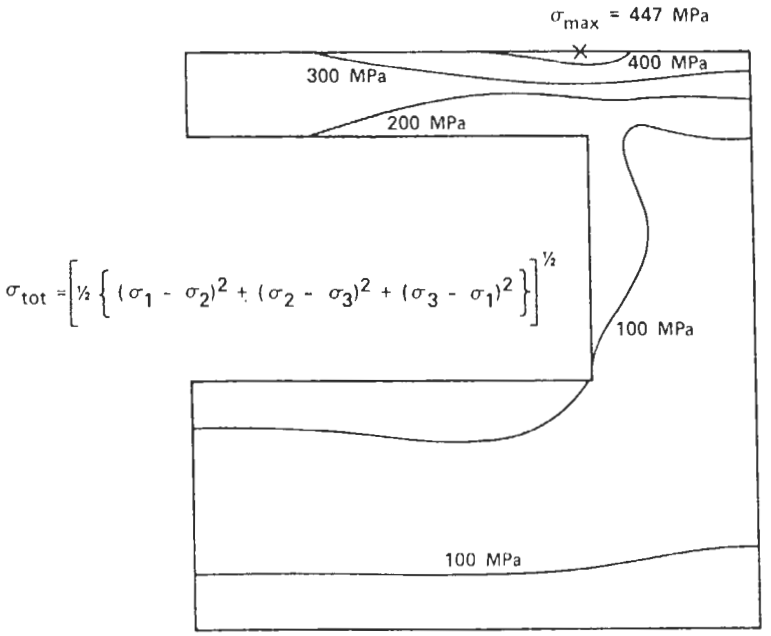

Fig. 45. Von Mises stress distribution (σ_6) in a lithium-cooled vanadium limiter with 6.0 MW/m^2 heat flux and coolant pressure of 5.5 MPa.

(with 1.5 mm wall thickness without coating), the maximum heat flux allowable is about 5.2 MW/m^2. A maximum coolant pressure of about 3.7 MPa is allowed based on the ASME code of stress limits for the structural material. On the other hand, lithium-cooled vanadium alloy limiters (with 1 mm wall thickness and no coating) have higher limits of 6.0 MW/m^2 heat flux and 8.0 MPa coolant pressure.

Fig. 45 shows an example of the Von Mises stress distribution (σ_t) in a cross-section of a lithium cooled vanadium limiter under a 6.0 MW/m^2 heat flux and coolant pressure of 5.5 MPa.

5. Concluding remarks

Nuclear technology plays a major role in the determination of fusion's feasibility and attractiveness as an economic power source. Yet there is currently a serious shortfall in data and understanding for the major issues of most component designs. Present activities on fusion nuclear technology need substantial enhancement in order to provide the needed data. This includes both increased experimental efforts as well as a strengthened program in modeling and analysis. Previous studies, most notably FINESSE [1–4], have provided the technical planning needed to identify the sequences and characteristics of major experiments and facilities in a logically consistent path for FNT development. The next logical step is implementation. This article has addressed a number of technical problems related to the implementation phase of FNT.

5.1. Near-term experiments and facilities

Required near-term (0–3 years) experiments and facilities have been examined, with particular emphasis on advanced solid breeder experiments in fission reactors and an advanced liquid metal flow facility, LMF1.

Presently, a large number of solid breeder materials are being considered worldwide. As experiments become more complex and expensive, screening of this material matrix must be performed. A study of the relative performance of the primary candidate solid breeder and multiplier materials (based on calculated neutronics, thermomechanics, tritium, activation and economics parameters) has led to several important recommendations. The conclusions from this study should serve as useful input to determining the priorities of solid breeder experiments.

Li_2O is the only solid breeder which has a chance for adequate tritium breeding without a multiplier (although uncertainties are currently too large to ensure fuel self-sufficiency). With Be as a multiplier, Li_2O is superior to all the ternary ceramics in achievable breeding ratio and power multiplication. Be-multiplied Li_4SiO_4 and, to a lesser extent, Li_2SiO_3 appear to be

the most attractive of the ternary ceramics from the viewpoint of better tritium breeding and power multiplication, lower activation and afterheat, and longer time to melt under accident conditions. This suggests that future emphasis should be placed on Li_2O with and without multiplier, and the silicates as the preferred candidate ternary ceramics. An important factor not considered in this study is the chemical and radiation stability of solid breeders, which favors $LiAlO_2$. It is, therefore, recommended that the experimental effort on $LiAlO_2$ be maintained.

Examination of the various neutron multipliers has shown Be to be a superior choice. BeO has poorer tritium breeding and energy production, and an exceptionally high tritium diffusive inventory. Li_7Pb_2 has favorable tritium breeding, but poorer energy multiplication, higher tritium inventory, and a limited operating temperature range.

A homogeneous mixture of Be and solid breeder provides superior neutronics performance over separate breeder and multiplier regions and is, therefore, recommended as a key configuration for experimental investigation in addition to the separate breeder and multiplier configuration. Thermomechanical and tritium behavior of sphere-pac material makes it preferable over a sintered block form.

In determining the most desirable characteristics of fission reactors for in-situ solid breeder experiments, several factors must be considered, including flux, spectrum, instrumentation capabilities, and test volume. Based on analysis of these, conclusions were reached regarding appropriate facilities for both material property testing and prototypic element testing.

For basic material property testing, fission reactors with either predominantly fast or mixed energy neutron spectra can be utilized. Care must be taken to choose the appropriate ^{6}Li enrichment and specimen size to achieve the desired test environment in a given test reactor.

For "prototypic" solid breeder testing with relevant temperature and tritium production gradients, the choice of an appropriate test reactor becomes more difficult. Fission reactors with significant thermal neutron flux are limited to small test specimen dimensions or low reaction rates, primarily due to self-shielding effects. Reasonable gradients for the initial tritium production and temperature within the test specimens can be obtained only for small test specimens with ^{6}Li enrichments of less than 2–3%. Also, the selective ^{6}Li burnup within the sample is quite severe and leads to a change in the tritium production gradient as a function of the test time.

Fission reactors with fast neutron spectra are less susceptible to self-shielding issues and, therefore, larger specimen sizes and higher burnup rates can be explored. Calculations for FFTF indicate that test specimens as large as 2.5 cm in diameter and ^{6}Li enrichments up to 20% can operate with minimal change in tritium production gradient with test time. The major limitation of fast neutron reactors is a minimum test temperature in the specimens of $\sim 360\,^\circ$C. Lower temperatures ($\sim 260\,^\circ$C) are possible only at significantly higher cost.

A facility called LMF1 (Liquid Metal Flow Facility) has been identified as a critical near-term experiment for self-cooled liquid metal blankets. Characteristics have been explored, including both the physical aspects of the facility and the experimental program.

The purpose of LMF1 is to carry out both isothermal and heat transfer tests on elements of future blanket designs for which there are unresolved MHD-related issues. LMF1 is different from previous experiments in its larger test volume and higher magnetic field, which allow achievement of the flow conditions much closer to a reactor. Microscopic studies of velocity and temperature profiles will be emphasized to expand our understanding of basic MHD phenomena. Macroscopic measurements will also be performed for verification of microscopic measurements as well as to provide empirical data for direct application to component design.

LMF1 will require construction of a new facility. The major elements include the flow loop, magnet systems, instrumentation, and test articles. The cost of the facility is expected to be dominated by the magnets, which cost roughly 10–15 M$.

5.2. Fusion testing issues

It is widely accepted by the world fusion community that an engineering test reactor will be needed to test and develop engineering components and systems prior to a committment to building a fusion power reactor. Major initiatives are already underway in Europe, Japan, USA and USSR.

Successful testing of fusion nuclear components requires that the physical and operating conditions of the test facility meet certain conditions. Extensive analysis to determine minimum and desirable test parameters has been performed in previous studies [1–4] and supplemented here. In particular, new calculations of the minimum burn time and maximum dwell time indicate that steady-state operation is highly desirable. Table 13 is a summary of the conclusions from the analysis of test requirements.

In addition to requirements on the test device characteristics, issues related to tritium supply and the reliability of a tritium-producing blanket also have been addressed. Since the amount of tritium available from external supplies is limited, internal production in tritium-producing blankets may be required. Examination of the possible civilian sources of tritium indicate a possible supply of 2–2.5 kg/yr from CANDU reactors and the potential for an additional 1 kg/yr from modified power reactors and fuel processing. While fusion nuclear testing requires only about 20 MW of fusion power, tokamaks generally require fusion power greater than ~ 300 MW at reasonable wall loading. It will be difficult to operate such a reactor at moderately high availability with only external tritium. Even if it could be made available, the cost (currently ~ $10000/g) might prove an unacceptable financial burden.

If tritium-producing blankets are used in the engineering test reactor, then blanket components will require a program of pre-operation testing and development. The required amount of testing has been evaluated by studying (1) the minimum mean time between failure (MTBF) required to achieve a particular blanket system availability, (2) the level of confidence in meeting this MTBF, and (3) the effect of parallel testing to reach a given confidence level. For a facility with 300 MW of fusion power and a blanket availability goal of 80%, the required MTBF may be 90000 hours or more, depending on the module replacement time. High confidence (~ 90%) in this level of performance will require testing time of several times the MTBF. It is unlikely that such lengthy testing will be achieved prior to fusion testing, which leads to low statistical confidence and high risk for the facility.

5.3. *Theory and modeling*

In general, modeling of fusion nuclear components is still in its infancy. Even in areas for which an established methodology exists for predicting component behavior (such as neutron transport), uncertainties in data and models are often larger than the margin for error, or design window. Computational efforts have been initiated in some of the most critical areas for which increased efforts are needed, including (1) heat transfer, fluid flow, and pressure drop in liquid metal blankets and high heat flux components, and (2) tritium transport in solid breeder materials.

Numerical methods to analyze MHD flows have been given special emphasis. Both finite difference (FDM) and finite element (FEM) solutions have been presented. While FEM methods have some potential advantages in complex geometries, a more extensive basis for finite difference techniques exists from ordinary fluid mechanics. Finite resources prohibit pursuing both methods, so future work will concentrate on FDM solution techniques.

Studies to date have utilized a pressure correction procedure based on the SIMPLE method. While this has proven successful at low and intermediate values of Ha and N, convergence is slow at very high Ha and N. Further work is proceeding on improvements to the numerical scheme which incorporates the electromagnetic force in the pressure correction procedure in order to extend the parameter range for which solutions can be obtained.

The tritium transport modeling includes the following transport mechanisms in steady or unsteady state: intragranular diffusion, grain boundary diffusion, surface adsorption/desorption, and pore diffusion. Solubility is not considered in the model, but it is intended for inclusion at a later stage. Early results are encouraging in that they show tritium release behavior expected from experimental observation. In the long run, such a model would be a valuable tool for: (a) providing input to the planning of experiments; (b) analyzing and interpreting experimental results; (c) providing predictive capability for design studies and for analysis of tritium selfsufficiency and safety; and (d) calculating the tritium behavior for pulsed vs. steady-state and providing input to the decision-making process regarding the mode of operating of the Engineering Test Reactor.

Models have been developed and preliminary results presented here; however, much further work will be needed to extend their applicability and completeness. Ultimately, it is intended that these models be incorporated into an overall framework for predicting component behavior.

Acknowledgements

This work is supported by the U.S. Department of Energy under Grant No. DE-FG03-86ER52123.

The authors wish to acknowledge the technical advice of many members of the fusion community. In particular, we are grateful to Dr. C.C. Baker (ANL), Prof. N. Ghoniem (UCLA), Prof. M. Hoffman (UC-Davis), Dr. G. Hollenberg (HEDL), Dr. C. Johnson (ANL), Dr. R. Mattas (ANL), Dr. S. Sharafat (UCLA), and Dr. M. Youssef (UCLA) for their review and comments on many parts of this article.

Many scientists and engineers from outside the U.S. have provided significant contributions to the study, and their efforts are gratefully acknowledged. Special acknowledgement is due to the Canadian Fusion Fuels Technology Project and the Japan Atomic Energy Research Institute.

We also wish to thank Ms. S. Ehrlich and Ms. M. Pagnusat for their assistance in preparing this manuscript.

References

[1] M.A. Abdou et al., FINESSE: a study of the issues, experiments, and facilities for fusion nuclear technology research and development (interim report), University of California, Los Angeles report, PPG-821, UCLA-ENG-84-30 (October 1984).

[2] M.A. Abdou et al., Technical issues and requirements of experiments and facilities for fusion nuclear technology (FINESSE phase I report), University of California, Los Angeles report, PPG-909, UCLA-ENG-85-39 (December 1985).

[3] M.A. Abdou et al., A study of the issues and experiments for fusion nuclear technology, Fusion Technol. 8 (1985) 2595–2645.

[4] M.A. Abdou et al., Technical issues and requirements of experiments and facilities for fusion nuclear technology, Nucl. Fusion 27, No. 4 (1987) 619–688.

[5] The NET Team, NET status report, NET Report 51 (1985).

[6] T. Tone et al., Nucl. Technol. Fusion 4 (1983) 573.

[7] C. Henning and B.G. Logan, TIBER-II: tokamak ignition/burn experimental reactor 1986 status report, Lawrence Livermore National Laboratory report, UCID-20863 (October 1986).

[8] Technical planning activity final report, Argonne National Laboratory report, ANL/FPP-87-1 (January 1987).

[9] M.A. Abdou et al., Modeling, analysis and experiments for fusion nuclear technology (FNT progress report: modeling & FINESSE), University of California, Los Angeles report, PPG-1021, UCLA-ENG-86-44, FNT-17 (January 1987).

[10] B.F. Picologlou, C.B. Reed, P.V. Dauzvardis and J.S. Walker, Experimental and analytical investigations of magnetohydrodynamic flows near the entrance to a strong magnetic field, Fusion Technol. 10 (1986) 860–865.

[11] W.M. Stacey, Jr. et al., The U.S. contribution to the international tokamak reactor phase 1 workshop, USA-INTOR/81-1 (June 1981).

[12] C.C. Baker et al., STARFIRE – a commercial fusion tokamak power plant study, Argonne National Laboratory report, ANL/FPP-80-1 (September 1980).

[13] D.L. Smith et al., Blanket comparison and selection study (final report), Argonne National Laboratory report, ANL/FPP-84-1 (September 1984). See also M.A. Abdou et al., Blanket comparison and selection study (interim report), Argonne National Laboratory report, ANL/FPP-83-1 (October 1983).

[14] M.A. Abdou et al., Deuterium-tritium fuel self-sufficiency in fusion reactors, Fusion Technol. 9 (1986) 250–285.

[15] M.C. Billone, The influence of surface desorption on tritium recovery and inventory in fusion solid breeders, J. Nucl. Mater. 141–143 (1986) 316–320.

[16] A.R. Raffray, Design and Cost Study of the ESPRESSO Blanket Concept for the Tandem Mirror Fusion Reactor, Doctor of Engineering Dissertation, Department of Mechanical Engineering, University of California, Davis, October 1985.

[17] F. Kreith, Principles of Heat Transfer, Third Edition (Harper & Row, New York, 1973).

[18] P.J. Gierszewski and R.J. Puigh, Testing needs and experiments for solid breeder blankets, J. Nucl. Mater. 141–143 (1986) 311–315.

[19] G.A. Deis, L.G. Miller and M. Youssef, Utilization of fission reactors for fusion engineering testing, Fusion Technol. 8 (1985) 1115–1123.

[20] P.J. Gierszewski, M.A. Abdou and R.J. Puigh, Fission reactor experiments for solid breeder blankets, Fusion Technol. 10 (1986) 1097–1101.

[21] Ja. Dekeyser and J.L. Walnier, Characteristics of experimental facilities for fusion research and development in lithium and lithium–lead technology, CEN/SCK report, FT/MOL/B4-7/T82-002 (1985).

[22] A. Inoue, H. Madarame and T. Tone, Outline of heat-removal studies in Japan, J. Fusion Energy 3 (1983) 425–428.

[23] M.A. Abdou et al., Fusion reactor design IV: report on the IAEA technical committee meeting and workshop. Yalta, USSR, 26 May–6 June 1986, Nucl. Fusion 26 (1986) 1377–1428.

[24] D. Ehst et al., Tokamak Power Systems Studies – FY 1986: A Second Stability Power Reactor, ANL/FPP/86-1 (March 1987).

[25] B. Kadomtsev et al., OTR – Experimental Fusion – Fission Tokamak Reactor Concept, IAEA Technical Committee Meeting and Workshop on Fusion Reactor Design and Technology, Yalta, USSR, 26 May–6 June, 1986, IAEA-TC392.3 (1986).

[26] International Tokamak Reactor, Phase Two A, Part I, STI/PUB/638 (IAEA, Vienna, 1983). See also, International Tokamak Reactor, Phase Two A, Part II, STI/PUB/714 (IAEA, Vienna, 1986).

[27] P.J. Gierszewski et al., Engineering scaling and quantification of the test requirements for fusion nuclear technology, Fusion Technol. 8 (1985) 1100–1108.

[28] C.C. Baker et al., Tokamak power systems studies – FY 1985, Argonne National Laboratory report, ANL/FPP-85-2 (1985).

[29] M.A. Abdou et al., A demonstration tokamak power plant study (DEMO), Argonne National Laboratory report, ANL/FPP-82-1 (1982).

[30] M.A. Abdou et al, Recent progress in design studies for

tokamak demonstration and commercial power plants, in: Fusion Reactor Design and Technology, IAEA-TC-392/15 (1983) p. 231–272.
[31] K. Taghavi, M.S. Tillack and H. Madarame, Special features of first wall heat transfer in liquid metal fusion reactor blankets, Fusion Technol. (July 1987) to appear.
[32] M.Z. Youssef and M.A. Abdou, Neutronic testing requirements in fusion devices, Trans. Am. Nuc. Soc. 46 (1984) 234–235.
[33] Y. Oyama, M.Z. Youssef and M.A. Abdou, Operating and geometrical arrangement requirements for fusion neutronics testing, Fusion Technol. 8 (1985) 1484–1490.
[34] M.A. Hoffman, Magnetic field effects on the heat transfer of potential fusion reactor coolants, Lawrence Livermore National Laboratory report, UCRL-73993 (1972).
[35] J.C.R. Hunt and R.J. Holroyd, Applications of Laboratory and Theoretical MHD Duct Flow Studies in Fusion Reactor Technology, CLM-R169 (May 1977).
[36] H. Branover, Magnetohydrodynamic Flow in Ducts (Keter Publishing House, Jerusalem, 1978).
[37] J.S. Walker, Liquid-metal flow in a thin conducting pipe near the end of a region of uniform magnetic field, Argonne National Laboratory report, ANL/FPP/TM-205 (1986).
[38] B. Brown, Tritium in the environment, Chalk River Nuclear Laboratories report, CRNL-2739-4 (1986).
[39] A. Bleier, R. Kroebel, K.H. Neeb and E. Schneider, Tritium inventories and behavior in zircaloy cladding of spent light water reactor fuel rods, in: Proc. Fuel Reprocessing and Waste Management Conf., Vol. 1 (1984) pp. 238–248.
[40] K.Y. Wong et al., Canadian tritium experience, Ontario Hydro report (1984).
[41] J. Couture, Status of the French reprocessing industry, in: Proc. Fuel Reprocessing and Waste Management Conf., Vol. 1 (1984) pp. 33–45.
[42] M. Chazalon and B. Libin, Strategy of breeding blanket introduction in NET and test requirements, Proc. 14th Symposium on Fusion Technology (SOFT), Avignon, France (September 1986) to appear.
[43] P.J. Gierszewski, et al., A low-risk aqueous lithium salt blanket for engineering test reactors, Proc. 14th Symposium on Fusion Technology (SOFT), Avignon, France (September 1986) to appear.
[44] D. Steiner, et al., a self-cooled heavy water breeding blanket, 11th Symposium on Fusion Engineering, pp. 539–543, Austin, Texas (November 1985).
[45] W.F. Bogaert, M.J. Embrecht and R. Waeber, Application of the Aqueous Self-Cooled Blanket Concept to Tritium Producing Shielding Blanket for NET, Final Report, University of Leuven (January 1987).
[46] J.C. Hunt, Magnetohydrodynamic flow in rectangular ducts, J. Fluid Mech. 21, Part 4 (1965) 577–590.
[47] J.S. Walker, G.S. Ludford and J.C. Hunt, Three-dimensional MHD duct flows with strong transverse magnetic fields, Part 2: Variable-area rectangular ducts with conducting sides, J. Fluid Mech. 46 (1971) 657–684.
[48] J.S. Walker and G.S. Ludford, Three-dimensional MHD duct flows with strong transverse magnetic fields, Part 4: Fully insulated, variable-area rectangular ducts with small divergences, J. Fluid Mech. 56 (1972) 481–496.
[49] J.C. Petrykowski and J.S. Walker, Liquid-metal flow in a rectangular duct with a strong, non-uniform magnetic field, J. Fluid Mech. 139 (1984) 309–324.
[50] S.V. Patankar, Numerical Heat Transfer and Fluid Flow (McGraw-Hill, New York, 1980).
[51] G.P. D'Arcy and P.S. Schmidt, Entry region effects on lithium flow and pressure drop in fusion-reactor blankets, Proc. Symp. on the Technology of Controlled Thermonuclear Fusion Experiments and the Engineering Aspects of Fusion Reactors, Austin, Texas (1972).
[52] E.O. Macagno and T.K. Hung, Computational and experimental study of a captive annular eddy, J. Fluid Mech. 28 (1967) 43–64.
[53] J.M. McMichael and S. Deutsch, Magnetohydrodynamics of laminar flow in slowly varying tubes in an axial magnetic field, Phys. Fluids 27 (1984) 110–118.
[54] P.L. Chambre, The laminar boundary layer with distributed heat sources or sinks, Applied Scientific Research, Section A, 6 (1957) 393–401.